Analysis of Low-Density Parity-Check Codes on Impulsive Noise Channels

Zhen Mei

Newcastle University

Newcastle upon Tyne, U.K.

A thesis submitted for the degree of

Doctor of Philosophy

April 2017

Abstract

Communication channels can severely degrade a signal, not only due to fading effects but also interference in the form of impulsive noise. In conventional communication systems, the additive noise at the receiver is usually assumed to be Gaussian distributed. However, this assumption is not always valid and examples of non-Gaussian distributed noise include power line channels, underwater acoustic channels and man-made interference. When designing a communication system it is useful to know the theoretical performance in terms of bit-error probability (BEP) on these types of channels. However, the effect of impulses on the BEP performance has not been well studied, particularly when error-correcting codes are employed. Today, advanced error-correcting codes with very long block lengths and iterative decoding algorithms, such as Low-Density Parity-Check (LDPC) codes and turbo codes, are popular due to their capacity-approaching performance. However, very long codes are not always desirable, particularly in communications systems where latency is a serious issue, such as in voice and video communication between multiple users. This thesis focuses on the analysis of short LDPC codes. Finite length analyses of LDPC codes have already been presented for the additive white Gaussian noise channel in the literature, but the analysis of short LDPC codes for channels that exhibit impulsive noise has not been investigated.

The novel contributions in this thesis are presented in three sections. First, uncoded and LDPC-coded BEP performance on channels exhibiting impulsive noise modeled by symmetric α-stable (SαS) distributions are examined. Different sub-optimal receivers are compared and a new low-complexity receiver is proposed that achieves near-optimal performance. Density evolution is then used to derive the threshold signal-to-noise ratio (SNR) of LDPC codes that employ these receivers. In order

to accurately predict the waterfall performance of short LDPC codes, a finite length analysis is proposed with the aid of the threshold SNRs of LDPC codes and the derived uncoded BEPs for impulsive noise channels.

Second, to investigate the effect of impulsive noise on wireless channels, the analytic BEP on generalized fading channels with SαS noise is derived. However, it requires the evaluation of a double integral to obtain the analytic BEP, so to reduce the computational cost, the Cauchy-Gaussian mixture model and the asymptotic property of SαS process are used to derive upper bounds of the exact BEP. Two closed-form expressions are derived to approximate the exact BEP on a Rayleigh fading channel with SαS noise. Then density evolution of different receivers is derived for these channels to find the asymptotic performance of LDPC codes. Finally, the waterfall performance of LDPC codes is again estimated for generalized fading channels with SαS noise by utilizing the derived uncoded BEP and threshold SNRs.

Finally, the addition of spatial diversity at the receiver is investigated. Spatial diversity is an effective method to mitigate the effects of fading and when used in conjunction with LDPC codes and can achieve excellent error-correcting performance. Hence, the performance of conventional linear diversity combining techniques are derived. Then the SNRs of these linear combiners are compared and the relationship of the noise power between different linear combiners is obtained. Non-linear detectors have been shown to achieve better performance than linear combiners hence, optimal and sub-optimal detectors are also presented and compared. A non-linear detector based on the bi-parameter Cauchy-Gaussian mixture model is used and shows near-optimal performance with a significant reduction in complexity when compared with the optimal detector. Furthermore, we show how to apply density evolution of LDPC codes for different combining techniques on these channels and an estimation of the waterfall performance of LDPC codes is derived that reduces the gap between simulated and asymptotic performance.

In conclusion, the work presented in this thesis provides a framework to evaluate the performance of communication systems in the presence

of additive impulsive noise, with and without spatial diversity at the receiver. For the first time, bounds on the BEP performance of LDPC codes on channels with impulsive noise have been derived for optimal and sub-optimal receivers, allowing other researchers to predict the performance of LDPC codes in these type of environments without needing to run lengthy computer simulations.

Acknowledgements

I would like to express my sincerest gratitude to my supervisor Dr. Martin Johnston, for his guidance and advice during my study in Newcastle university. His experience and enthusiasm inspired me to work on channel coding and impulsive noise, which is the focus of the thesis. I am very grateful to his insightful ideas and many hours spent on me discussing my research and proofreading my papers. I would also like to thank my second supervisor Dr. Stéphane Le Goff for his encouragement and valuable suggestions during my master and PhD period. I have learnt a lot from him.

I would like to acknowledge my friends and colleagues Bin Dai, Yuanyi Zhao, Zheng Chu, Pengming Feng, Yulong Chen, Jiachen Yin, Yang Sun, Zeyu Fu, Huan Cao, Jamal Ahmed Hussein, Wael Abd Alaziz and Zaid Abdullah for their help and friendship during the past few years in the UK.

Finally, I would like to express my deepest love and gratitude to my family. I really thank my parents for their encouragement and support in innumerable ways throughout my study in the UK. No words are enough to express my appreciation for them. Especially, I am grateful to my girlfriend, Wenqi Hu. She always supported and encouraged me during my PhD period in Newcastle university. Her great love and patience inspired me to work harder and made this thesis possible.

Contents

List of Figures

List of Tables

List of Acronyms & Symbols

Symbols

α	Characteristic exponent of α-stable process
β	Skewness of α-stable pdf
δ	Location parameter of α-stable process
ϵ	The mixture ratio of distributions
Γ	The ratio of Gaussian to impulsive noise power
γ	Dispersion of α-stable process
$\lambda(x)$	The edge degree distributions of variable nodes
μ	The mean of the normal distribution
$\otimes$	Convolution Operation
$\rho(x)$	The edge degree distributions of check nodes
σ^2	The variance of the Gaussian noise
$\mathrm{SNR_G}$	Geometric signal-to-noise ratio
$\varphi(t)$	The characteristic function
C_g	The exponential of the Euler constant
d_c	The maximum check node degree
d_v	The maximum variable node degree
$E\{\cdot\}$	Expectation Operator
E_b	The energy per bit

E_s	The energy per symbol
N_0	Noise power
$Q(x)$	The tail probability of the standard normal distribution
$Q_\alpha(x)$	The tail probability of the standard symmetric α-stable distribution
R_c	Code rate

Acronyms/Abbreviations

BCGM	Bi-parameter Cauchy-Gaussian Mixture
BEC	Binary Erasure Channel
BEP	Bit Error Probability
BER	Bit Error Rate
BI-AWGN	Binary Input - Additive White Gaussian Noise
BICM-ID	Bit-Interleaved Coded Modulation with Iterative Decoding
BLEP	Block Error Probability
BPSK	Binary Phase-Shift Keying
BSC	Binary Symmetric Channel
BSMC	Binary-input Symmetric Memoryless Channel
CDF	Cumulative Density Function
CND	Check-Node Decoder
DE	Density Evolution
DVB	Digital Video Broadcasting
EGC	Equal-Gain Combining
EMI	Electromagnetic Interference
EXIT	Extrinsic Information Transfer
FLOM	Fractional Lower Order Moments

GA	Gaussian Approximation
GMM	Gaussian Mixture Model
IFT	Inverse Fourier transform
LDPC	Low-density Parity-Check
LLR	Log-Likelihood Ratio
M-QAM	M-ary Quadrature Amplitude Modulation
MAI	Multiple Access Interference
MIMO	Multiple-Input Multiple-Output
ML	Maximum Likelihood
MRC	Maximal-Ratio Combining
MSA	Min-Sum Algorithm
MSE	Mean Square Error
OFDM	Orthogonal Frequency-Division Multiplexing
PDF	Probability Density Function
PEG	Progressive Edge-Growth
QDE	Quantized Density Evolution
RFI	Radio Frequency Interference
SαS	Symmetric α-Stable
SAA	Small Argument Approximation
SC	Selection Combining
SIMO	Single-Input Multiple-Output
SISO	Single-Input Single-Output
SNR	Signal-to-Noise Ratio
SPA	Sum-Product Algorithm

VND	Variable Node Decoder
ZOS	Zero-Order Statistics

Chapter 1

Introduction

1.1 Introduction

The performance of the communication system degraded by fading effects and additive Gaussian noise has been investigated for many years in the literature. However, there are many applications where the dominant background noise has a non-Gaussian distribution, such as impulsive noise. The presence of non-Gaussian impulsive noise can severely degrade a communication system since many decoders assume the noise is still Gaussian. As a class of powerful error-correction codes, low-density parity-check (LDPC) codes have been employed in many applications. In addition, the LDPC code was adopted as a part of the standard for powerline communications, which suffer from impulsive noise. In this thesis, the uncoded and LDPC-coded performance on impulsive noise channels is examined. Moreover, fading channels with impulsive noise are also investigated and the performance of diversity combining techniques to mitigate fading are analyzed.

1.2 Motivation and Challenges

Several famous models have been proposed to model impulsive noise, such as the Gaussian mixture model, Middleton Class A model and symmetric alpha stable (SαS) distributions [2–4]. Recently, the class of SαS distributions was shown to be an accurate model for impulsive noise, namely, radio frequency interference (RFI) in laptop and desktop computers [5] and background noise in power-line communications [6]. However, unlike Gaussian distributions, the probability density function

(pdf) of SαS distributions is not given in closed-form. Hence, the first error probability analysis of the communication system with SαS noise is presented.

As we know, LDPC codes have been adopted in many applications, such as powerline communications. Hence, it motivates us to examine the LDPC-coded performance in an impulsive environment. Conventionally, the noise is assumed to be Gaussian and the corresponding log-likelihood ratio (LLR) demapper is linear, which is far from the optimal LLR for impulsive noise. Since the optimal LLR is not given in closed-form, sub-optimal receivers need to be designed to reduce the complexity and it is important to examine the coded performance of optimal and sub-optimal receivers. Diversity combining techniques have been used for many years to mitigate fading effects and different combiners have been investigated for fading channels with impulsive noise in the literature. To the best of our knowledge, there is no literature on LDPC coded performance in impulsive noise with spatial diversity and one of the major contributions of this thesis is the evaluation of the performance of LDPC codes in such environments with diversity combining methods.

1.3 Aims and Objectives

The aim of this thesis is to provide a framework to analyze the error probability of communication channels in the presence of SαS noise. More importantly, the performance of LDPC codes will be explored and analyzed on these channels by simulations and density evolution, respectively. To closely estimate the simulated bit-error rate (BER) and block-error rate (BLER) performance of LDPC codes, a method to predict the waterfall performance is proposed. The objectives of this thesis are:

- To derive the theoretical performance of communication channels with SαS noise.
- To investigate the LDPC-coded performance with optimal and sub-optimal receivers for channels with SαS noise.
- To derive an estimation of the waterfall performance of LDPC codes on memoryless channels with SαS noise.
- To examine diversity combining methods and the performance of LDPC codes

combined with different combiners on fading channels with impulsive noise.

1.4 Statement of Originality

The contributions of this thesis are focused on the performance analysis of uncoded and coded system with impulsive noise. The novelty of the thesis is described as follows:

In Chapter 4, the uncoded error probability of SαS noise channels is derived. To examine the performance of LDPC codes on these channels, density evolution (DE) is performed to find the threshold SNRs of different receivers. Moreover, a near-optimal receiver is proposed to reduce the complexity and maintain good performance. Finally, an accurate estimation of the waterfall performance of finite length LDPC codes is proposed.

In Chapter 5, the bit error probability (BEP) of generalized fading channels with SαS noise is derived. To reduce the computational cost, we present two closed-form approximations of the exact error probability on Rayleigh fading channels with SαS noise. Then we present a DE analysis to find the asymptotic performance of LDPC codes with optimal and sub-optimal receivers on fading channels with SαS noise. Finally, the finite length performance LDPC codes on these channels is also predicted.

In Chapter 6, we first derive the uncoded BEP of traditional linear diversity combining methods and non-linear detectors on Rayleigh fading channels with SαS noise. In addition, a near-optimal non-linear detector is proposed. Similarly, to examine the LDPC-coded performance, we derive the threshold SNR of linear combiners by using DE and the waterfall performance is predicted using the same approach we have given in the thesis.

1.5 Organization of the Thesis

This thesis is organized as follows:

Chapter 2 introduces the background and current research in impulsive noise in the relevant literature. In addition, the development and applications of LDPC codes are presented. Moreover, the signal detection and the performance of error correction codes with soft decision decoders on impulsive noise channels are described.

Chapter 3 presents the background theory related to this work. Different models of non-Gaussian noise are introduced with particular focus on symmetric alpha-stable (SαS) distributions. The properties, generation and parameter estimation of SαS random variables are presented. In terms of LDPC codes, a very efficient construction method called the progressive edge-growth (PEG) algorithm is introduced. In addition, the message passing decoding algorithm: sum-product algorithm (SPA) and the asymptotic analysis of this algorithm are described.

In Chapter 4, the performance of LDPC codes on SαS noise channels with different receivers are investigated and we propose a near-optimal receiver with low complexity. Then a density evolution analysis is performed to find the asymptotic performance of these receivers. In addition, to reduce the gap between asymptotic and simulated performance, a finite length analysis of LDPC codes on SαS noise channels is presented. In order to calculate the estimation of the waterfall performance of LDPC codes, the uncoded bit error probability (BEP) of SαS noise channels is first derived. By observing the real-time channel quality, the block and bit error probability of finite length LDPC codes are then predicted.

In Chapter 5, we have derived the analytic BEP of BPSK on generalized fading channels with SαS noise. To reduce the computational cost, we have derived two approximations of the exact BEP on Rayleigh fading channels with SαS noise, which are based on the bi-parameter Cauchy-Gaussian mixture (BCGM) model and the asymptotic expansion of SαS process. These two bounds are given in closed-from, which can greatly reduce the complexity. Then we have investigated the LDPC-coded BEP of generalized fading channels with SαS noise. We propose a DE analysis to find the asymptotic performance of LDPC codes with optimal and sub-optimal receivers on these channels. Finally, the waterfall performance of finite length LDPC codes on these channels is predicted.

In Chapter 6, the uncoded and LDPC-coded performance of linear diversity combining techniques and non-linear detectors are examined on Rayleigh fading channels with independent SαS noise. The decoding threshold of linear combiners is derived by using DE. By utilizing uncoded BEP and threshold, a closed-form approximation of the waterfall performance is obtained. In addition, the performance of LDPC codes with non-linear detectors are investigated and a near-optimal detector based on the BCGM model is proposed.

The thesis is concluded in Chapter 7 and we also provide some suggestions for

future research in this field.

1.6 Publications Related to the Thesis

1. **Z. Mei**, M. Johnston, S. Le Goff and L. Chen, "Density Evolution Analysis of LDPC codes with Different Receivers on Impulsive Noise Channels", *in Proc. IEEE/CIC International Conference on Communications in China (IEEE/CIC ICCC)*, Shenzhen, China, 2015.

2. **Z. Mei**, M. Johnston, S. Le Goff and L. Chen, "Error Probability Analysis of M-QAM on Rayleigh Fading channels with Impulsive Noise", *in Proc. IEEE international workshop on Signal Processing advances in Wireless Communications (SPAWC)* , Edinburgh, UK, 2016.

3. **Z. Mei**, M. Johnston, S. Le Goff and L. Chen, "Finite Length Analysis of LDPC codes on Impulsive Noise Channels", *IEEE Access*, IEEE, 2017.

4. **Z. Mei**, M. Johnston, S. Le Goff and L. Chen, "Performance Analysis of LDPC-Coded Diversity Combining on Rayleigh Fading Channels with Impulsive Noise", *IEEE Transactions on Communications*, 2017 (Early Access).

5. **Z. Mei**, M. Johnston, S. Le Goff and L. Chen, "Performance Analysis of LDPC codes over Fading Channels with Impulsive Noise", submitted to *IET Communications*.

Chapter 2

Literature Survey

2.1 Introduction

In this chapter, signal detection and channel coding schemes, with particular focus on LDPC codes on impulsive noise channels, will be reviewed. First, examples of common communication systems are presented that are modelled as symmetric alpha stable processes. This is followed by different types of signal detection for additive impulsive noise channels. A review of the different design methods for LDPC codes is presented and finally the design of receivers for soft-decision decoders on impulsive noise channels concludes this chapter.

2.2 Impulsive Noise

In conventional communication systems, noise is usually modeled as Gaussian and is called additive white Gaussian noise (AWGN). However, in some scenarios, the system suffers from non-Gaussian noise which contains a significant interference component. This type of noise is also known as impulsive noise. Impulsive noise can be generated naturally or by man-made noise, which includes atmospheric noise, underwater acoustic noise, the background noise of powerline communications, multiple access interference (MAI) in ultra-wideband systems and the electromagnetic interference (EMI) [2, 7, 8]. The presence of impulses will severely degrade the communication system, which is likely to assume the noise is Gaussian and a redesigning of the system is required. Hence a statistical-physical model is required to describe the behavior of impulsive noise. Based on this, several famous models have been

proposed to model impulsive noise, such as the Gaussian mixture model, Middleton Class A model and symmetric alpha stable (SαS) distributions [2–4]. In particular, the SαS family of distributions can accurately model impulsive noise present in underwater acoustic noise and atmospheric noise [9], as well as realistically modeling the statistics of radio frequency interference (RFI) generated by clocks and buses in laptop and desktop computers [5] and impulsive noise in power-line communications [6].

Recently, SαS noise was employed as an accurate model of multiple access interference (MAI) in a wireless *ad hoc* network and as near-field interference in wireless transceivers [5, 8]. If we also consider fading effects, the underwater acoustic channel can be modeled as a Rayleigh fading channel with SαS noise [9]. Theoretically, to exploit the spatial diversity, different diversity combining techniques and space time coding were investigated in [10, 11]. In addition, SαS noise had been used to model the multiple-access interference (MAI) at the receiver for Nakagami-m and Rician fading channels [12, 13]. In this thesis, we will focus on the SαS model and investigate signal detection and LDPC-coded performance in the presence of SαS noise.

2.3 Signal detection in Impulsive Noise

The conventional receiver assumes the additive noise is Gaussian, which is not correct when impulse occurs, and leads to a severe performance degradation. The optimal receiver needs to have the knowledge of the pdf of the non-Gaussian SαS noise [14, 15]. However, the pdf of SαS distributions is not given in closed-form which will lead to high computational cost. Hence, suboptimal receivers that do not need to know the exact pdf of the noise are more desirable for practical use. Some suboptimal receivers have been proposed that estimate the pdf or reduce the effect of impulses [16], such as the Cauchy receiver, which assume the noise has a fixed Cauchy pdf since it has algebraic tails, and the much simpler limiter and hole-puncher [17], which limits or blanks the magnitude of the received values. Recently, a soft limiter with an adaptive threshold was proposed to further improve the performance [18]. To achieve near-optimal performance, a new analytic expression of the SαS pdf, which is based on the finite mixture of Gaussian approximations, was proposed in [19].

Diversity combining is an important technique that combats fading effects by exploiting spatial diversity. Traditional combining schemes such as maximal-ratio combining (MRC), equal-gain combining (EGC) and selection combining (SC) are chosen depending on the required trade-off between performance and complexity at the receiver. Conventionally, the noise added at each branch of the diversity combiner is assumed to be Gaussian. However, interference can exhibit an impulsive behavior [2, 20] and it is important to take this impulsive nature into account when analyzing spatial diversity. The optimal receivers on fading channels with impulsive noise were investigated in [21] and [22]. An adaptive diversity receiver was proposed to combat the impulsive noise with unknown parameters [23]. The receivers which are designed for Gaussian noise was investigated for fading channels with impulsive noise in [24] to examine the robustness of these combiners to impulsive noise and the impulsive noise was modeled as Middleton Class-A distributions. Nasri *et al* have analyzed the asymptotic BEP of diversity combining schemes under general non-Gaussian noise [25], but this work cannot be applied to SαS distributions because they have an infinite variance. Rajan *et al* also performed a diversity combining analysis for Rayleigh fading channels and isotropic SαS noise with dependent components [10], where diversity gain and asymptotic BEP were derived. We note that a complex SαS variable can be classified as a sub-Gaussian variable where its real and imaginary components are dependent [26]. However, if the bandpass sampling frequency f_s is at least four times the carrier frequency f_c, components become independent and this type of SαS noise is called additive white SαS noise (AWSαSN) [27, 28]. As we mentioned above, optimal and sub-optimal detectors for AWSαSN have already been investigated in the literature [16, 29]. For diversity combining, different linear combiners were compared in [30, 31]. However, the analytic BEP has not been derived for these linear combiners and it will be addressed in this thesis.

2.4 Low-Density Parity-Check codes

Low-Density Parity-Check (LDPC) codes were first proposed in Robert Gallager's doctoral thesis in 1960 and then published in [32]. However, LDPC codes were overlooked at that time due to the computational limitation of hardware and the development of Reed-Solomon codes. In 1981, a graphical representation of LDPC

codes called Tanner graph was proposed [33]. Until 1996, after the invention of turbo codes in 1993, LDPC codes were rediscovered by David Mackay and also shown to achieve near Shannon limit performance [34] followed by LDPC codes over finite field proposed in [35]. LDPC codes over GF(q) were shown better performance than their binary counterparts, but with a much higher decoding complexity and some algorithms were proposed to reduce the complexity of the decoder of non-binary LDPC codes [36–40]. Recently, LDPC codes have been adopted in many modern applications such as DVB-S2/T2, WiFi 802.11 standard and ITU-T G.hn standard. LDPC codes are preferred to turbo codes in these applications due to their lower decoding complexity and lower error floor.

The iterative message passing algorithm of LDPC codes has shown near Maximum likelihood (ML) decoding performance with very low complexity. To analyze the iterative decoder, the density evolution (DE) technique was proposed to find the asymptotic performance of iterative decoders [41]. By using DE, the decoding threshold SNR of a specific LDPC ensemble can be found. Naturally, when DE is extended to irregular LDPC ensembles, this method can be used to design irregular LDPC codes [42]. To avoid instability due to large amounts of numerical calculations and reduce the complexity, a quantized density evolution (QDE) was proposed in [43] and showed very accurate estimation of the threshold SNR with only 11-bit quantization. Furthermore, an alternative method called Gaussian approximation (GA) was proposed to simplify DE on binary-input additive white Gaussian noise (BI-AWGN) channels [44]. Instead of tracking densities in the decoding process, GA assumes the message passed through the iterative decoder is Gaussian or Gaussian mixtures. Hence it only needs to track the mean and variance of the message's pdf which results in a huge reduction in the complexity. Compared with DE and GA, an alternative method called extrinsic information transfer (EXIT) chart was proposed to visualize the exchange of extrinsic information between component decoders [45, 46]. Then the EXIT chart was extended to LDPC codes [47] and it is a tool to find the decoding threshold SNR as well as design good codes by reducing it to a curve fitting problem.

It is well known that the performance of LDPC codes degrades as the code length decreases. Hence, the asymptotic analysis of LDPC codes is not useful to predict the actual performance since it assumes that the code length is infinite and cycle-free. Finite length analyses need to be studied to evaluate the performance of short length

LDPC codes. In the literature, a finite length analysis of LDPC code ensembles on the binary erasure channel (BEC) was presented in [48] using a recursive approach. In [49], the waterfall region of LDPC codes was proved to follow a scaling law over the BEC and the performance was predicted accurately. However, the procedure of finding the scaling parameters on the BEC cannot be easily transferred to other channels and decoding algorithms. Recently, a waterfall region analysis based only on the threshold SNR was proposed [50, 51]. This method estimates the block-error probability by observing the real-time channel quality which is worse than the decoding threshold. Then an EXIT chart and GA combined with the block-error probability were used to obtain the bit-error probability. This method is simple and provides a good estimation of the waterfall region performance of short LDPC codes without any scaling parameters or curve fitting. In [52, 53], Noor-A-Rahim *et al* present a similar approach, which observes the actual channel quality and provides a more accurate estimation, but has a higher complexity.

To the best of our knowledge, the finite length analysis of LDPC codes is only investigated on the BEC, binary symmetric channel (BSC) and BI-AWGN channel, but not impulsive noise channels. Recently, LDPC codes were adopted in the proposed standard for powerline channels (G.hn/G.9960) [54], which are impulsive in nature and therefore, show that LDPC codes are good error-correcting codes in this kind of environment. However, there is no literature on the finite length analysis of LDPC codes on channels with impulses. Hence a method to closely predict the actual performance of LDPC codes on impulsive noise channels is required.

2.5 Soft Decision decoders and Receiver design on Impulsive Noise Channels

It is known that the soft decision decoders have shown better performance than hard decision decoders on AWGN channels and the fundamental limit of the coded systems with impulsive noise was give in [55]. For SαS noise, the capacity of the channel is also calculated [56, 57] and different code schemes were employed to approach this capacity. The soft decision decoders have shown better performance than hard decision decoders on AWGN channels. Conventionally, the log-likelihood ratio (LLR) is chosen as the metric of reliability and the initial input of the soft decision

decoders. For impulsive noise channels, sub-optimal LLR demappers were proposed for convolutional codes to achieve good performance with low complexity [58,59]. In addition, the bit-interleaved coded modulation with iterative decoding (BICM-ID) system with impulsive noise was analyzed by EXIT chart [60]. For turbo codes, the performance of different receivers was investigated in [61–63] and a robust p-norm receiver was proposed suitable for very impulsive environment [64]. As a class of powerful error correction codes, the performance of LDPC codes with different receivers on impulsive noise channels have also been presented in the literature [65–67]. The LDPC codes combined with a limiter in coded OFDM system with impulsive noise was investigated in [68,69]. In [70], a robust LLR which is suitable for different non-Gaussian noise models was proposed. Recently, a new type of soft limiter which is called the clipper was proposed. It combines with the LLR demapper to achieve good LDPC coded performance. In [71], the threshold of the clipper was further optimized by three methods. To approach near-optimal performance of iterative decoders, some receivers were proposed to approximate the optimal LLR demapper [29, 58, 72, 73]. We call this type of receiver the LLR approximation receiver. The LLR demapper was closely estimated in [72] and [73] by dividing the LLR into two parts (a linear part and asymptotic part) and using the asymptotic expansions of SαS pdf. In [58], the authors approximated the optimal piecewise linear LLR and corresponding coefficients were computed by minimizing the mean square error (MSE). Hence, the design of sub-optimal receivers for LDPC codes is still an open problem which needs to be explored.

If we take the fading into account, diversity combining techniques should be considered to mitigate the fading effect. The performance of LDPC codes with spatial diversity on AWGN channels was investigated in [74–76] and the cascaded combining techniques with LDPC codes is also shown in the literature [77, 78]. Recently, the performance of protograph-based LDPC codes with diversity was analyzed [79]. However, there are no publications that have examined the performance of LDPC codes with diversity combining on non-Gaussian channels.

2.6 Conclusion

As we discussed in this chapter, for the signal detection problem, different sub-optimal detectors were proposed to reduce the complexity of the optimal detector.

Recently, in cooperation with the decoder, the sub-optimal receivers based on LLR approximation were also proposed. We will follow this methodology to design the receiver and investigate the asymptotic performance of LDPC codes with different receivers. In addition, the finite length analysis for impulsive noise channels has not been examined in the literature. Inspired by [50], we will propose a method to closely estimate the waterfall performance of LDPC codes on these channels. Finally, to combat fading effects, optimal linear combiners and non-linear detectors were investigated for impulsive noise channels in the literature. In this thesis, we will derive theoretical uncoded and LDPC-coded performance for linear combiners to provide a benchmark when evaluating these systems.

Chapter 3

Theoretical Background

3.1 Symmetric alpha-stable noise

In this chapter, background theory on symmetric alpha-stable noise (SαS) is first explained, which includes the definition of the probability density function, a modified signal-to-noise ratio known as geometric SNR, the generation of SαS noise samples and estimation of the different parameters of SαS noise. The chapter concludes with detailed explanations on the construction of low-density parity-check (LDPC) codes using the Progressive Edge Growth algorithm, the decoding of LDPC codes using the message passing algorithm and the asymptotic performance of LDPC codes using density evolution, Gaussian approximation and Extrinsic Information Transfer charts. This is the essential prerequisite material for the novel work presented in chapters four, five and six.

3.1.1 Impulsive Noise Models

There are various distributions to model a non-Gaussian environment. In this chapter, we introduce some famous models including the Gaussian mixture model (GMM), Middleton Class A model and α-stable model. As a widely used model, the pdf of Symmetric α-stable (SαS) distribution has no closed-form expression which makes it difficult to analyze and we will focus on this model in this thesis. However, we will begin by reviewing the other popular models first.

3.1.1.1 Gaussian Mixture Model

The Gaussian Mixture model (GMM) is defined by the weighted sum of N Gaussian densities. The pdf is given as

$$f_{\mathrm{GMM}}(x) = \sum_{i=1}^{N} c_i f_{\mathrm{G}}(x; \mu_i; \sigma_i^2), \tag{3.1}$$

where $f_{\mathrm{G}}(x; \mu_i; \sigma_i^2)$ is the Gaussian pdf with mean μ_i and variance σ_i^2. This model is quite general since the Middleton Class A model is a GMM with infinite number of components and the symmetric α-stable (SαS) model can also be approximated by a scaled GMM model [2, 80].

In this thesis, we also introduce a commonly used GMM model which has two components [81]. The pdf is defined as

$$f_\epsilon(x) = (1-\epsilon) f_{\mathrm{G}}(x; 0; \sigma^2) + \epsilon f_{\mathrm{G}}(x; 0; \kappa\sigma^2), \tag{3.2}$$

with $0 \leq \epsilon \leq 1$ and $\kappa \geq 1$. In this two-component GMM model, $f_{\mathrm{G}}(x; 0; \sigma^2)$ represents the background noise and $f_{\mathrm{G}}(x; 0; \kappa\sigma^2)$, which has a larger variance that represents the impulsive component. As a mathematical model, the two-component GMM has been widely used in the analysis of many non-Gaussian channels [81, 82].

3.1.1.2 Middleton Class A Model

Three statistics-physical models of non-Gaussian noise were proposed by Middleton, which are called the Middleton Class A, B and C models [2]. The Middleton Class A model describes narrowband noise while the Class B model represents broadband noise and the Class C model is the sum of the Class A and Class B models. In this section, we introduce the most famous Middleton Class A model which has been shown accurately model electromagnetic interference (EMI) and background noise in powerline channels [2, 83]. As we mentioned above, the pdf of Middleton Class A model is a GMM with an infinite number of normal distributions. Hence the pdf is defined as

$$f_{\mathrm{GMM}}(x) = \sum_{m=1}^{\infty} P_m f_{\mathrm{G}}(x; 0; \sigma_m^2), \tag{3.3}$$

where

$$P_m = \frac{A^m e^{-A}}{m!}, \tag{3.4}$$

and

$$\sigma_m^2 = \sigma_I^2 \frac{m}{A} + \sigma_g^2 = \sigma_g^2 \left(\frac{m}{A\Gamma} + 1 \right). \tag{3.5}$$

σ_g^2 is the variance of the AWGN background noise and σ_I^2 is the variance of the impulsive noise component. Parameter Γ represents the ratio of Gaussian to impulsive noise power and A is the density of the impulses.

3.1.1.3 α-stable model

The stable law is a generalization of normal distribution and includes the normal distribution as a special case. Compared with other models, the α-stable distribution is very flexible and is an accurate model in many areas, including signal processing, underwater acoustic communications and powerline communications [6,9]. The characteristic function of α-stable distributions is

$$\varphi(t) = \exp\left\{ j\delta t - \mid \gamma t \mid^{\alpha} (1 - j\beta \mathrm{sign}(t)\omega(t,\alpha)) \right\}. \tag{3.6}$$

where

$$\omega(t,\alpha) = \begin{cases} \tan(\pi\alpha/2), & \alpha \neq 1, \\ -2/\pi \log|t|, & \alpha = 1. \end{cases}$$

There are four parameters to determine the pdf of an α-stable variable $x \sim S(\alpha, \beta, \delta, \gamma)$. 1) α is the characteristic exponent ($0 < \alpha \leq 2$) which controls the heaviness of the tail of the pdf [4] and indicates the impulsiveness of the channel. 2) β is the skewness of the pdf. 3) δ is location parameter which represents the mean or the median of the pdf. 4) γ is called the dispersion which measures the spread of the SαS pdf, which is similar to the variance of a Gaussian distribution.

3.1.2 Symmetric α-stable (SαS) noise

As an important class of heavy-tailed distributions, symmetric alpha-stable (SαS) distributions have successfully modeled multiple access interference in ad-hoc networks, near-field interference in wireless transceivers and underwater acoustic noise [5, 9, 84]. Compared with general α-stable distributions, the skewness parameter β of SαS pdf is 0. Then the characteristic function is given as

$$\varphi(t) = \exp\left(j\delta t - \gamma^{\alpha} \mid t \mid^{\alpha} \right). \tag{3.7}$$

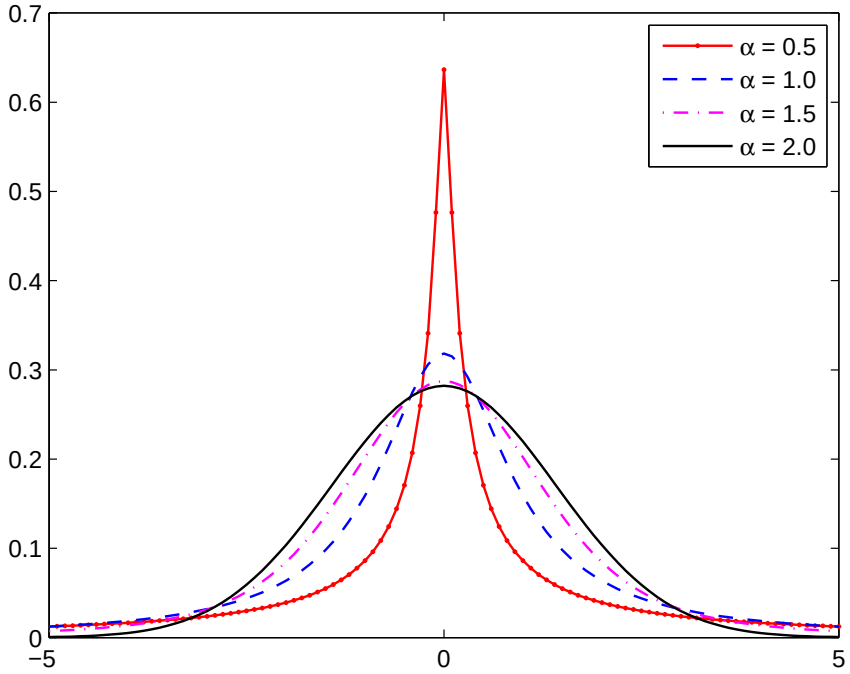

Figure 3.1: Standard SαS distributions($\gamma = 1, \delta = 0$)

The pdf of symmetric alpha stable distributions can be obtained by performing the inverse Fourier transform (IFT) of the characteristic function. Hence a SαS random variable, $x \sim S(\alpha, 0, 0, \gamma)$ has a pdf denoted as

$$f_\alpha(x; \delta, \gamma) = \frac{1}{2\pi} \int_{-\infty}^{\infty} \exp(j\delta t - \gamma^\alpha |t|^\alpha) e^{-jtx} dt. \tag{3.8}$$

A general SαS distribution has no closed-form expressions, except for two special cases: $\alpha = 2$ and $\alpha = 1$. When $\alpha = 1$, the distribution is Cauchy and the pdf is given as

$$f_1(x; \delta, \gamma) = \frac{1}{\pi} \frac{\gamma}{\gamma^2 + (x - \delta)^2}, \tag{3.9}$$

when $\alpha = 2$, the distribution is Gaussian and the standard pdf is

$$f_2(x; \delta, \gamma) = \frac{1}{2\sqrt{\pi}\gamma} \exp\left[-\frac{(x - \delta)^2}{4\gamma^2}\right], \tag{3.10}$$

when $\alpha = 2$, the variance is finite and the relationship between variance and dispersion is $\sigma^2 = 2\gamma^2$. For convenience, we also denote $f_\alpha(x; \delta, \gamma)$ as $f_\alpha(x - \delta; \gamma)$. Fig. 3.1 plots the pdf of SαS distributions with different αs. As shown in Fig. 3.1, when α decreases the tail of the pdf becomes thicker.

SαS distribution has some useful properties, which is described in [4, 26]. Here we list several important properties:

Property 1. A random variable X is stable if and only if

$$a_1X_1 + a_2X_2 \overset{d}{=} aX + b, \tag{3.11}$$

where a_1, a_2, a and b are constants and X_1 and X_2 have the same distribution as X. $X \overset{d}{=} Y$ denotes that X and Y follow the same distribution.

Property 2. The generalized central limit theorem states that the sum of a number of SαS distributed random variables will tend to a stable distribution.

Property 3. For a SαS random variable v with dispersion γ, we have

$$\lim_{x\to\infty} P(v > x) = \frac{\gamma^\alpha C_\alpha}{x^\alpha}, \tag{3.12}$$

where $C_\alpha = \frac{1}{\pi}\Gamma(\alpha)\sin\left(\frac{\pi\alpha}{2}\right)$.

Property 4. If $v_i \sim S(\alpha, 0, 0, \gamma_i)$, $i = 1, 2, \cdots, N$, then $\sum_{i=1}^N v_i \sim S(\alpha, 0, 0, \gamma)$, where $\gamma = \left(\sum_{i=1}^N \gamma_i^\alpha\right)^{\frac{1}{\alpha}}$.

Property 5. Let $v \sim S(\alpha, 0, 0, \gamma)$ and c is a constant. Then $cv \sim S(\alpha, 0, 0, |c|\gamma)$.

Property 6. Any SαS random variable $v \sim S(\alpha, 0, 0, \gamma)$ can be classified as α-sub-Gaussian, which can be expressed as

$$Z = \sqrt{A}G, \tag{3.13}$$

where A and G are independent. $A \sim S(\alpha/2, 1, 0, [\cos(\pi\alpha/4)]^{2/\alpha})$ is a skewed α-stable random variable and $G \sim \mathcal{N}(0, 2\gamma^2)$ is a Gaussian random variable.

3.1.3 Geometric Signal-to-Noise Ratio

Conventionally, the power is defined as the second-order moment of a process and it has been widely accepted as a measure of the signal strength. However, the second-order moment of a SαS process is infinite, which means the definition of traditional noise power is not feasible. In [4], fractional lower order moments (FLOM) are proposed to characterize the SαS process since only moments of order less than α exist. Let X be a SαS random variable, then

$$E\{|X|^p\} < \infty, \quad \text{if } 0 \leq p < \alpha, \tag{3.14}$$

where $E\{\cdot\}$ is the expectation operator. The FLOM can be calculated from the characteristic exponent α and dispersion γ^α and it is given as

$$E\{|X|^p\} = D(p,\alpha)\gamma^p, \quad \text{if } 0 < p < \alpha, \tag{3.15}$$

where

$$D(p,\alpha) = \frac{2^{p+1}\Gamma\left(\frac{p+1}{2}\right)\Gamma\left(-\frac{p}{\alpha}\right)}{\alpha\sqrt{\pi}\Gamma\left(-\frac{p}{2}\right)}, \tag{3.16}$$

and $\Gamma(\cdot)$ is the Gamma function. However, if $p \geq \alpha$, the FLOMs are not defined. Recently, zero-order statistics (ZOS) were proposed to characterize the SαS process [85]. The logarithmic-order moments $E\{\log|X|\}$ are employed to define the power, since $E\{\log|X|\} < \infty$. Then the geometric power of X is defined as

$$S_0(X) = e^{E\{\log|X|\}}. \tag{3.17}$$

After some derivation, a closed-form expression for geometric power is given as

$$S_0 = \frac{(C_g)^{1/\alpha}\gamma}{C_g}, \tag{3.18}$$

where $C_g \approx 1.78$ is the exponential of the Euler constant. Hence the geometric SNR, $\mathrm{SNR_G}$ is defined as

$$\mathrm{SNR_G} = \frac{1}{2C_g}\left(\frac{A}{S_0}\right)^2, \tag{3.19}$$

where A is the signal amplitude and $1/(2C_g)$ is a normalization constant to ensure $\mathrm{SNR_G}$ can still be applied when the noise is Gaussian ($\alpha = 2$). For a coded system, we can define $\frac{E_b}{N_0}$ for binary phase-shift keying (BPSK) modulation in terms of the

geometric SNR and code rate, R as

$$\frac{E_b}{N_0} = \frac{\mathrm{SNR_G}}{2R} = \frac{1}{4RC_g}\left(\frac{A}{S_0}\right)^2, \tag{3.20}$$

where R is the code rate and $A = 1$. For M-ary modulation, we have

$$\frac{E_b}{N_0} = \frac{1}{4\log_2(M)RC_g}\left(\frac{A}{S_0}\right)^2, \tag{3.21}$$

where $A^2 = E_s$. When $M = 2$ and $A = 1$, which is BPSK, (3.21) becomes (3.20). Hence (3.21) is a universal expression of $\frac{E_b}{N_0}$.

3.1.4 Generation of SαS random variables

The generation of SαS random variables is given in [16] and we give the procedure here. Let U be uniform in $(-\pi/2, \pi/2)$ and W is the standard exponential. To generate U and W we need two uniformly distributed samples u_1 and u_2. Then $U = \pi(u_1 - 0.5)$ and $W = -\ln(u_2)$.

When $\alpha = 1$, the SαS random variables are

$$Z = \gamma \tan(U). \tag{3.22}$$

When $\alpha \neq 1$,

$$Z = \gamma \frac{\sin(\alpha U)}{(\cos(U))^{\frac{1}{\alpha}}}\left[\frac{\cos[(1-\alpha)U]}{W}\right]^{\frac{1-\alpha}{\alpha}}, \tag{3.23}$$

where γ is obtained from (3.21).

There is an alternative method to generate SαS random variables by using property 6, so that any SαS random variable $w \sim S(\alpha, 0, \gamma, 0)$ can be expressed as

$$Z = \sqrt{A}G, \tag{3.24}$$

where $A \sim S(\alpha/2, 1, [\cos(\pi\alpha/4)]^{2/\alpha}, 0)$ and $G \sim \mathcal{N}(0, 2\gamma^2)$.

We notice that A is a skewed α-stable random variable which does not follows SαS pdf. To generate a standard α-stable random variable $A_s \sim S(\alpha, \beta, 0, 1)$, the following expression is derived [86]:

$$S(\alpha, \beta, 0, 1) = D_{\alpha,\beta}\frac{\sin\alpha(U - U_0)}{(\cos U)^{1/\alpha}}\left(\frac{\cos(U - \alpha(U - U_0))}{W}\right)^{\frac{1-\alpha}{\alpha}}, \alpha \neq 1, \tag{3.25}$$

and

$$S(1,\beta,0,1)=\frac{2}{\pi}\left[\left(\frac{\pi}{2}+\beta U\right)\tan U-\beta\ln\left(\frac{\frac{\pi}{2}W\cos U}{\frac{\pi}{2}+\beta U}\right)\right],\alpha=1, \tag{3.26}$$

where W is standard exponential and U is uniform distributed on $(-\pi/2,\pi/2)$. In addition, $D_{\alpha,\beta}=[\cos(\arctan(\beta\tan(\pi\alpha/2)))]^{1/\alpha}$, and $U_0=-\frac{\pi}{2}\beta(k(\alpha)/\alpha)$ with $k(\alpha)=1-|1-\alpha|$. Then the α-stable variable A with dispersion γ can be obtained from A_s as

$$A=\gamma A_s. \tag{3.27}$$

In this section, we introduce two methods to generate SαS random variables. By using these methods, the noise samples with different αs are shown in Fig. 3.2-3.7, which shows the behavior of noise from Gaussian ($\alpha=2$) to extremely impulsive ($\alpha=1$).

Figure 3.2: $\alpha = 2$

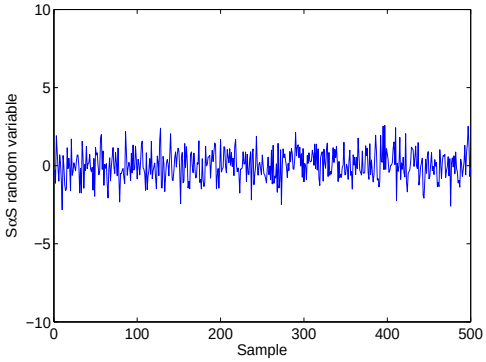

Figure 3.3: $\alpha = 1.99$

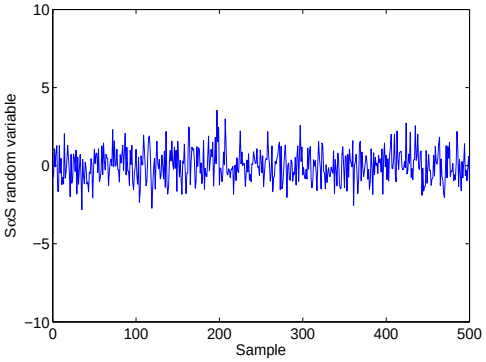

Figure 3.4: $\alpha = 1.8$

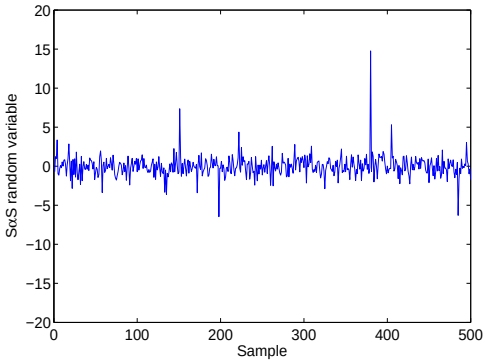

Figure 3.5: $\alpha = 1.5$

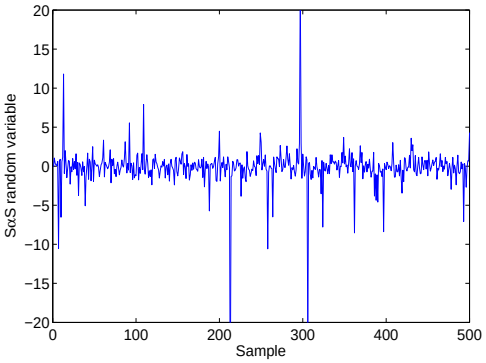

Figure 3.6: $\alpha = 1$

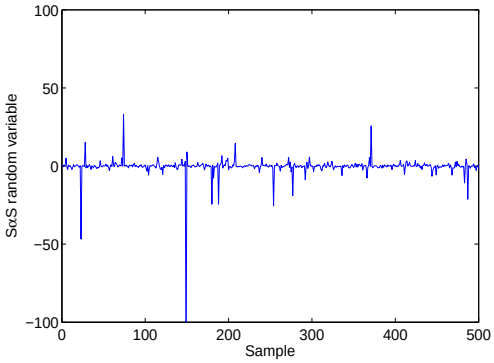

Figure 3.7: $\alpha = 0.5$

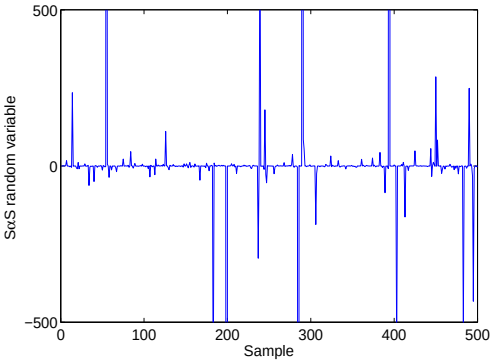

3.1.5 Parameter Estimation

After SαS noise has been received, the knowledge of the parameters of SαS is very important since most detectors require this to achieve a good performance. In this section, we introduce a method to accurately estimate the parameters α, γ and δ of SαS noise [87].

The algorithm is described as follows: assume we receive N independent samples with the same parameters from a SαS distribution. These N samples are denoted as $X_1, X_2, \cdots, X_N$. Then α, γ and δ will be estimated by these N samples.

(1) *Estimation of* δ

To estimate the mean or the median of the SαS pdf, the sample median is used. The estimated location parameter δ is given as

$$\hat{\delta} = \text{median}\left\{X_1, X_2, \cdots, X_N\right\}. \tag{3.28}$$

If N is odd, the median is the center order statistic. If N is even, the sample median is defined as the average of two center values. This estimator has shown to be very close to the maximum-likelihood (ML) estimator [87].

(2) *Estimation of* α

To estimate α, the knowledge of δ is required. Hence δ should be estimated first. The algorithm is given as follows: the N samples are divided into L non-overlapping segments. The length of each segment is $K = N/L$ and these L segments are expressed as

$$\left\{X_1 - \hat{\delta}, X_2 - \hat{\delta}, \cdots, X_N - \hat{\delta}\right\} = \left\{\boldsymbol{X}(1), \boldsymbol{X}(2), \cdots, \boldsymbol{X}(L)\right\}, \tag{3.29}$$

where $\boldsymbol{X}(l) = \left\{X_{(l-1)K+1} - \hat{\delta}, X_{(l-1)K+2} - \hat{\delta}, \cdots, X_{lK} - \hat{\delta}\right\}$ and $l = 1, 2, \cdots, L$. If $\overline{X_l}$ and $\underline{X_l}$ represent the maximum and minimum of $\boldsymbol{X}(l)$, we define

$$\widetilde{X_l} = \log \overline{X_l}, \tag{3.30}$$

$$\widehat{X_l} = -\log(-\underline{X_l}). \tag{3.31}$$

The standard deviations of defined $\widetilde{X_l}$ and $\widehat{X_l}$ are

$$\overline{s} = \sqrt{\frac{1}{L-1}\sum_{l=1}^{L}(\widetilde{X_l} - \mu)^2}, \tag{3.32}$$

and

$$\underline{s} = \sqrt{\frac{1}{L-1}\sum_{l=1}^{L}(\widehat{X_l} - \zeta)^2}, \tag{3.33}$$

where $\mu = \frac{1}{L}\sum_{l=1}^{L}\widetilde{X_l}$ and $\zeta = \frac{1}{L}\sum_{l=1}^{L}\widehat{X_l}$. The estimation of α can be expressed by $\overline{s}$ and $\underline{s}$ as

$$\hat{\alpha} = \frac{\pi}{2\sqrt{6}}\left(\frac{1}{\overline{s}} + \frac{1}{\underline{s}}\right). \tag{3.34}$$

(3) *Estimation of* γ

The estimation of γ is based on FLOM of the pdf. The estimated γ is given as

$$\hat{\gamma} = \left[\frac{\frac{1}{N}\sum_{k=1}^{N}|X_k - \hat{\delta}|^p}{C(p,\hat{\alpha})}\right]^{\hat{\alpha}/p}, \tag{3.35}$$

where

$$C(p,\hat{\alpha}) = \frac{1}{\cos\left(\frac{\pi}{2}p\right)}\frac{\Gamma\left(1-\frac{p}{\hat{\alpha}}\right)}{\Gamma\left(1-p\right)}. \tag{3.36}$$

The value of p $(0 < p < \frac{\hat{\alpha}}{2})$ is arbitrary and the simulations shown that this estimation is most accurate when $p \approx \frac{\hat{\alpha}}{3}$. As presented above, the estimation of the characteristic exponent α requires the knowledge of δ and the estimation of dispersion γ can only be performed after δ and α. We note these estimators provide better performance as N and L increase.

3.2 LDPC codes

Low-density parity-check (LDPC) codes were discovered by Gallager [32] and shown to have near Shannon limit performance in [34]. As a class of capacity-approaching error correction codes, low-density parity-check (LDPC) codes have been widely used in many applications such as DVB-S2/T2, WIMAX and G.hn/G.9960. In this section, we introduce the construction and decoding algorithms of LDPC codes.

Moreover, the asymptotic performance of LDPC codes on AWGN and more general BMSC (binary memoryless symmetric channel) is analyzed.

3.2.1 Construction of LDPC codes

Normally, there are two ways to construct a LDPC code: random construction and algebraic construction [88]. In this subsection, a well-known construction method called the Progressive Edge-Growth (PEG) algorithm, which can effectively construct short or medium length LDPC codes, is presented.

3.2.1.1 PEG Construction Algorithm

Most LDPC codes are randomly constructed by eliminating cycles of length 4. For LDPC codes with large code lengths, random construction gives very good performance since they avoid short cycles in the Tanner graph. However, when constructing short length LDPC codes, the probability of obtaining short cycles is very high and the minimum distance becomes a critical issue for an irregular LDPC ensemble.

The Progressive Edge-Growth (PEG) algorithm was proposed in [1] and it can construct the Tanner graph with a large girth by progressively establishing edges between check nodes and symbol nodes. The inputs of this algorithm are the number of check nodes m, the number of symbol nodes n and symbol nodes degree sequence of the graph D_s. Then an edge selection procedure is performed to make the placement of a new edge have the least impact on the girth. The PEG algorithm has two advantages: 1. it is simple to construct LDPC codes and a good girth property can be guaranteed by the lower bound. 2. it can be used to generate good codes for any given code length and code rate which is very flexible. Moreover, with some modifications, linear time encoding is also feasible for PEG algorithm. In the following, we will define the notation and introduce the PEG algorithm.

As we defined above, a parity check matrix H can be characterized by a bipartite graph with n symbol and m check nodes nodes. Such a graph is called a Tanner graph and we define a Tanner graph as (V, E). V is the set of nodes where $V = V_c \cup V_s$. V_c is the set of check nodes and V_s is set of symbol nodes with $V_c = \{c_0, c_1, \cdots, c_{m-1}\}$ and $V_s = \{s_0, s_1, \cdots, s_{n-1}\}$. E is the set of edges and edge $(c_j, s_j) \in E$ if $h_{i,j} \neq 0$.

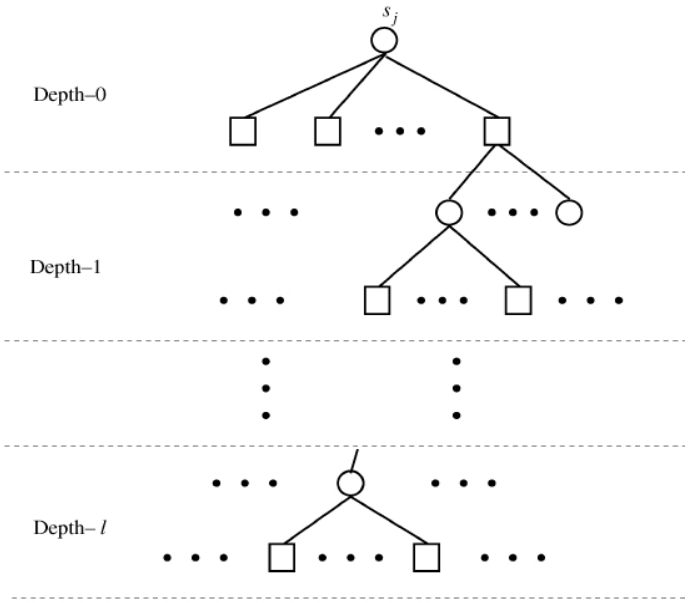

Figure 3.8: Sub-graph spreading from s_j [1]

Hence the symbol nodes degree sequence D_s is given as

$$D_s = \left\{ d_{s_0}, d_{s_1}, \cdots, d_{s_{n-1}} \right\}, \tag{3.37}$$

where d_{s_j} is the degree of the symbol node s_j with $0 \leq j \leq n-1$ and $d_{s_0} \leq d_{s_1} \leq \cdots \leq d_{s_{n-1}}$. Similarly, the check nodes degree sequence is denoted as

$$D_c = \left\{ d_{c_0}, d_{c_1}, \cdots, d_{c_{n-1}} \right\}, \tag{3.38}$$

where d_{c_j} is the degree of the check node c_j, $0 \leq j \leq m-1$, in non-decreasing order. Also, E can be divided into subsets as $E = E_{s_0} \cup E_{s_1} \cup \cdots \cup E_{s_{n-1}}$, where E_{s_j} contains all edges connected to s_j. The k-th edge incident on s_j is denoted by $E_{s_j}^k$ with $0 \leq k \leq d_{s_j} - 1$.

For a given s_j, its neighborhood with depth l, $N_{s_j}^l$ can be defined as the set containing all check nodes reached by s_j within depth l. Its complementary set is defined as $N_{s_j}^{-l}$. This spreading graph is shown in Fig. 3.8. The sub-graph starts from s_j and traverses all edges incident on s_j, which are $(s_j, c_{i_1}), (s_j, c_{i_2}), \cdots, (s_j, c_{i_{d_{s_j}}})$. Then all other edges which are incident on $c_{i_1}, c_{i_2}, \cdots, c_{i_{d_{s_j}}}$ are traversed and this procedure will continue until the desired depth is reached. In the following, we introduce the PEG algorithm in detail.

Two situations need to be noticed when spreading the sub-graph of s_j: (1) $N_{s_j}^l$ is

smaller than m, but it stops increasing. It means some check nodes are not reachable from s_j. In this case, the PEG algorithm chooses the unreachable one, hence it does not create additional cycles. (2) $N_{s_j}^{-l} \neq \varnothing$ and $N_{s_j}^{-(l+1)} = \varnothing$. In this situation, all check nodes are reached from s_j, hence the PEG algorithm chooses the check node with the largest distance from s_j at depth $l+1$. The PEG algorithm is summarized as follows:

Progressive Edge-Growth Algorithm
from $j = 0$ **to** $n - 1$
begin
from $k = 0$ **to** $d_{s_j} - 1$
begin
if $k = 0$

Edge (c_i, s_j), which is represented by $E_{s_j}^0$, is established. $E_{s_j}^0$ is the first edge incident to s_j and c_i is the check node with the lowest degree under the current graph.

else

Expand the subgraph from s_j to depth l and there are two stop conditions: (1) $N_{s_j}^l$ is smaller than m, but it stops increasing. (2) $N_{s_j}^{-l} \neq \varnothing$ and $N_{s_j}^{-(l+1)} = \varnothing$. Then edge $E_{s_j}^k$ is established, where the check node is chosen from $N_{s_j}^l$ with the lowest check node degree.

end
end

When s_j has multiple choices to connect, the one with smallest number of incident edges is chosen. If there are multiple check nodes in $N_{s_j}^{-l}$ that have same lowest degree, then we can randomly choose one of these or always select the first one.

3.2.2 Message Passing Decoding of LDPC codes

A class of algorithms to decode LDPC codes is called the message passing algorithms since the decoding process is based on the passing of message along the edges of the Tanner graph. If the messages passing through the graph are binary, these algorithms are called hard decision decoding algorithms such as the bit flipping algorithm. If the messages are probabilities or log-likelihood ratios (LLRs), these

algorithms are soft decision decoding algorithms such as the sum-product algorithm (SPA). Soft decision decoding performs much better than hard decision decoding and it has been shown that a near Shannon-limit performance can be achieved by the SPA [34].

In this subsection, LLR based SPA is described. Compared with the probability based SPA decoder, log-SPA calculates LLRs instead of probabilities. The initial LLR of the i-th coded bit is given as

$$L_i = \ln \frac{P(c_i = 0|y_i)}{P(c_i = 1|y_i)} = \ln \frac{P(y_i|c_i = 0)}{P(y_i|c_i = 1)}, \tag{3.39}$$

where y_i is the i-th received signal and c_i is the i-th coded bit. If we rearrange (3.39) and use the relationship that $P(y_i|c_i = 0) + P(y_i|c_i = 1) = 1$, we can obtain

$$P(y_i|c_i = 0) = \frac{e^{L_i}}{1 + e^{Li}}. \tag{3.40}$$

If there are l variables where $c_1, c_2, ..., c_l$ are binary random variables and $y_1, y_2, ..., y_l$ are independent random variables, then

$$2P(y_1, y_2, ...y_l|c_1 + c_2 + ... + c_l = 0) - 1 = \prod_{i=1}^{l}(2P(y_i|c_i = 0) - 1). \tag{3.41}$$

Substituting (3.40) to (3.41), we have

$$2P(y_1, y_2, ...y_l|c_1 + c_2 + ... + c_l = 0) - 1 = \prod_{i=1}^{l} \frac{e^{L_i} - 1}{e^{L_i} + 1} = \prod_{i=1}^{l} \tanh \frac{L_i}{2}. \tag{3.42}$$

Hence for multiple variables, the LLR is given as:

$$L(y_1, y_2, ...y_l|c_1 + c_2 + ... + c_l = 0) = \ln \frac{1 + \prod_{i=1}^{l} \tanh \frac{L}{2}}{1 - \prod_{i=1}^{l} \tanh \frac{L_i}{2}}. \tag{3.43}$$

With knowledge of the above derivations, the log-SPA algorithm is given as follows:

- **Initialization**

Initialize the LLR L_j of the j-th coded bit according to (3.39), where ($j = 1, 2, ..., n$). Use L_j to initialize matrix $\boldsymbol{Q}$, where $q_{ij} = L_j$, when $h_{ij} = 1$.

- **Check Node Update**

Update $\boldsymbol{R}$ by calculating r_{ij} for each check node i ($i = 1, 2, ..., m$). Note that the check node i itself should be excluded since what we calculate is the extrinsic information. The updating equation is given as

$$r_{ij} = \ln \frac{1 + \prod_{k \in N(i) \backslash j}^{l} \tanh\left(\frac{q_{ik}}{2}\right)}{1 - \prod_{k \in N(i) \backslash j}^{l} \tanh\left(\frac{q_{ik}}{2}\right)}. \tag{3.44}$$

- **Variable Node Update**

For each variable (symbol) node j ($j = 1, 2, ..., n$), calculate q_{ij} as

$$q_{ij} = L_j + \sum_{i' \in M(j) \backslash i} r_{i'j}. \tag{3.45}$$

- **Hard Decision**

The decision metric is calculated as

$$\hat{q}_j = L_j + \sum_{i \in M(j)} r_{ij}. \tag{3.46}$$

This final decision contains both intrinsic and extrinsic information. If $q_j^{'} > 0$, the estimated coded bit $\hat{c}_j = 0$. Otherwise, $\hat{c}_j = 1$. If $\hat{\mathbf{c}} = [\hat{c}_1, \hat{c}_2, \cdots, \hat{c}_n]$ satisfy $\hat{\mathbf{c}} \cdot \mathbf{H^T} = \mathbf{0}$, stop the iterations. Otherwise go back to check node update to continue the loop until it either satisfies the parity check equations or reaches the maximum number of iterations.

3.2.3 Asymptotic Performance of LDPC codes

3.2.3.1 Density Evolution

The asymptotic behavior of the log-SPA decoder had been analyzed numerically in [41] by the density evolution (DE) algorithm. It demonstrated that for binary-input symmetric memoryless channels (BSMC), the threshold of an ensemble of LDPC codes can be calculated which determines the upper bound of the channel parameter to guarantee error-free transmission, as the length of the codeword goes to infinity and assuming the Tanner graph is cycle-free. Moreover, the threshold provides us with a tool to find good irregular ensembles. In [42], a code design based on DE and differential evolution was proposed. The designed optimized ensembles

were shown to achieve near-capacity performance. In the following, we will introduce DE in detail.

First we provide some definitions of the ensemble of LDPC codes. The regular LDPC ensemble can be defined by a degree pair (d_v, d_c), where d_v is the maximum variable node degree and d_c is the maximum check node degree. In this thesis, symbol nodes and variable nodes are used interchangeably. An irregular LDPC ensemble can be characterized by edge degree distributions $\lambda(x)$ and $\rho(x)$, which are defined as

$$\lambda(x) = \sum_{j=2}^{d_v} \lambda_j x^{j-1}, \tag{3.47}$$

and

$$\rho(x) = \sum_{i=2}^{d_c} \rho_i x^{i-1}, \tag{3.48}$$

where λ_j and ρ_i are the fraction of edges that are connected to variable and check nodes with degree j and i, respectively. In this section, we introduce DE for regular LDPC codes, and then we will extend it to irregular LDPC codes. To perform the DE, the symmetric conditions of channels are required and we assume that the all-zero codeword $\mathbf{c} = [0, 0, \cdots, 0]$ is transmitted. According to the BPSK mapping, the modulated signal is $\mathbf{x} = [+1, +1, \cdots, +1]$. Under this assumption, an error will occur if the output message of the variable node is negative. Conventionally, we use LLRs to represent the message and $v = \ln \frac{P(y|x=+1)}{P(y|x=-1)}$ is the outgoing message for variable nodes where x is the BPSK symbol. Hence, there is no decision error if

$$\lim_{l\to\infty} \int_{-\infty}^{0} p_v^{(l)}(\tau) d\tau = 0, \tag{3.49}$$

where $p_v^{(l)}$ is the pdf of v in the l-th iteration. The decoding threshold κ^* is defined as the maximum noise level which allows error-free transmission for LDPC codes with an infinite length. Hence, κ^* is expressed as

$$\kappa^* = \sup \left\{ \kappa : \lim_{l\to\infty} \int_{-\infty}^{0} p_v^{(l)}(\tau) d\tau = 0 \right\}. \tag{3.50}$$

For the BSC, κ is the crossover probability ε and for the AWGN channel, κ is the standard deviation σ. For the SαS channel which is the focus of this thesis, κ becomes the dispersion γ. The corresponding SNR of κ^* is called threshold SNR.

Now we describe the process of the DE algorithm for computing $p_v^{(l)}$. First, the

initial pdf $p_v^{(0)}$ of the message from the channel is calculated. Then we perform an iterative two-stage algorithm which contains the pdf evolution of the check node update and variable node update. The check node update in (3.44) can be rewritten as

$$u_j^{(l)} = 2\tanh^{-1}\left(\prod_{i=1}^{d_c-1}\tanh\left(\frac{v_i^{(l-1)}}{2}\right)\right), \tag{3.51}$$

where $u_j^{(l)}$ is the message of j-th check node in the l-th iteration. To calculate the densities of this step, we define a G-density $g(z)$ which represents the pdf of $g(z)$ [89], where

$$g(z) = \left(\text{sign}\left(z\right), -\ln\tanh\left|z/2\right|\right). \tag{3.52}$$

Hence, (3.51) can also be written in terms of $g(\cdot)$ and $g^{-1}(\cdot)$ as

$$u_j^{(l)} = g^{-1}\left(\sum_{i=1}^{d_c-1} g(v_i^{(l-1)})\right). \tag{3.53}$$

With this notation, the DE of the check node update is given as

$$p_u^{(l)} = \Gamma^{-1}\left[\left(\Gamma\left[p_v^{(l-1)}\right]\right)^{\otimes(d_c-1)}\right], \tag{3.54}$$

where $p_v^{(l)}$ is the pdf of each $v_i^{(l)}$ in the l-th iteration. Similarly, $p_u^{(l)}$ is the pdf of each $u_j^{(l)}$. $\Gamma(\cdot)$ and $\Gamma^{-1}(\cdot)$ represent the change of density due to $g(\cdot)$ and $g^{-1}(\cdot)$. $\otimes$ is the convolution operation.

For variable node update, the DE for the sum of messages is the convolution of their densities, such that

$$p_v^{(l)} = p_v^{(0)} \otimes \left(p_u^{(l)}\right)^{\otimes(d_v-1)}. \tag{3.55}$$

Then (3.54) and (3.55) are performed iteratively as $l \to \infty$. We note that convolution operations can be efficiently performed by using the fast Fourier transform (FFT).

For irregular LDPC codes, only small modifications are required on (3.54) and (3.55), which we should average over all variable and check node degrees. The DE of the check node update and variable node update is given as

$$p_u^{(l)} = \Gamma^{-1}\left[\sum_{i=2}^{d_c}\rho_i\left(\Gamma\left[p_v^{(l-1)}\right]\right)^{\otimes(i-1)}\right], \tag{3.56}$$

and

$$p_v^{(l)} = p_v^{(0)} \otimes \sum_{i=2}^{d_v} \lambda_i \left(p_u^{(l)}\right)^{\otimes(i-1)}. \tag{3.57}$$

Finally, the probability of errors occurring at l-th iteration is given as

$$P_e^{(l)} = \int_{-\infty}^{0} p_v^{(l)}(\tau) d\tau. \tag{3.58}$$

3.2.3.2 Gaussian Approximation

DE tracks the change of pdf during the decoding process. Although it is valid for general BMSC channels, the computational cost is high. In many applications, the noise added at the receiver is assumed to be Gaussian. Hence, a simple method to estimate the threshold of LDPC codes on binary-input AWGN channels was proposed, which is called Gaussian approximation (GA) [44]. It approximates the densities as Gaussian or Gaussian mixtures. In this way, instead of tracking densities, it can track the mean of the Gaussian pdf which greatly reduces the complexity. In this section, we will show how to use GA to find the asymptotic performance of LDPC codes on AWGN channels.

If we assume the channel is Gaussian, the initial message can be calculated as

$$v = \ln \frac{P(y|x=+1)}{P(y|x=-1)} = \frac{2y}{\sigma^2}, \tag{3.59}$$

where σ^2 is the variance of the noise. It is easy to determine that v is still Gaussian with mean $2/\sigma^2$ and variance $4/\sigma^2$. We note that the symmetry condition is preserved under DE and it can be expressed as $f(\tau) = f(-\tau)e^{\tau}$ [42], where $f(\tau)$ is the pdf of LLR. Hence for AWGN channels, we observe that $\sigma^2 = 2m$, where m is the mean. It implies that we only need to monitor the mean of the messages when performing GA with the symmetry condition, which greatly reduces the complexity. First we investigate GA for regular LDPC ensembles.

For the check node update, (3.51) can be rewritten as

$$\tanh\left(\frac{u_j^{(l)}}{2}\right) = \prod_{i=1}^{d_c-1} \tanh\left(\frac{v_i^{(l-1)}}{2}\right). \tag{3.60}$$

We take the expectations of this equation as

$$E\left[\tanh\left(\frac{u^{(l)}}{2}\right)\right] = E\left[\tanh\left(\frac{v^{(l-1)}}{2}\right)\right]^{d_c-1}, \tag{3.61}$$

where index i and j are omitted since v_j's and u_j's are i.i.d. (independent and identically distributed). The $v^{(l-1)}$ and $u^{(l)}$ are Gaussian with $\mathcal{N}(m_{u^{(l)}}, 2m_{u^{(l)}})$ and $\mathcal{N}(m_{v^{(l-1)}}, 2m_{v^{(l-1)}})$. Hence, we have

$$E\left[\tanh\left(\frac{u}{2}\right)\right] = \frac{1}{\sqrt{4\pi m_u}}\int_{-\infty}^{\infty}\tanh\frac{u}{2}\exp\left(-\frac{(u-m_u)^2}{4m_u}\right)du. \tag{3.62}$$

According to this equation, a function $\phi(x)$ for $x \geq 0$ can be defined as

$$\phi(x) = 1 - \frac{1}{\sqrt{4\pi x}}\int_{-\infty}^{\infty}\tanh\frac{u}{2}\exp\left(-\frac{(u-x)^2}{4x}\right)du, \quad \text{if} \quad x > 0. \tag{3.63}$$

When $x = 0$, $\phi(x) = 1$. The means of the variable node update can be expressed as

$$m_v^{(l)} = m_{v_0} + (d_v - 1)m_u^{(l)}, \tag{3.64}$$

where m_{v_0} is the mean of v_0. $m_v^{(l)}$ and $m_u^{(l)}$ represents the mean of u and v in the l-th iteration. According to (3.62), the GA updating rule is given as

$$m_u^{(l)} = \phi^{-1}\left(1 - \left[1 - \phi\left(m_{v_0} + (d_v - 1)m_u^{(l-1)}\right)\right]^{d_c-1}\right), \tag{3.65}$$

where $m_u^{(0)} = 0$ to initialize the algorithm. Also, to reduce the complexity for computing $\phi(x)$, an accurate approximation was proposed in [44] and it is given as

$$\phi(x) = \begin{cases} \exp(-0.4527x^{0.86} + 0.0218), & 0 < x < 10, \\ \sqrt{\frac{\pi}{x}}e^{-\frac{x}{4}}\left(1 - \frac{10}{7x}\right), & x > 10. \end{cases}$$

For irregular LDPC codes, the mean of the message from the variable node of degree j is expressed as

$$m_{v,j}^{(l)} = m_{v_0} + (j-1)m_u^{(l)}. \tag{3.66}$$

Hence, the message $v^{(l)}$ has a Gaussian mixture pdf $f_v^{(l)}$ as

$$f_v^{(l)} = \sum_{j=2}^{d_v}\lambda_i\mathcal{N}(m_{v,j}^{(l)}, 2m_{v,j}^{(l)}). \tag{3.67}$$

By using (3.67), the mean $m_{u,i}^{(l)}$ of the check node with degree i is given as

$$m_{u,i}^{(l)} = \phi^{-1}\left(1 - \left[1 - \sum_{j=2}^{d_v} \lambda_j \phi\left(m_{v,j}^{(l-1)}\right)\right]^{i-1}\right). \tag{3.68}$$

By combining the mean of check nodes with different degrees, $m_u^{(l)}$ is calculated as

$$m_u^{(l)} = \sum_{i=2}^{d_c} \rho_i \phi^{-1}\left(1 - \left[1 - \sum_{j=2}^{d_v} \lambda_j \phi\left(m_{v_0} + (j-1)m_u^{(l-1)}\right)\right]^{i-1}\right). \tag{3.69}$$

The error probability of the l-th iteration is

$$P_e^l = \sum_{i=2}^{d_v} \lambda_i' Q\left(\sqrt{\frac{m_{v_0} + i m_u^l}{2}}\right), \tag{3.70}$$

where

$$\lambda_i' = \frac{\lambda_i / i}{\sum_{j=2}^{d_v} \lambda_j / j}. \tag{3.71}$$

3.2.3.3 EXIT charts

Compared with DE and GA, an alternative method called an extrinsic information transfer (EXIT) chart was proposed to visualize the exchange of the extrinsic information between component decoders [45]. The EXIT chart is a tool to find the decoding threshold as well as design good codes by reducing it to a curve fitting problem. In this section, we will briefly introduce the EXIT charts for regular and irregular LDPC codes on the AWGN channel.

To derive the EXIT chart of LDPC codes, the check node update and variable node update are considered as two component decoders, respectively [47]. Then the EXIT chart can plot the input and output mutual information of the variable-node decoder (VND) and the check-node decoder (CND). The input of the VND and CND is called *a priori* information, denoted by "A". The output is extrinsic information which is denoted as "E". Hence the mutual information between inputs (*a priori*) or outputs (extrinsic) of the VND and the coded bit are denoted as $I_{A,V}$ or $I_{E,V}$, respectively. Similarly, $I_{A,C}$ or $I_{E,C}$ are defined for the CND.

We first derive the $I_{E,V}$ versus $I_{A,V}$ transfer function for the VND. The output

of VND can be expressed as

$$L_{i,\text{out}} = L_{\text{ch}} + \sum_{j \neq i} L_{j,\text{in}}, \tag{3.72}$$

where extrinsic LLR $L_{i,\text{out}}$ is Gaussian with $\sigma^2 = \sigma_{ch}^2 + (d_v - 1)\sigma_A^2$, σ_{ch}^2 is the variance of input from the channel and σ_A^2 is the variance of the *a priori* inputs. Now we can use the definition of mutual information to calculate $I_{E,V}$ as

$$I_{E,V} = J(\sigma) = J\left(\sqrt{(d_v - 1)\sigma_A^2 + \sigma_{ch}^2}\right), \tag{3.73}$$

where

$$J(\sigma) = 1 - \int_{-\infty}^{\infty} \frac{e^{-(\xi - \sigma^2/2)/2\sigma^2}}{\sqrt{2\pi\sigma^2}} \log_2\left(1 + e^{-\xi}\right) d\xi. \tag{3.74}$$

We can express $I_{E,V}$ by $I_{A,V}$ by using the relationship that $I_{A,V} = J(\sigma_A)$. Hence,

$$I_{E,V} = J(\sigma) = J\left(\sqrt{(d_v - 1)\left[J^{-1}(I_{A,V})\right]^2 + \sigma_{ch}^2}\right), \tag{3.75}$$

where $J^{-1}(\cdot)$ is the inverse function of $J(\cdot)$. The accurate approximations of $J(\cdot)$ and $J^{-1}(\cdot)$ are also given in [47]. Similarly, the EXIT function for CND is given as

$$I_{E,C} = 1 - J\left(\sqrt{d_c - 1} \cdot J^{-1}(1 - I_{A,C})\right). \tag{3.76}$$

We note the EXIT curve of the VND is dependent on the channel condition while the EXIT curve for the CND remains unchanged. As an example, the EXIT curves of the VND and CND for regular $(4, 6)$ LDPC codes at $E_b/N_0 = 3$ dB and 0.5 dB are plotted in Fig. 3.9. As indicated in this figure, as E_b/N_0 decreases, the tunnel between VND and CND curves becomes smaller, which means the decoder needs more iterations to converge. If E_b/N_0 is below the threshold, the tunnel will be closed, which means the decoder cannot guarantee an error-free transmission. The red-dashed lines represent the number of iterations required for the decoder to converge. For irregular LDPC codes, similar to DE and GA, the mutual information can be expressed as the sum of the fractions of mutual information for different degrees, where

$$I_{E,V} = \sum_{j=2}^{d_v} \lambda_j I_{E,V}(j, I_{A,V}). \tag{3.77}$$

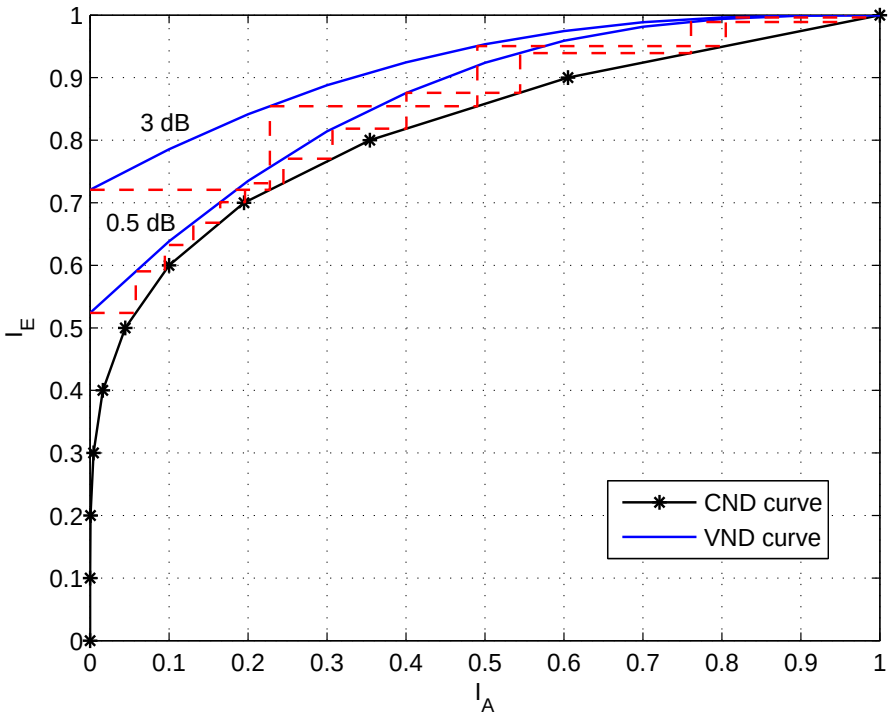

Figure 3.9: EXIT curves of (4,6) LDPC codes at $E_b/N_0 = 3$ dB and 0.5 dB

$I_{E,V}(j, I_{A,V})$ is obtained by replacing d_v in (3.75) with j. Similarly, $I_{E,V}$ is given as

$$I_{E,C} = \sum_{i=2}^{d_c} \lambda_i I_{E,C}(i, I_{A,C}). \tag{3.78}$$

Hence the optimization of LDPC codes can be regarded as a curve-fitting problem, which can be solved efficiently by linear programming. For a given SNR (close to the capacity), if we can find a VND curve which is just above the CND curve, then the selected degree distributions are nearly optimized values.

3.3 Conclusion

In this chapter, different impulsive noise models have been presented. In particular, the SαS noise model has been explained in detail, which includes the definition of the pdf, a new definition of SNR, the generation of SαS samples and the parameter estimation. This chapter has also given the details of the construction and the decoding of LDPC codes. To analyze the asymptotic performance of LDPC codes, density evolution, Gaussian approximation and EXIT charts have been described in detail. To conclude, this chapter provides the essential background theory for the

following novel chapters.

Chapter 4

Receiver Design and Finite Length Analysis of LDPC codes on Impulsive Noise Channels

In this chapter, different detectors for SαS noise are compared and a near-optimal detector is proposed that can achieve almost optimal performance as well as reduce the complexity. In addition, a density evolution analysis is employed to examine the asymptotic performance of LDPC codes with different receivers. However, there is still a gap between asymptotic and practical performance of finite length LDPC codes. Finite length analyses of LDPC codes have already been presented in the literature for the AWGN channel, but in this chapter we consider the analysis of short LDPC codes for channels that exhibit impulsive noise. We propose a method to estimate the waterfall performance of LDPC codes on SαS channels, which requires knowledge of the uncoded BEP and the decoding threshold SNR of LDPC codes on such channels. Hence, the uncoded BEP is also derived in this chapter.

4.1 Channel Model

We consider an LDPC-coded system with a codeword of length N bits. The codeword is mapped to a binary phase shift keying (BPSK) constellation to generate the transmitted signal. The received signal is contaminated by additive impulsive noise with a SαS distribution and is defined as

$$y_j = x_j + \eta_j, \tag{4.1}$$

where y_j is the j-th received signal, $x_j \in \{-1, +1\}$ is the BPSK symbol, η_j is an SαS distributed noise sample and $j = 1, 2, \ldots, n$.

4.2 Receivers Design and Asymptotic Performance Analysis

4.2.1 Optimal and Suboptimal Receivers

The LLR of the channel output is assumed to have the knowledge of the channel and it is given as

$$L_j = \ln\left(\frac{P(y_j|x_j = 1)}{P(y_j|x_j = -1)}\right) = \ln\left(\frac{f_\alpha(y_j - 1; \gamma)}{f_\alpha(y_j + 1; \gamma)}\right), \tag{4.2}$$

where $f_\alpha(x; \gamma)$ is the pdf of the SαS noise. However, if we use this optimum LLR as the input of the decoder, the complexity is high due to the integration in the calculation of pdf. Hence, a suboptimal receiver is necessary to reduce the complexity and still maintain a good performance.

In this section, we discuss some well known and recent suboptimal receivers presented in the literature. As we know, the pdf of SαS distributions has a closed-form expression when $\alpha = 2$ and $\alpha = 1$. When $\alpha = 2$, the conventional Gaussian receiver is given as

$$L_j = \ln\left(\frac{f_2(y_j - 1; \gamma)}{f_2(y_j + 1; \gamma)}\right) = \frac{y_j}{\gamma^2}, \tag{4.3}$$

where $\sigma^2 = 2\gamma^2$. This linear demapper is optimum when the channel is AWGN. However, it is not suitable for non-Gaussian noise since it does not consider the impulsive nature. A well-known receiver is based on the Cauchy distribution ($\alpha = 1$)

to detect SαS signals, since it exhibits algebraic tails which shares the same property as other SαS pdfs ($\alpha < 2$). The LLR of the Cauchy receiver is given as

$$L_j = \ln\left(\frac{\gamma^2 + (y_j + 1)^2}{\gamma^2 + (y_j - 1)^2}\right). \tag{4.4}$$

Another way to cope with impulses is to use non-linear operations to limit the received values, such as a soft limiter and hole-puncher [17]. Recently, a variant of the soft limiter, called the clipper, was proposed in [71]. The equation of this LLR demapper is

$$L_j = \begin{cases} py_j, & \text{if } -h/p < y_j < h/p, \\ h\text{sign}(y_j), & \text{otherwise.} \end{cases} \tag{4.5}$$

where p is the signal amplitude and h is the clipping level of the impulse. The optimized p and h can be found through density evolution.

The third type of detector approximates the optimal LLR values of the received symbols. Recently, a LLR-approximation based demapper was proposed and shown to achieve near-optimal performance [72]. This LLR demapper is divided into two parts: a linear part and an asymptotic part. The linear part of the demapper is proportional to the received signal and is related to γ. The asymptotic part is obtained by using the asymptotic property (Property 3) of the $S\alpha S$ process. The LLR demapper for $y_j > 0$ is expressed as

$$L_j = \min\left(\frac{\sqrt{2}y_j}{\gamma}, \frac{2(\alpha + 1)}{y_j}\right). \tag{4.6}$$

For $y_j < 0$, the LLR demapper is calculated by replacing the min in (4.6) by a max operation. However, this receiver requires knowledge of α and γ.

We propose a new demapper which can achieve a near-optimal performance without knowledge of the dispersion γ. For our receiver, the LLR demapper is still decomposed into linear and asymptotic parts. However, the linear part of (4.6) is replaced with py_j where p is the optimized gradient which can be obtained from density evolution and only related to α. Hence this receiver only requires knowledge of α and the estimation of parameters of SαS noise can be obtained by referring to

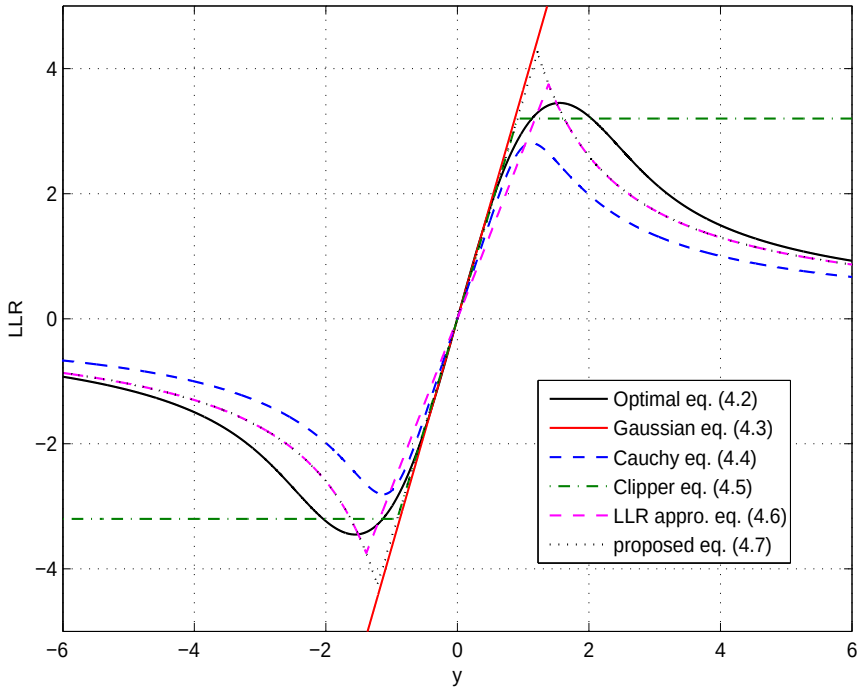

Figure 4.1: LLR demapper ($\alpha = 1.6$, $E_b/N_0 = 2$ dB)

Chapter 3. The new LLR demapper is

$$L_j = \begin{cases} \min(py_j, \frac{2(\alpha+1)}{y_j}), & y_j \geq 0, \\ \max(py_j, \frac{2(\alpha+1)}{y_j}), & y_j < 0. \end{cases} \tag{4.7}$$

Fig. 4.1 gives curves of different LLR demappers which are discussed in this section when $\alpha = 1.6$ and $E_b/N_0 = 2$ dB. It is clear that Gaussian receiver is linear and becomes incorrect when $|y|$ is large. Compared with the Cauchy receiver and the clipper, our demapper matches the optimal demapper closely, which implies that it should approach the performance of the optimal demapper. Compared with LLR approximation demapper, our demapper gives a better approximation of the linear part of the true LLR. In the next section, the asymptotic performance of the these receivers will be evaluated through density evolution.

4.2.2 Asymptotic Performance of LDPC codes on SαS channels

4.2.2.1 The Capacity of SαS channels

Channel capacity is a fundamental upper bound on the rate at which information can be reliably transmitted. For the AWGN channel, the channel capacity has been well studied in the literature [89]. For binary memoryless symmetric channels (BMSC), the capacity can be evaluated as a function of the pdf of log-likelihood ratios (LLRs) [89]. As a type of BMSC, the capacity of SαS channels can be expressed as

$$C_\alpha = 1 - E\left\{\log_2\left(1 + e^{-L}\right)\right\}, \tag{4.8}$$

where $L = \ln \frac{P(x=+1|y)}{P(x=-1|y)}$ is the channel LLR. The expectation operator in (4.8) can be replaced by a time average. Hence the capacity of SαS channels can be obtained as

$$C_\alpha = 1 - \lim_{N\to\infty} \left\{ \frac{1}{N} \sum_{n=1}^{N} \log_2\left(1 + e^{-x_n L_n}\right) \right\}, \tag{4.9}$$

where x_n is the modulated signal. This capacity limit can be measured by a large number, N, of LLR values and it will be used as a benchmark for the coded performance in the result section.

4.2.2.2 Density Evolution of LDPC codes on SαS Channels

The asymptotic performance of an LDPC ensemble can be accurately predicted by several tools, namely, DE, GA and EXIT chart. These tools assume the LDPC codes are cycle-free with an infinite codeword length. As introduced in Chapter 3, the EXIT chart and GA assume that the channel is Gaussian which is not of interest in this chapter. However, DE can be applied to any binary memoryless symmetric channels (BMSC). The impulsive noise we study has a non-Gaussian SαS distribution, hence, DE can be employed to analyze the iterative behavior of the Sum-Product decoder.

DE starts with the calculation of the pdf of the initial LLR. The optimal LLR of the i-th variable node for the i-th iteration is expressed as

$$v_i^{(0)} = \ln \frac{P(x_i = +1|y_i)}{P(x_i = -1|y_i)} = \ln \frac{f_\alpha(y_i - 1; \gamma)}{f_\alpha(y_i + 1; \gamma)}. \tag{4.10}$$

For suboptimal receivers, the expression of the LLR demapper has been given above. With the exception of the Gaussian linear receiver ($\alpha = 2$), there is no analytic expression for the densities of LLRs for other receivers. Hence, we employ a Monte-Carlo simulation and histogram method to find the pdf of these LLRs. The DE tracks the pdf of the LLRs between check nodes and variable nodes during the iterative decoding and it allows us to calculate the threshold SNR of a LDPC ensemble which indicates where the waterfall region begins. For SαS noise, the threshold can be defined by the dispersion γ_{th}:

$$\gamma_{\text{th}} = \sup\left\{\gamma : \lim_{l\to\infty} \int_{-\infty}^{0} p_v^{(l)}(x)dx = 0\right\}, \tag{4.11}$$

where $p_v^{(l)}$ is the pdf of $v_i^{(0)}$ at the l-th iteration. If $\gamma < \gamma_{\text{th}}$, the error converges to zero as $l \to \infty$ and if $\gamma > \gamma_{\text{th}}$, the decision error diverges from zero. The DE of the check node update and the variable noise update have been introduced in Chapter 3, and they are given as

$$p_u^{(l)} = \Gamma^{-1}\left[\sum_{i=2}^{d_c} \rho_i \left(\Gamma\left[p_v^{(l-1)}\right]\right)^{\otimes(i-1)}\right], \tag{4.12}$$

and

$$p_v^{(l)} = p_v^{(0)} \otimes \sum_{i=2}^{d_v} \lambda_i \left(p_u^{(l)}\right)^{\otimes(i-1)}, \tag{4.13}$$

respectively. According to (4.12) and (4.13), we can obtain densities passed from variable nodes to check nodes in the l-th iteration as

$$p_v^{(l)} = p_v^{(0)} \otimes \lambda\left(\Gamma^{-1}\left(\rho\left(\Gamma\left(p_v^{(l-1)}\right)\right)\right)\right). \tag{4.14}$$

We assume that the all-zero codeword is transmitted, Hence, the BEP is

$$P_e^{(l)} = \int_{-\infty}^{0} p_v^{(l)}(x)dx. \tag{4.15}$$

The effectiveness of our DE analysis will be shown in the results section. We note that DE only gives us the asymptotic performance of LDPC codes since it assumes the LDPC code has an infinite length and cycle-free. However, there is a large gap between the asymptotic performance and practical performance when we consider finite length LDPC codes. In order to estimate the performance more accurately,

we propose a method to analyze the finite length LDPC codes in the next section.

4.3 Finite Length Analysis of LDPC codes on SαS Channels

In this section, the analytic BEP of SαS channels will be derived first. Then we will combine the analytic BEP and DE analysis which has been given above to calculate the estimated block and BEP for finite length LDPC codes.

4.3.1 Uncoded Bit Error Probability on SαS Channels

In this part, we will derive the BEP, P_b^α, of BPSK modulation on SαS channels, which will be employed to estimate the block and BEP of the LDPC-coded system. When $\alpha = 2$, the pdf of the noise is known but the cdf is not given in closed-form. Hence the right tail probability function is defined as

$$Q(x) = \frac{1}{\sqrt{2\pi}} \int_x^\infty \exp\left(-\frac{t^2}{2}\right) dt. \tag{4.16}$$

We can define a right tail probability function $Q_\alpha(x)$ for SαS noise as

$$Q_\alpha(x) = \int_x^\infty f_\alpha(t; 0, 1) dt, \tag{4.17}$$

where $f_\alpha(t; 0, 1)$ is the standard SαS distribution which is defined by letting $\gamma = 1$. We note that the integral in (4.17) can be calculated by a numerical method given in [90]. Hence, P_b^α for SαS channels is derived as

$$\begin{aligned} P_b^\alpha &= P(x = +1)P(e|x = +1) + P(x = -1)P(e|x = -1) \\ &= \frac{1}{2} \int_{-\infty}^0 f_\alpha(t - 1; \gamma) dt + \frac{1}{2} \int_0^\infty f_\alpha(t + 1; \gamma) dt \\ &= \int_1^\infty f_\alpha(u; \gamma) du, \end{aligned} \tag{4.18}$$

where e is a symbol error and $P(x = +1) = P(x = -1) = \frac{1}{2}$. According to the standardization of SαS random variables, if $x \sim S(\alpha, \gamma)$, then $x/\gamma \sim S(\alpha, 1)$ and the pdf should be scaled by $1/\gamma$ [90]. By using this parametrization of the SαS process,

(4.18) can be rewritten as

$$\begin{aligned} P_b^{\alpha} &= \int_1^{\infty} \frac{1}{\gamma} f_{\alpha}\left(\frac{u}{\gamma}; 1\right) du \\ &= \int_{\frac{1}{\gamma}}^{\infty} f_{\alpha}(v; 1) dv \\ &= Q_{\alpha}\left(\frac{1}{\gamma}\right). \end{aligned} \tag{4.19}$$

Since the geometric SNR is defined for the whole range of α, (4.19) is a general expression for all SαS channels. From (3.20) and (4.19), we can obtain P_b^{α} in terms of E_b/N_0 as

$$P_b^{\alpha} = Q_{\alpha}\left(\frac{1}{\gamma}\right) = Q_{\alpha}\left(\sqrt{4R_c C_g^{(\frac{2}{\alpha}-1)} \frac{E_b}{N_0}}\right). \tag{4.20}$$

When $R_c = 1$, (4.20) represents the BEP of an uncoded BPSK system on SαS channels.

There are two special cases of SαS random variables which have a closed-form expression for the pdf: $\alpha = 1$ and $\alpha = 2$. Hence their BEP can be derived to further verify the correctness of our analysis. First we consider the case of Cauchy noise ($\alpha = 1$), where P_b^{Cauchy} is given as

$$\begin{aligned} P_b^{\text{Cauchy}} &= \int_0^{\infty} \frac{\gamma}{\pi} \frac{1}{(t+1)^2 + \gamma^2} dt \\ &= \int_{\frac{1}{\gamma}}^{\infty} \frac{1}{\pi} \frac{1}{x^2+1} dx, \end{aligned} \tag{4.21}$$

The Cauchy distribution of (4.21) has been converted to a standard pdf and P_b^{Cauchy} can be expressed in terms of $Q_{\alpha}(x)$ as

$$P_b^{\text{Cauchy}} = Q_{\alpha}\left(\frac{1}{\gamma}\right). \tag{4.22}$$

Now we examine the case for AWGN ($\alpha = 2$). Notice that according to the definition of the standard SαS pdf, the variance of the normal distribution is equal to two, since $\sigma^2 = 2\gamma^2$. Hence the standard SαS distribution when $\alpha = 2$ is

$$f_{\alpha=2}(t; 1) = \frac{1}{2\sqrt{\pi}} \exp(-\frac{t^2}{4}). \tag{4.23}$$

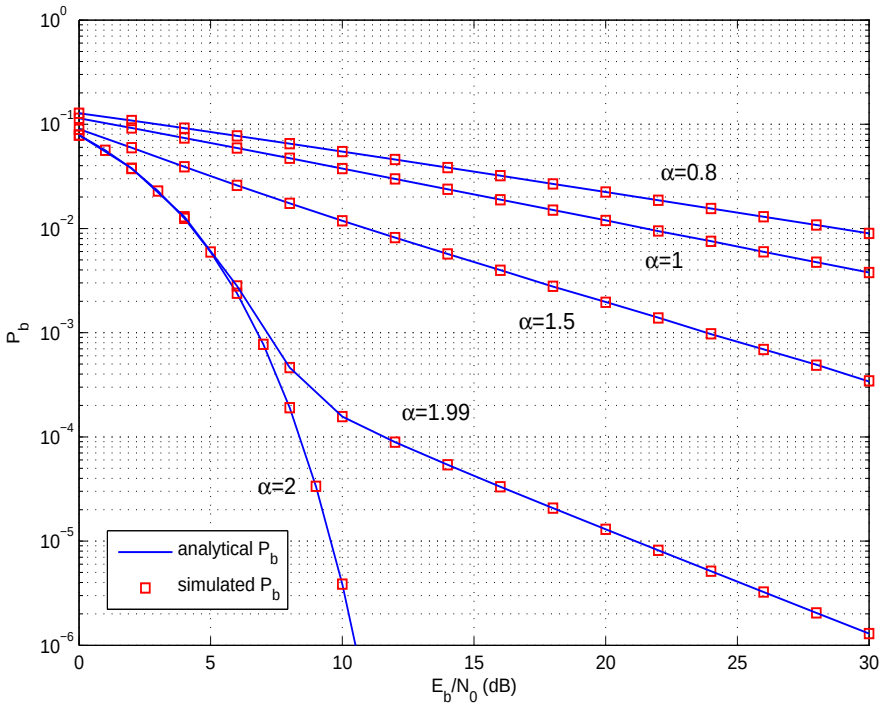

Figure 4.2: Uncoded performance of BPSK on SαS channels at $\alpha = 2, 1.99, 1.5, 1$ and 0.8, respectively.

Then the uncoded BEP of BPSK on the AWGN channel can be expressed in terms of the Q_α-function as

$$P_b^{\text{Gauss}} = Q\left(\sqrt{\frac{2E_b}{N_0}}\right) = Q_{\alpha=2}\left(2\sqrt{\frac{E_b}{N_0}}\right). \tag{4.24}$$

When $\alpha = 2$, (4.20) reduces to (4.24), hence (4.20) is universal for all values of α. The derived analytic expression is verified by Fig. 4.2, where P_b^α in (4.20) for different α's are shown to be identical to the simulated BER.

4.3.2 Block and Bit Error Probability of finite length LDPC codes on SαS Channels

4.3.2.1 Estimating the Block Error Probability

The block error probability (BLEP) of finite length LDPC codes can be derived by considering the real-time channel quality for transmitting each codeword. First we define the observed bit error rate P_{obs}^α as the bit error rate of any received word of length N [51]. Assuming the all-zero codeword $\boldsymbol{c}$ is transmitted, an error will occur if $L(y_j) = \frac{P(c_j=0|y_j)}{P(c_j=1|y_j)}$ is negative. The pdf of P_{obs}^α can be found by taking N samples

from the LLR distribution with a BEP of P_b^α. Hence, the probability mass function (pmf) of P_{obs}^α is given as

$$f_{P_{\text{obs}}^\alpha}(N, P_{\text{obs}}^\alpha) = \binom{N}{NP_{\text{obs}}^\alpha} (P_b^\alpha)^{NP_{\text{obs}}^\alpha} (1 - P_b^\alpha)^{N - NP_{\text{obs}}^\alpha}, \tag{4.25}$$

where NP_{obs}^α is the average number of errors in the codeword of length N and it has a binomial distribution $B(N, P_b^\alpha)$. When $N \to \infty$, the pdf of NP_{obs}^α is well approximated by the Gaussian distribution $\mathcal{N}(NP_b^\alpha, NP_b^\alpha(1 - P_b^\alpha))$. Hence, the pdf of P_{obs}^α is approximated by $\mathcal{N}(P_b^\alpha, P_b^\alpha(1 - P_b^\alpha)/N)$.

Now we employ a threshold method to predict the BLEP P_B^α for LDPC codes with block length N in SαS noise. As defined above, the threshold SNR of a specific ensemble of LDPC codes is the maximum channel parameter where the decision error of the SPA decoder can converge to zero. The threshold γ_{th} of LDPC codes on SαS channels can be calculated by the DE analysis which we introduced in this chapter. Then we give the procedure for estimating P_B^α by using the obtained threshold SNR.

First, we calculate the threshold BEP P_{th} which corresponds to the threshold dispersion γ_{th} on the SαS channel using (4.20). Hence,

$$P_{\text{th}} = Q_\alpha \left(\sqrt{4R_c C_g^{(\frac{2}{\alpha}-1)} \left(\frac{E_b}{N_0} \right)_{\text{th}}} \right), \tag{4.26}$$

where $\left(\frac{E_b}{N_0}\right)_{\text{th}}$ is the threshold SNR defined by γ_{th}. To find P_B^α for short LDPC codes, the probability that the observed channel behaves worse than the decoding threshold is calculated by using the pdf of P_{obs}^α. Hence, the probability that $P_{\text{obs}}^\alpha > P_{\text{th}}$ can be calculated by $f_{P_{\text{obs}}^\alpha}(N, P_{\text{obs}}^\alpha)$ and the block length N. Hence, the BLEP is estimated as

$$P_{\text{B}}^\alpha(N, \lambda, \rho) = \int_{P_{\text{th}}}^{1} f_{P_{\text{obs}}^\alpha}(N, x) dx, \tag{4.27}$$

where (4.27) gives the BLEP for a LDPC ensemble with code length N and edge degree distributions $\lambda(x)$ and $\rho(x)$. As discussed earlier, when N is large, $f_{P_{\text{obs}}^\alpha}(N, P_{\text{obs}}^\alpha)$ can be approximated by a Gaussian distribution. Hence the BLEP is given as

$$P_{\text{B}}^\alpha(N, \lambda, \rho) = Q\left(\frac{P_{\text{th}} - \mu_{P_{\text{obs}}^\alpha}}{\sigma_{P_{\text{obs}}^\alpha}} \right), \tag{4.28}$$

where $\mu_{P_{\text{obs}}^\alpha} = P_b^\alpha$ and $\sigma_{P_{\text{obs}}^\alpha} = P_b^\alpha(1 - P_b^\alpha)/N$.

4.3.2.2 Estimating the Probability of Bit Error

The BEP is derived from the BLEP by observing that the error rate does not change significantly for channel parameters which are slightly worse than the threshold when the decoder fails to converge. There is a BEP P_e when the decoder fails, as given in (4.15). As derived above, each block has the probability $P_{\mathrm{B}}^{\alpha}(N, \lambda, \rho)$ of an error occuring, hence the coded BEP is given as

$$P_{\mathrm{b}}^{\alpha}(N, \lambda, \rho) = P_e^{(l_{\max})} P_{\mathrm{B}}^{\alpha}(N, \lambda, \rho), \tag{4.29}$$

where $l_{\max}$ is the maximum number of iterations in the process of DE. We note that $P_e^{(l)}$ is the BEP obtained from GA in [51], but this is not valid in our situations since the SαS noise channel is non-Gaussian. Hence density evolution is essential to calculate $P_e^{(l)}$.

4.4 Results

4.4.1 LDPC codes with Different Receivers on SαS Channels

Table 4.1: the threshold SNRs in dB for the different receivers

	optimal	LLR appro.	proposed	Cauchy	Clipper
$\alpha = 1.8$	1.54	1.64	1.63	1.90	1.65
$\alpha = 1.6$	1.88	1.98	1.98	2.08	2.05
$\alpha = 1.2$	2.72	2.79	2.78	2.76	3.55
$\alpha = 1.0$	3.31	3.38	3.36	3.31	4.80

The threshold SNRs of optimal and suboptimal receivers derived from DE are given in table 4.1. As shown in table 4.1, the threshold SNRs for the LLR approximation receiver and the proposed receiver are similar and both of them are very close to the optimal receiver for a large range of α. When $\alpha = 1$, the Cauchy receiver is the optimal receiver. It also exhibits a good performance for various val-

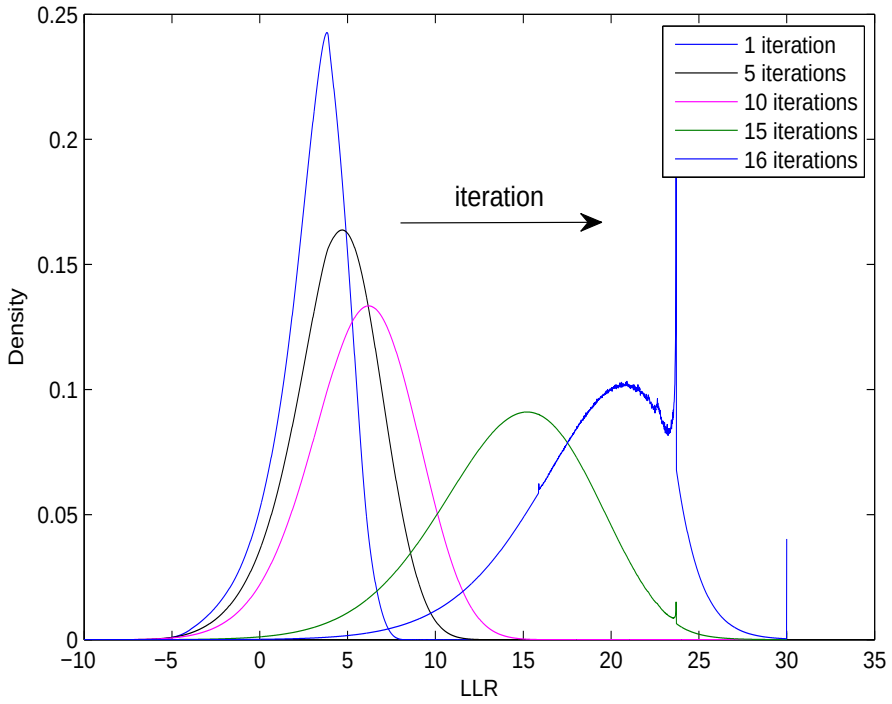

Figure 4.3: Density evolution at variable node with the optimal receiver, when $\alpha = 1.8$ and $E_b/N_0 = 2$ dB.

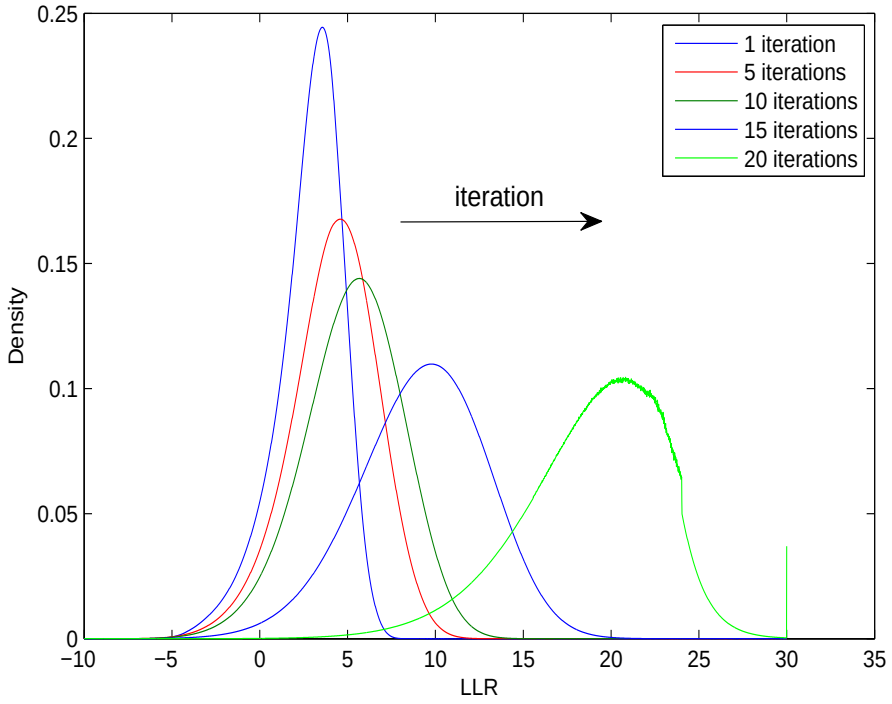

Figure 4.4: Density evolution at variable node with our proposed receiver, when $\alpha = 1.8$ and $E_b/N_0 = 2$ dB.

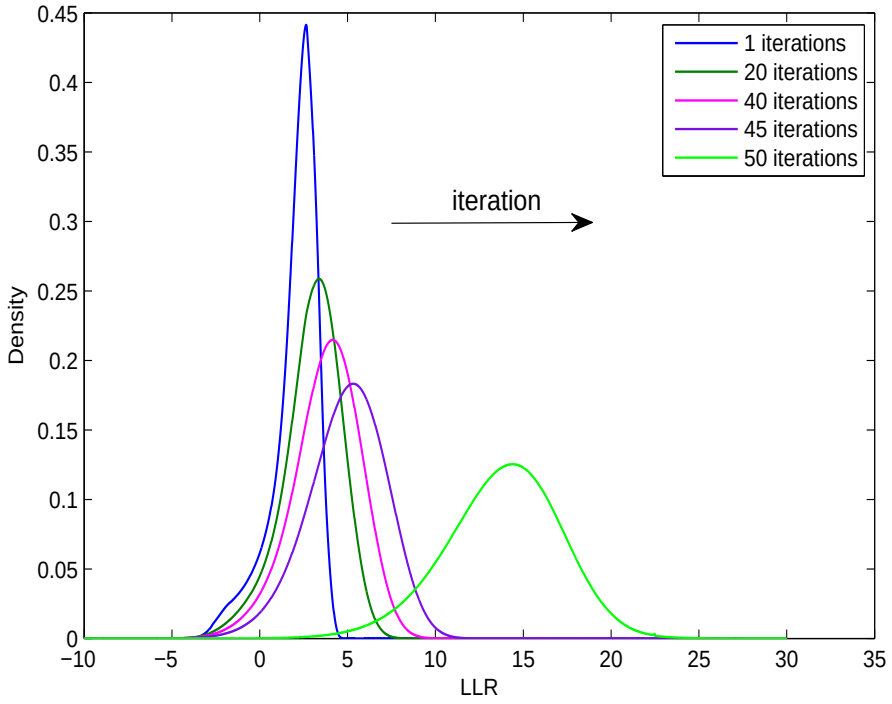

Figure 4.5: Density evolution at variable node with Cauchy receiver when $\alpha = 1.8$ and $E_b/N_0 = 2$ dB

ues of α. However, we observe that the performance of the Cauchy receiver suffers from degradation when the channel is only slightly impulsive, such as $\alpha = 1.8$. The simple clipper receiver is also attractive in this case since it achieves near-optimal performance at $\alpha = 1.8$. In addition, the threshold SNR of the clipper approaches the optimal receiver as α increases. This implies that the clipper receiver is very suitable for lightly impulsive environments compared with the other receivers due to its excellent performance and low complexity.

Additionally, we plot the pdf of the message passed from variable nodes for different receivers at $\alpha = 1.8$ and $E_b/N_0 = 2$ dB in Fig. 4.3 - Fig. 4.5. As given in (4.11), the error probability P_e of the decoder is the integration of $p_\omega^{(l)}$ evaluated in the range $(-\infty, 0]$. As shown in Fig. 4.3 - Fig. 4.5, the area of the density for negative LLRs which corresponds to P_e becomes smaller as the number of iterations increases. For example, it requires 50 iterations for the Cauchy receiver to make $P_e \to 0$ while the optimal receiver and proposed receiver only require 16 and 20 iterations, respectively. This observation verify the thresholds given in table 4.1 for the Cauchy, optimal and proposed receivers, which are 1.90 dB, 1.54 dB and 1.63 dB respectively. We also observe that the LLR becomes larger as the number of

iterations increases and there are a few spikes at LLR = 25 and 30 for 16 iterations and 20 iterations in Fig. 4.3 and Fig. 4.4, respectively. It is known that LLR measures the reliability of the received signal. This implies that as the number of iterations increases, the decoder is more confident on the decision of the received symbols and the LLR will converge to a specific value and no longer increase.

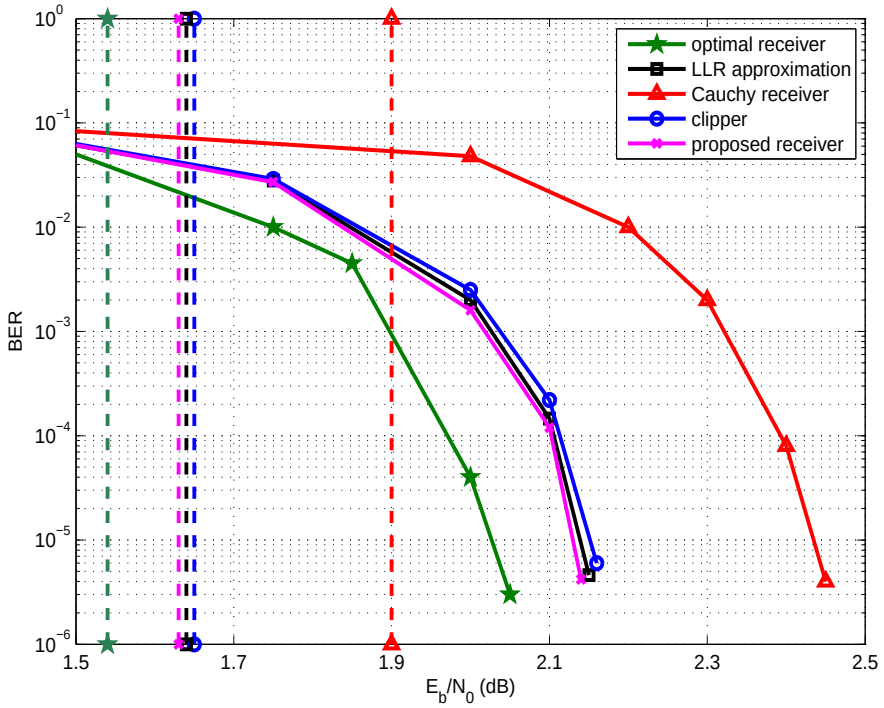

Figure 4.6: LDPC codes ($n_b = 20000$ bits) on the SαS channel with $\alpha = 1.8$

To examine the simulated performance of optimal and suboptimal receivers and validate the obtained thresholds, we use a $(3, 6)$ LDPC code with code length $n_b = 20000$ and code rate $R_c = 0.5$. The LDPC code is randomly constructed and the maximum iterations number is set to 20. The BER performance is evaluated for SαS channels with $\alpha = 1.8$ and $\alpha = 1$ which represent lightly impulsive and extremely impulsive noise, respectively. As shown in Fig. 4.6, when $\alpha = 1.8$, the clipper receiver, the proposed receiver and the LLR approximation receiver achieve similar performances and are 0.1 dB worse than the optimal receiver, but the Cauchy receiver is 0.4 dB away from the optimal receiver. In Fig. 4.7, $\alpha = 1$ and the Cauchy receiver is optimal, but the proposed receiver still matches the performance of the optimal receiver while the LLR approximation receiver achieves a slightly worse performance. However, in this situation, the clipper receiver is 1.7 dB worse than the optimal receiver.

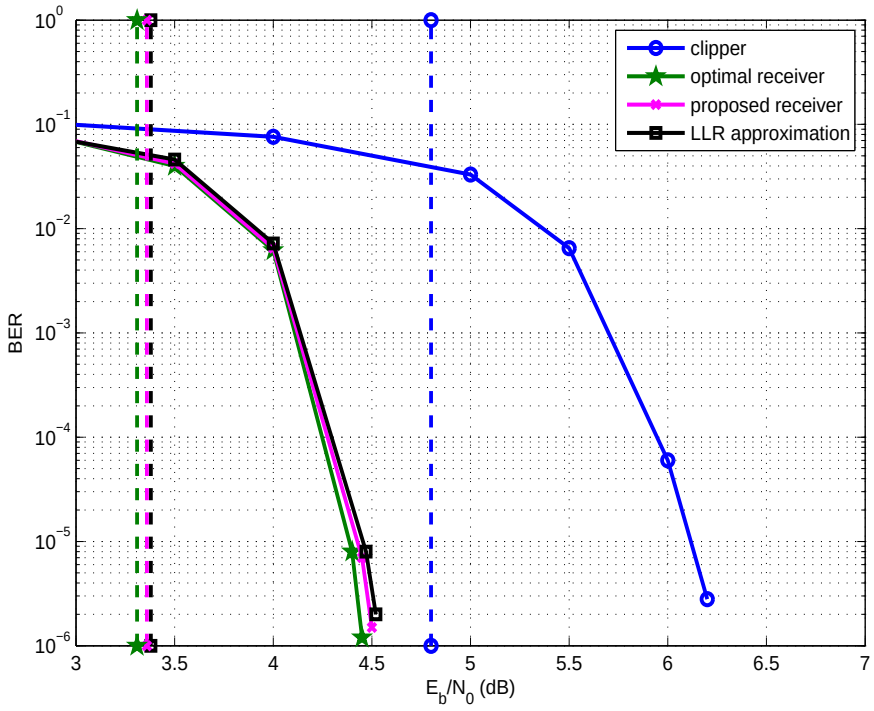

Figure 4.7: LDPC codes ($n_b = 20000$ bits) on the SαS channel with $\alpha = 1$

We note that the threshold SNRs for the different receivers obtained from DE analysis are denoted by dashed vertical lines in these figures and the threshold SNRs match the beginning of the waterfall region for these BER curves. Hence, this shows that our asymptotic analysis is valid on these channels.

4.4.2 Waterfall performance of LDPC codes on SαS Channels

We investigate the accuracy of our estimated BLEPs and BEPs for finite length LDPC codes by comparing analytic BEP with the simulated BER of LDPC codes. We employ both rate 1/2 regular and irregular LDPC codes with different codeword lengths ($N = 1000, 4000, 20000$) at different values of α ($\alpha = 0.8, 1, 1.5, 1.9$). The decoding algorithm is the SPA and the maximum number of iterations is 100. For regular LDPC codes, the degree of d_v and d_c are 3 and 6, respectively. For irregular codes, the degree distributions are selected to be $\lambda(x) = 0.30013x + 0.28395x^2 + 0.41592x^7$, $\rho(x) = 0.22919x^5 + 0.77081x^6$ and $\lambda(x) = 0.4x^2 + 0.4x^5 + 0.2x^8$, $\rho(x) = x^8$. The first degree distribution pair is chosen from [42] which is an optimized code with maximum variable node degree of 8. The second degree distribution pair is chosen from [51]. In the simulation, LDPC codes with short or medium length ($N \leq 4000$

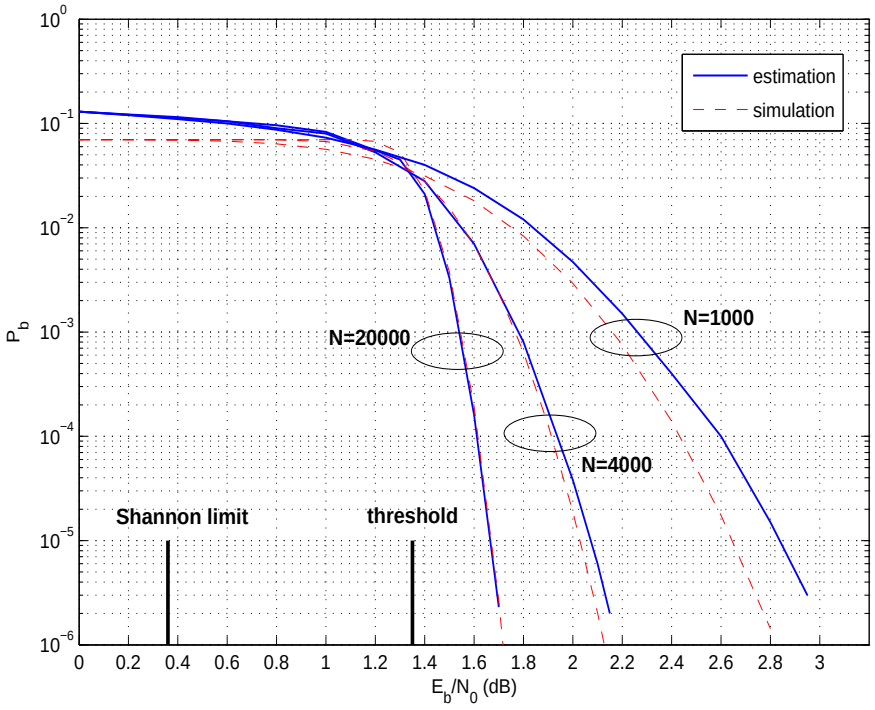

Figure 4.8: BEP comparison of regular $(3, 6)$ LDPC codes showing estimated and simulation results with different block lengths on SαS channels when $\alpha = 1.9$.

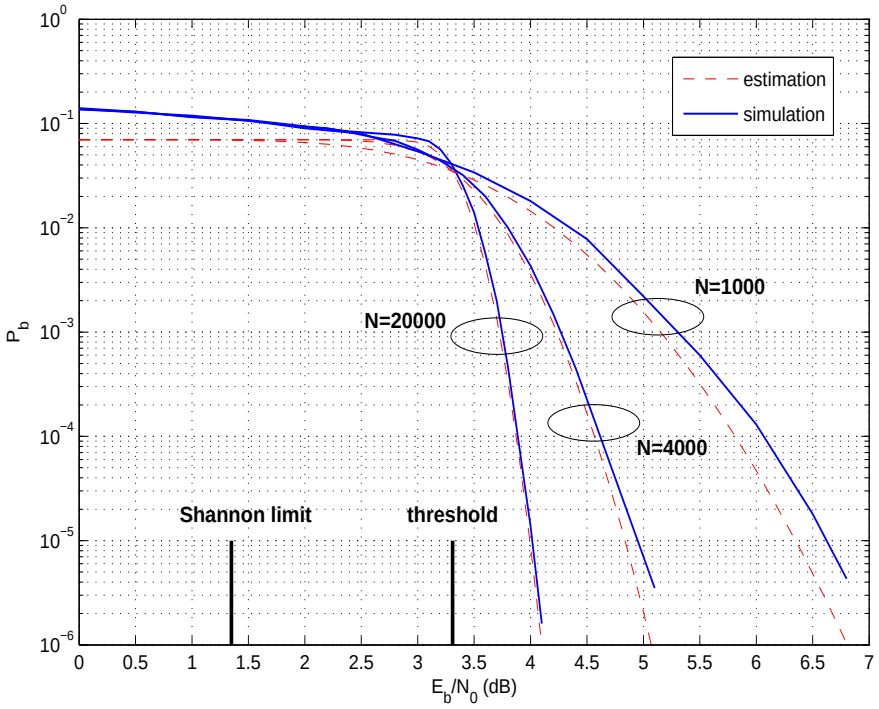

Figure 4.9: BEP comparison of regular $(3, 6)$ LDPC codes showing estimated and simulation results with different block lengths on SαS channels when $\alpha = 1$.

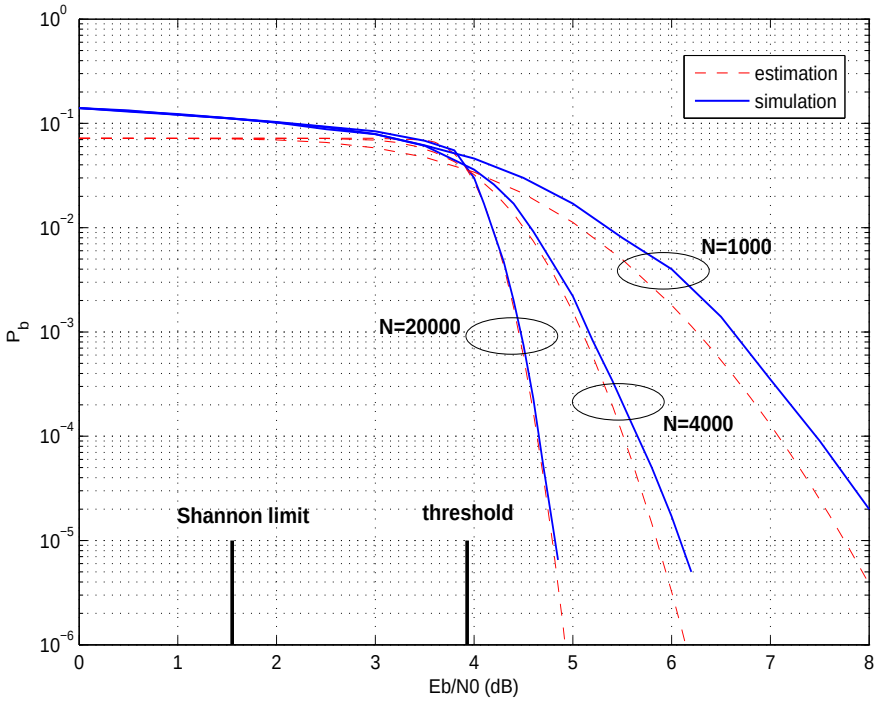

Figure 4.10: BEP comparison of regular $(3, 6)$ LDPC codes showing estimated and simulation results with different block lengths on SαS channels when $\alpha = 0.8$.

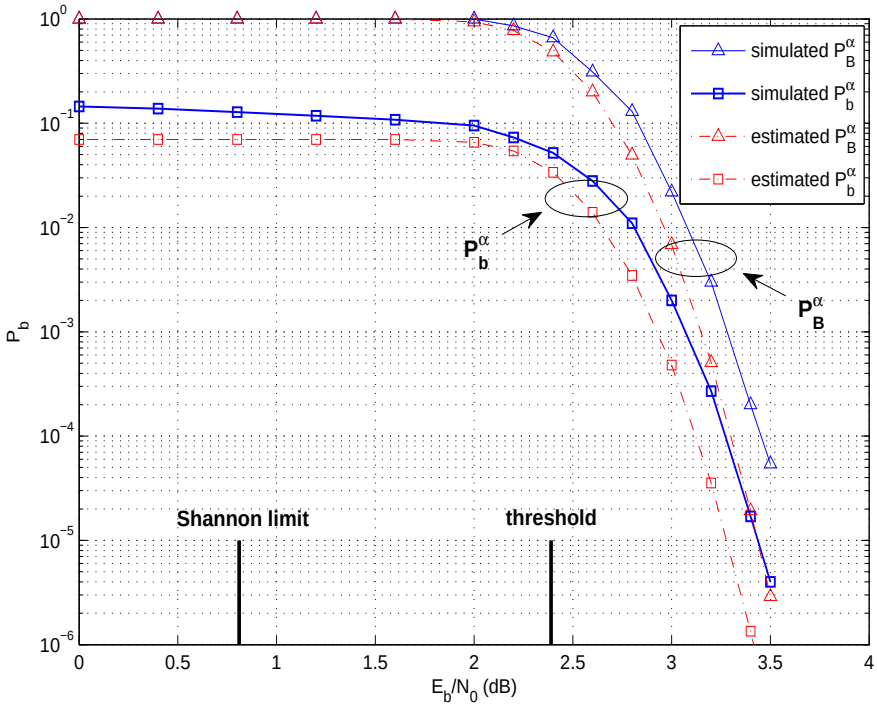

Figure 4.11: Block and bit error probability of irregular LDPC codes with degree distribution $\lambda(x) = 0.4x^2 + 0.4x^5 + 0.2x^8$, $\rho(x) = x^8$ showing estimated and simulation results with $N = 4000$ on SαS channels when $\alpha = 1.5$.

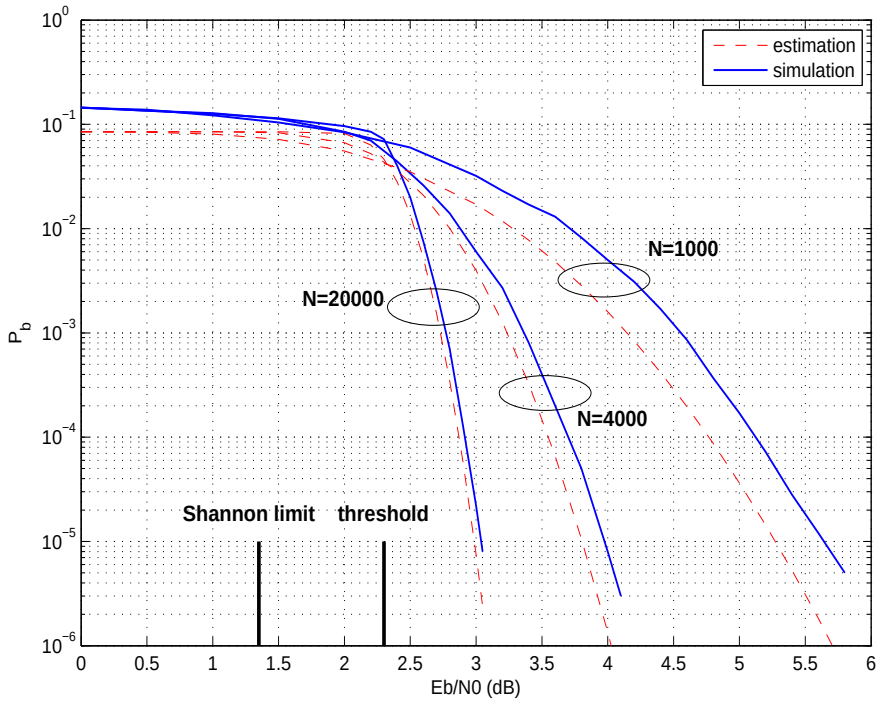

Figure 4.12: BEP comparison of irregular LDPC codes with degree distribution $\lambda(x) = 0.30013x + 0.28395x^2 + 0.41592x^7$, $\rho(x) = 0.22919x^5 + 0.77081x^6$ showing estimated and simulation results with different block lengths on SαS channels when $\alpha = 1$.

bits) are constructed using the progressive edge-growth (PEG) algorithm [1], which maximizes the local girth. For long LDPC codes, random construction is used since the computational cost of the PEG algorithm for long LDPC codes is very high.

As shown in Figs. 4.8 - 4.10, the gap between the estimated and simulated bit error rate becomes smaller as the code length increases for each value of α. When $N = 1000$, the gap between the estimated and simulated performance is about 0.2 dB and it reduces to 0.1 dB when N increases to 4000. For long LDPC codes where $N = 20000$, the estimation and the simulation result are almost the same. We also observe that these performance differences are independent of α.

For irregular LDPC codes, our estimation method is also shown to be effectiveness. As shown in Fig. 4.11, the actual performance is accurately predicted by the analytically derived P_B^{α} and P_b^{α} in (4.28) and (4.29) with only a 0.15 dB difference at a bit error rate of 10^{-5}, while the gap to the threshold SNR is 1.04 dB. In Fig. 4.12, the performance of optimized LDPC codes is presented when $\alpha = 1$. It is shown that the gaps between the estimated and simulated performance for different block lengths are similar to the results for the regular LDPC codes, with both sets

of results becoming almost identical when $N = 20000$ bits. Compared with Fig. 4.9, we note that the performance of this optimized code is about 1 dB better than regular $(3, 6)$ LDPC codes with the same block lengths.

It is observed that the gap between the estimated and simulated results is greater at shorter block lengths. There are two reasons for this result: First, the threshold γ_{th} and its corresponding P_{th} obtained from DE assumes the LDPC code is cycle-free. However, short cycles cannot be avoided for short LDPC codes. Hence, the effect of cycles on short block length LDPC codes is more serious and this degrades performance [1]. For long LDPC codes, the prediction becomes more accurate since the concentration theorem states that the average behavior of individual codes concentrates around its expected behavior as the block length grows and this average behavior converges to the cycle-free case [41]. Second, the pdf of P_{obs}^{α} is not well approximated as a Gaussian distribution when N is small, which means (4.28) and (4.29) become less accurate. To numerically evaluate the accuracy of the Gaussian approximation, the Kullback-Leibler (KL) divergence is employed to calculate the difference between the two pdfs. KL divergence is defined as $D_{\text{KL}}(P||Q) = \sum_i P(i) \log \frac{P(i)}{Q(i)}$, where P is the true pdf and Q is an approximation of P. In our case, P is the binomial pdf $B(N, P_0^{\alpha})$ and Q is the normal distribution $\mathcal{N}(P_0^{\alpha}, P_0^{\alpha}(1 - P_0^{\alpha})/N)$. For example, the threshold E_b/N_0 is given in Fig. 4.8 and the corresponding BEP P_{th} can be calculated by (4.26). Knowing the value of block length N and P_{th}, the pdf of P_{obs}^{α} can be determined. Therefore, the KL divergence between the pdf of P_{obs}^{α} and Gaussian distribution is obtained as $1.4\times10^{-3}, 3\times10^{-4}, 6.7\times10^{-5}$ for $N = 1000, 4000, 20000$, respectively. This indicates that the approximation becomes more accurate as the block length increases and when $N = 20000$, these two pdfs are almost identical.

4.5 Conclusion

In this chapter, we have examined the performance of LDPC codes on SαS channels with different receivers. A sub-optimal receiver has been proposed that provides a good approximation of the exact LLR but does not require calculation of the SαS pdf or its dispersion, which greatly reduces the complexity. In addition, a DE analysis of the LDPC code for each receiver on SαS channels was presented. With DE, we have derived the threshold SNRs which represent the start of the waterfall

region. Moreover, simulation results of LDPC codes with different receivers have been presented to validate the DE analysis.

The asymptotic and simulated results show that the proposed receiver can achieve near-optimal performance with only the knowledge of the channel impulsiveness α. We also observe that the clipper receiver is most suitable for only slightly impulsive(as α approaches two) since it is simple and presents excellent performance, while the Cauchy receiver approaches optimum performance as α approaches one. The LLR approximation receiver also shows good performance over a large range of α, but it also requires the knowledge of γ and additionally the proposed receiver is slightly better for some α values due to the better approximation of the LLR. We can conclude that the proposed receiver is a good choice for SαS channels and it can achieve a good performance at a low complexity.

In order to better estimate the waterfall performance of LDPC codes on impulsive noise channels, we have analyzed finite length performance of regular and irregular LDPC codes by deriving the BLEP and BEP on SαS impulsive noise channels. We observed that at long block lengths ($N = 20000$ bits), the estimated BEPs are almost identical to the simulated bit error rates for different values of α, but it is also found that the gap between theoretical and simulation results increases as the block length decreases. The reasons for this are the effect of short cycles on the Tanner graph and the Gaussian approximation of the observed error probabilities becoming weaker as the block length is reduced, although the gap was still only around 0.2 dB when the block length is as low as $N = 1000$ bits. Hence, we have shown that for a given degree distribution pair our method can be used to obtain accurate estimates of the BLEP and BEP of finite length LDPC codes on SαS additive impulsive noise channels. Furthermore, our analysis implies that for a given uncoded BEP and threshold, predictions of the actual performance for short LDPC codes could be accomplished on more general memoryless channels.

Chapter 5

Performance Analysis of LDPC codes over Fading Channels with Impulsive Noise

5.1 Introduction

In chapter 4, a performance analysis of LDPC codes on additive impulsive noise channels was presented and closed form expressions for the coded BEP were derived. In this chapter, we extend the work from chapter 4 to first derive the uncoded BEP on generalized fading channels, encompassing Rayleigh, Ricean and Nakagami-m fading channels, with additive SαS noise. In order to reduce the computational cost of calculating the exact BEP we derive two approximations for the case of the BEP of Rayleigh fading channels with SαS noise. One approximation is based on the utilization of a bi-parameter Cauchy-Gaussian mixture (BCGM) model and the other one uses the asymptotic property of SαS random variables. Both of them are given as closed-form expressions which greatly reduce the complexity and show accurate estimation of the exact BEP.

We then derive the asymptotic performance of LDPC codes on these channels with optimal and sub-optimal receivers using density evolution (DE). Finally, we extend this analysis to estimate the BEP of finite length LDPC codes, which becomes more accurate as block size increases.

5.2 Error Probability Analysis of Generalized Fading Channels with SαS Noise

We consider a point-to-point system with a coherent receiver. The n-th received signal $y(n)$ is described as

$$y(n) = ae^{j\phi}x(n) + z(n), \tag{5.1}$$

where $x(n)$ is the BPSK modulated signal with $x(n) \in \{-1, 1\}$, a is the normalized fading amplitude with $E[a^2] = 1$ and ϕ is the phase of the channel. $z(n)$ is complex noise where the real part $z_R(n)$ and imaginary part $z_I(n)$ are i.i.d. and they both follow a symmetric alpha-stable (SαS) distribution. According to [27], the real and imaginary components of any complex SαS noise samples are independent and identically distributed if the bandpass sampling frequency is four times greater than the carrier frequency. Hence, with this assumption the BEP for SαS channels is derived as

$$\begin{aligned} P_b^\alpha &= P(x=+1)P(e|x=+1) + P(x=-1)P(e|x=-1) \\ &= \int_1^\infty f_\alpha(u;\gamma)du, \end{aligned} \tag{5.2}$$

where e is a symbol error and $P(x=+1) = P(x=-1) = \frac{1}{2}$. According to the standardization of SαS random variables, if $x \sim S(\alpha, \gamma)$, then $x/\gamma \sim S(\alpha, 1)$ and the pdf should be scaled by $1/\gamma$. By using this parametrization of the SαS process, (5.2) can be rewritten as

$$P_b^\alpha = \int_1^\infty \frac{1}{\gamma} f_\alpha\left(\frac{u}{\gamma}; 1\right) du = \int_{\frac{1}{\gamma}}^\infty f_\alpha(v;1)dv = Q_\alpha\left(\frac{1}{\gamma}\right). \tag{5.3}$$

Since geometric SNR is defined for the whole range of α, (5.3) is a general expression for all SαS channels. From (3.20) and (5.3), we can obtain P_b^α in terms of E_b/N_0 as

$$P_b^\alpha = Q_\alpha\left(\frac{1}{\gamma}\right) = Q_\alpha\left(\sqrt{4R_c C_g^{(\frac{2}{\alpha}-1)}\frac{E_b}{N_0}}\right). \tag{5.4}$$

Table 5.1: PDF $p(a)$ and $p(\omega;\Omega)$ for normalized fading amplitude a and instantaneous SNR for selected fading channels

Channel Type	PDF of Fading Amplitude a and SNR/bit, ω
Rayleigh	$p(a) = 2a\exp(-a^2); \quad a \geq 0$ $p(\omega;\Omega) = \frac{1}{\Omega}\exp(-\omega/\Omega); \quad \omega \geq 0$
Rician $K \geq 0$	$p(a) = 2(1+K)e^{-K}a\exp\left(-(1+K)a^2\right)$ $\times I_0\left(2a\sqrt{K(1+K)}\right); \quad a \geq 0$ $p(\omega;\Omega) = \frac{(1+K)e^{-K}}{\Omega}\exp\left(-\frac{(1+K)\omega}{\Omega}\right)$ $\times I_0\left(2\sqrt{\frac{K(1+K)\omega}{\Omega}}\right); \quad \omega \geq 0$
Nakagami-m $m \geq 1/2$	$p(a) = \frac{2m^m a^{2m-1}}{\Gamma(m)}\exp\left(-ma^2\right); \quad a \geq 0$ $p(\omega;\Omega) = \frac{m^m\omega^{m-1}}{\Omega^m\Gamma(m)}\exp\left(-\frac{m\omega}{\Omega}\right); \quad \omega \geq 0$

The BEP on generalized fading channels with SαS noise for BPSK is given as

$$\begin{aligned} P_b^{\alpha,\mathrm{F}} &= \int_0^\infty P_{b|a}^{\alpha}(\omega)p(\omega;\Omega)d\omega \\ &= \int_0^\infty Q_\alpha\left(\sqrt{4R_c C_g^{(\frac{2}{\alpha}-1)}\omega}\right)p(\omega;\Omega)d\omega, \end{aligned} \tag{5.5}$$

where $p(\omega;\Omega)$ is the pdf of ω and $\Omega = \frac{E_b}{N_0}$. We note that (5.5) is valid for generalized fading channels. In this chapter, we consider Rayleigh, Rician and Nakagami-m fading to verify our analysis. Their corresponding pdfs $p(a)$ of the fading amplitude a and pdfs $p(\omega;\Omega)$ of the instantaneous SNR ω are given in Table 5.1.

We note that the calculation of $Q_\alpha(x)$ requires a double integral, but this can be reduced to only one integral. We can first write $Q_\alpha(x) = 1 - F_\alpha(x)$ where $F_\alpha(x)$ is the cumulative distribution function (cdf) of the SαS distribution. Hence, we propose to use an alternative expression of $F_\alpha(x)$ [90] to reduce the complexity of calculating $Q_\alpha(x)$. For $x > 0$:

(a) When $\alpha \neq 1$,

$$Q_\alpha(x) = c_1 + \frac{\mathrm{sign}(\alpha-1)}{\pi}\int_0^{\frac{\pi}{2}}\exp\left(-x^{\frac{\alpha}{\alpha-1}}V(\theta;\alpha)\right)d\theta, \tag{5.6}$$

where

$$c_1 = \begin{cases} \frac{1}{2}, & \alpha < 1, \\ 0, & \alpha > 1, \end{cases}$$

and

$$V(\theta;\alpha) = \left(\frac{\cos\theta}{\sin\alpha\theta}\right)^{\frac{\alpha}{\alpha-1}} \frac{\cos(\alpha-1)\theta}{\cos\theta}.$$

(b) When $\alpha = 1$,

$$Q_\alpha(x) = -\frac{1}{2} - \frac{1}{\pi}\arctan(x). \tag{5.7}$$

This new general expression of Q_α-function reduces the complexity of calculating $Q_\alpha(x)$ by replacing the double integral with a single integral. Hence, by using this alternate expression of $Q_\alpha(x)$, we can efficiently calculate the analytic BEP for fading channels with SαS noise.

5.3 Approximated Error Probabilities of Rayleigh Fading Channels with SαS Noise

We have derived the exact BEP for generalized fading channels with SαS noise. However, as discussed earlier, the computational cost of calculating the exact BEP is very high. A double-integral is needed if we use the alternative expression of $F_\alpha(x)$. In this section, two closed-form approximations of the BEP on Rayleigh fading channels with SαS noise will be derived to greatly reduce the complexity.

5.3.1 BEP approximation from the BCGM model

The first approximation is to use a recently proposed bi-parameter Cauchy-Gaussian mixture (BCGM) model to approximate SαS distributions ($1 \leq \alpha \leq 2$) [91]. This model mixes a Gaussian distribution ($\alpha = 2$) and a Cauchy distribution ($\alpha = 1$) with only two parameters, ϵ and γ which is very simple. The pdf of the BCGM model is given as [91]

$$f_{\mathrm{CG}}(x) = (1-\epsilon)\frac{1}{2\sqrt{\pi}\gamma}\exp\left(-\frac{x^2}{4\gamma^2}\right) + \epsilon\frac{\gamma}{\pi(x^2+\gamma^2)}, \tag{5.8}$$

where ϵ is the mixture ratio and its near-optimal value is given as

$$\epsilon = \frac{2\Gamma(-p/\alpha) - \alpha\Gamma(-p/2)}{2\alpha\Gamma(-p) - \alpha\Gamma(-p/2)}. \tag{5.9}$$

The gamma function is $\Gamma(x) = \int_0^\infty e^{-t}t^{x-1}dt$ and $p < \alpha$ [91]. Then we can define the standard BCGM distribution as

$$f^s_{\mathrm{CG}}(x) = (1-\epsilon)\frac{1}{2\sqrt{\pi}}\exp\left(-\frac{x^2}{4}\right) + \epsilon\frac{1}{\pi(x^2+1)}. \tag{5.10}$$

The BEP of SαS channel can be approximated by $f^s_{\mathrm{CG}}(x)$ as

$$P_b^{\alpha,\mathrm{BCGM}} = \int_{\sqrt{4C_g^{(\frac{2}{\alpha}-1)}\frac{E_b}{N_0}}}^{\infty} f^s_{\mathrm{CG}}(x)dx. \tag{5.11}$$

Hence, the BEP on Rayleigh fading channels with SαS noise can be approximated as

$$\begin{aligned} P_b^{\alpha,\mathrm{Ray}} &\approx \frac{1}{\Omega}\int_0^\infty P_{b|a}^{\alpha,\mathrm{BCGM}}(\omega)\exp(-\omega/\Omega)d\omega \\ &= \frac{1}{\Omega}\int_0^\infty \left(\int_{\sqrt{4C_1\omega}}^\infty f^s_{\mathrm{CG}}(t)dt\right)\exp(-\omega/\Omega)d\omega \\ &= \frac{1-\epsilon}{2}\left(1-\sqrt{\frac{C_1\Omega}{1+C_1\Omega}}\right) + \frac{\epsilon}{2}\left(1-\exp\left(\frac{1}{4C_1\Omega}\right)\mathrm{erfc}\left(\sqrt{\frac{1}{4\mathrm{C}_1\Omega}}\right)\right), \end{aligned} \tag{5.12}$$

where $C_1 = C_g^{(\frac{2}{\alpha}-1)}$. It is observed that the original expression of the approximated $P_b^{\alpha,\mathrm{Ray}}$ requires a double-integral. After some simplifications, a closed-form expression of BEP is obtained which is given in (5.12). Compared with the exact analytic BEP, this approximation can greatly reduce the computational cost. We note that when $\epsilon = 0$, (5.12) is reduced to the exact BEP for Rayleigh fading channels with Gaussian noise. When $\epsilon = 1$, (5.12) is the exact BEP of Rayleigh fading channels with Cauchy noise. The derivation of (5.12) is given in the Appendix.

5.3.2 Asymptotic performance of Rayleigh Fading Channels with SαS noise

In addition to approximating the pdf of SαS distributions by the BCGM model, another approximation uses the asymptotic property of SαS distributions to approximation the tail probability function $Q_\alpha(x)$. According to [4] and Property 3, for a α-stable random variable X with dispersion γ^α, we have

$$\lim_{x\to\infty} P(X > x) = \frac{\gamma^\alpha C_\alpha}{x^\alpha}, \tag{5.13}$$

where

$$C_\alpha = \frac{1}{\pi}\Gamma(\alpha)\sin\left(\frac{\pi\alpha}{2}\right). \tag{5.14}$$

Hence the asymptotic right-tail probability function $Q_\alpha(x)$ is given as

$$\lim_{x\to\infty} Q_\alpha(x) = \frac{C_\alpha}{x^\alpha}, \tag{5.15}$$

By substituting (5.15) into (5.4), we can obtain the asymptotic BEP of uncoded BPSK on SαS channels as

$$P_b^{\alpha,\text{asy}} = C_\alpha\left(\sqrt{4C_g^{(\frac{2}{\alpha}-1)}\Omega}\right)^{-\alpha}. \tag{5.16}$$

After some manipulations, the asymptotic BEP of uncoded BPSK on Rayleigh fading channels with SαS noise is given as

$$\begin{aligned} P_b^{\alpha,\text{Ray}} &\to \frac{1}{\Omega}\int_0^\infty P_{b|a}^{\alpha,\text{asy}}(\omega)\exp(-\omega/\Omega)d\omega \\ &= \frac{C_\alpha}{\left(4C_g^{(\frac{2}{\alpha}-1)}\Omega\right)^{\frac{\alpha}{2}}}\Gamma\left(1-\frac{\alpha}{2}\right). \end{aligned} \tag{5.17}$$

The derived expression of the asymptotic BEP is very simple as it only contains a Gamma function $\Gamma(\cdot)$ and the derivation of this final expression is given in the Appendix . Numerical and simulated results for the exact and approximated BEP of BPSK on Rayleigh fading channels with SαS noise are shown in Fig. 5.1.

As shown in Fig. 5.1, our analytic BEPs match the simulation results for different values of α. The BCGM model gives a very accurate approximation of the exact

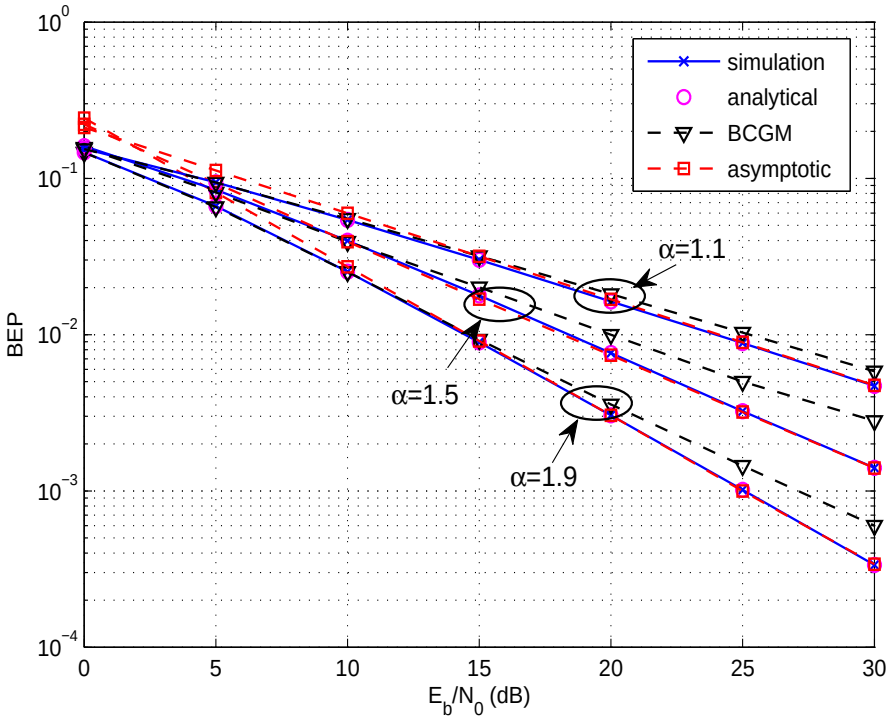

Figure 5.1: The BEP of BPSK on Rayleigh fading channels with SαS noise at $\alpha = 1.9, 1.5, 1.1$.

BEP at the high error-rate region. As an example, when $\alpha = 1.9$, the BCGM's BEP curve for uncoded BPSK closely matches the exact BEP when BEP $> 10^{-2}$. However, as SNR increases, the estimation becomes less accurate. In contrast, the asymptotic BEP closely approximates the low error-rate region of the exact BEP, but the approximation is less accurate in the high error-rate region. As presented in Fig. 5.1, for each α, the asymptotic BEP matches the exact BEP closely when the BEP is equal to or less than 10^{-2}.

5.4 BEP on Rayleigh fading channel with SαS noise with extensions to M-QAM

As we know, the the BEP of BPSK on the AWGN channel is given as

$$P_b^{\text{Gauss}} = Q\left(\sqrt{\frac{2E_b}{N_0}}\right). \tag{5.18}$$

Hence, according to (5.4), the mapping between $Q(x)$ and $Q_\alpha(x)$ is

$$Q(x) \to Q_\alpha\left(\sqrt{2C_g^{(\frac{2}{\alpha}-1)}}x\right). \tag{5.19}$$

For AWGN channels, according to [92], the closed-form BEP of M-QAM is calculated as

$$P_b^{\mathrm{M}} = \frac{2}{\sqrt{M}\log_2\sqrt{M}} \sum_{k=1}^{\left\{\log_2\sqrt{M}\right\}} \sum_{i=0}^{\left\{(1-2^{-k})\sqrt{M}-1\right\}} \left\{ f(k,i) Q\left((2i+1)\sqrt{\frac{3\Omega\log_2 M}{M-1}}\right)\right\}, \tag{5.20}$$

where $\Omega = \frac{E_b}{N_0}$ and $\lfloor x \rfloor$ is the largest integer which is not greater than x. $f(k,i)$ is defined as

$$f(k,i) = (-1)^{\left\lfloor \frac{i2^{k-1}}{\sqrt{M}} \right\rfloor} \left(2^{k-1} - \left\lfloor \frac{i2^{k-1}}{\sqrt{M}} + \frac{1}{2} \right\rfloor\right). \tag{5.21}$$

From the relationship between $Q(x)$ and $Q_\alpha(x)$, the theoretical BEP of M-QAM over SαS noise is given as

$$P_{b,\alpha}^{\mathrm{M}} = \frac{2}{\sqrt{M}\log_2\sqrt{M}} \sum_{k=1}^{\left\{\log_2\sqrt{M}\right\}} \sum_{i=0}^{\left\{(1-2^{-k})\sqrt{M}-1\right\}} \left\{ f(k,i) Q_\alpha\left((2i+1)\sqrt{\frac{6C_g^{(\frac{2}{\alpha}-1)}\Omega\log_2 M}{M-1}}\right)\right\}. \tag{5.22}$$

Hence, the exact BEP of uncoded M-QAM on Rayleigh fading channels with SαS noise is given as

$$P_{b,\alpha}^{\mathrm{M,Ray}} = \int_0^\infty P_{b|a,\alpha}^{\mathrm{M}}(\omega) p(\omega) d\omega, \tag{5.23}$$

where $p(\omega) = \frac{1}{\Omega}\exp(-\omega/\Omega)$.

5.4.1 BEP approximation from the BCGM model

The BEP of uncoded M-QAM on the SαS channel can be approximated by the BCGM model as

$$P_{b,\alpha}^{\mathrm{M,BCGM}} = \frac{2}{\sqrt{M}\log_2\sqrt{M}} \sum_{k=1}^{\left\{\log_2\sqrt{M}\right\}} \sum_{i=0}^{\left\{(1-2^{-k})\sqrt{M}-1\right\}} \left\{ f(k,i) \int_{\sqrt{g(i)\Omega}}^\infty f_{\mathrm{CG}}^s(x) dx\right\}, \tag{5.24}$$

$$P_{b,\alpha}^{\mathrm{M,Ray}} \approx \frac{1}{\Omega}\int_0^\infty P_{b|a,\alpha}^{\mathrm{M,BCGM}}(\omega)\exp(-\omega/\Omega)d\omega$$
$$= \frac{2}{\sqrt{M}\log_2\sqrt{M}} \sum_{k=1}^{\left\{\log_2\sqrt{M}\right\}} \sum_{i=0}^{\left\{(1-2^{-k})\sqrt{M}-1\right\}}$$
$$\left\{ f(k,i)\left[\frac{1-\epsilon}{2}\left(1-\sqrt{\frac{g(i)\Omega}{4+g(i)\Omega}}\right)+\frac{\epsilon}{2}\left(1-\exp\left(\frac{1}{g(i)\Omega}\right)\mathrm{erfc}\left(\sqrt{\frac{1}{g(i)\Omega}}\right)\right)\right]\right\}, \tag{5.27}$$

where

$$g(i) = \frac{6C_g^{(\frac{2}{\alpha}-1)}\log_2 M}{M-1}(2i+1)^2. \tag{5.25}$$

The exact BEP on Rayleigh fading channels with SαS noise is now approximated by using the BCGM model as

$$P_{b,\alpha}^{\mathrm{M,Ray}} \approx \frac{1}{\Omega}\int_0^\infty P_{b|a,\alpha}^{\mathrm{M,BCGM}}(\omega)\exp(-\omega/\Omega)d\omega. \tag{5.26}$$

It is observed that (5.26) contains a double integral. Similar to uncoded BPSK, a closed-form expression of BEP for M-QAM is obtained in (5.27).

5.4.2 Asymptotic performance of a Rayleigh fading channel with SαS noise

Another approximation can be obtained by using the heavy tailed property of SαS distributions. By substituting (5.15) into (5.22), we obtain the asymptotic BEP for M-QAM on SαS channels

$$P_{b,\alpha}^{\mathrm{M,asy}} = \frac{2C_\alpha}{\sqrt{M}\log_2\sqrt{M}} \sum_{k=1}^{\left\{\log_2\sqrt{M}\right\}} \sum_{i=0}^{\left\{(1-2^{-k})\sqrt{M}-1\right\}} \left\{ f(k,i)\left(g(i)\Omega\right)^{-\frac{\alpha}{2}}\right\}. \tag{5.28}$$

After the simplification, the asymptotic BEP of M-QAM on Rayleigh fading

channels with SαS noise is obtained as

$$P_{b,\alpha}^{\mathrm{M,Ray}} \to \frac{1}{\Omega}\int_0^{\infty} P_{b|a,\alpha}^{\mathrm{M,asy}}(\omega)\exp(-\omega/\Omega)d\omega$$
$$= \frac{2C_\alpha}{\sqrt{M}\log_2\sqrt{M}} \sum_{k=1}^{\{\log_2\sqrt{M}\}} \sum_{i=0}^{\{(1-2^{-k})\sqrt{M}-1\}} \left\{ f(k,i)\,(g(i)\Omega)^{-\frac{\alpha}{2}}\,\Gamma\left(1-\frac{\alpha}{2}\right)\right\}. \tag{5.29}$$

The resulting expression of the asymptotic BEP is also very simple, containing only a Gamma function. We note that for Rayleigh fading channels with slightly impulsive noise (i.e. $\alpha = 1.8$), only the first two terms ($i = 0, 1$) of (5.23), (5.27) and (5.29) are needed to provide a good estimate of the exact BEP. However, when the channel becomes very impulsive (i.e. $\alpha = 1$), more terms ($i = 0, 1, 2...$) should be included since $Q_\alpha(x)$ decays slowly for small α's as SNR increases.

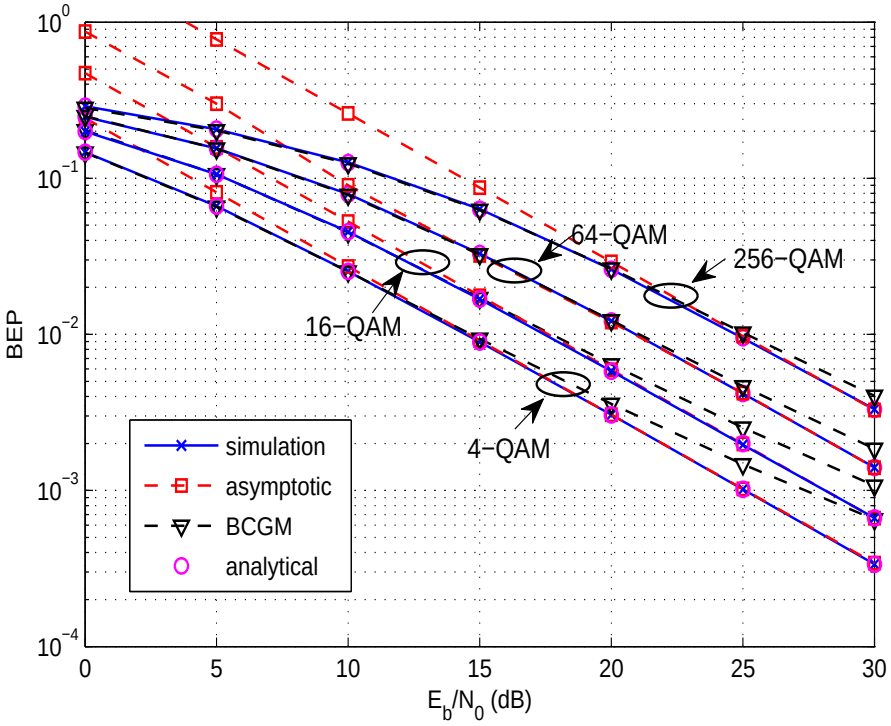

Figure 5.2: BEP of M-QAM on Rayleigh fading channels with SαS noise when $\alpha = 1.9$.

Numerical and simulated results for the exact and approximated BEP's of M-QAM on Rayleigh fading channels with SαS noise are shown in Fig 5.2 - 5.4. When the channel is slightly impulsive ($\alpha = 1.9$) or extremely impulsive ($\alpha = 1.1$), our analytic BEPs closely match the simulated BERs for different order M of QAM. The BCGM model gives a good estimation of the exact BEP at the high error-

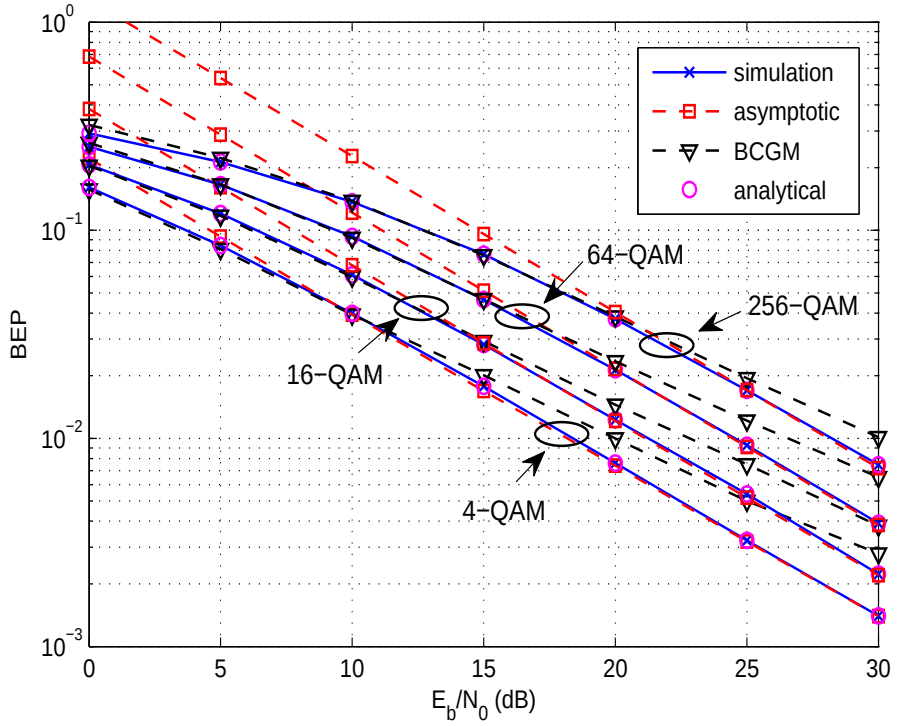

Figure 5.3: BEP of M-QAM on Rayleigh fading channels with SαS noise when $\alpha = 1.5$.

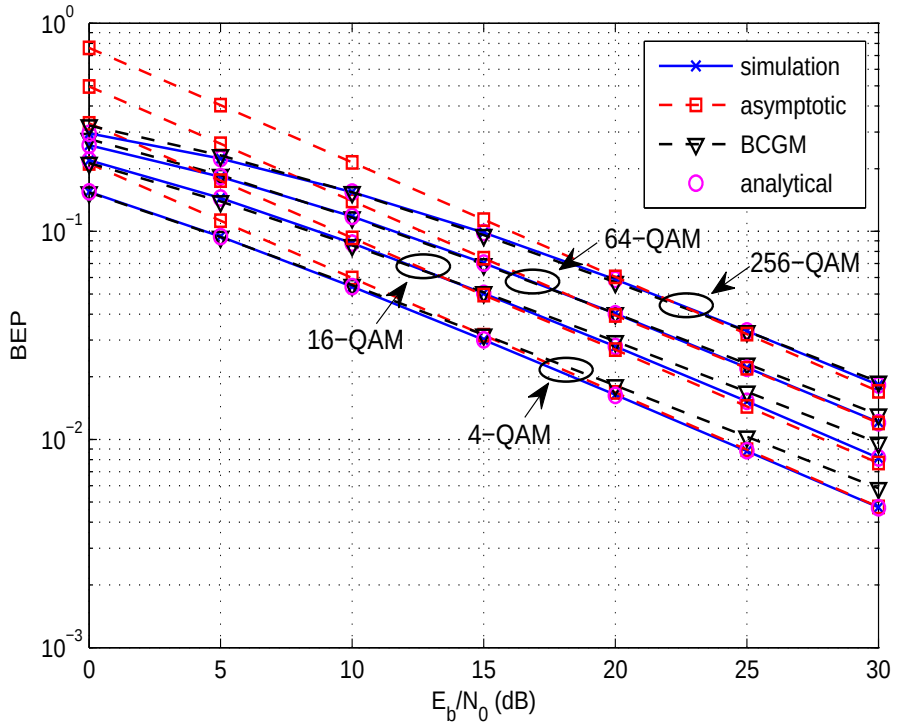

Figure 5.4: BEP of M-QAM on Rayleigh fading channels with SαS noise when $\alpha = 1.1$.

rate region, but when the SNR increases this estimation becomes less accurate. In contrast, the asymptotic BEPs approximate the low error-rate region of the exact BEPs very accurately, but are less accurate in the high error-rate region.

When the channel is moderately impulsive ($\alpha = 1.5$), our analytic BEPs still closely match the simulated BER curves in Fig. 5.3. Similar to the case of $\alpha = 1.9$ and $\alpha = 1.1$, the asymptotic BEP accurately approximates the low error-rate region of the exact BEP. However, for the BCGM model it is less accurate compared with $\alpha = 1.9$ and $\alpha = 1.1$. This is because the BCGM model can better estimate the actual SαS pdf when α is close to 2 or 1.

5.5 Performance Analysis of LDPC codes over Generalized Fading Channels with SαS noise

5.5.1 Asymptotic performance of LDPC codes

As discussed in previous sections, only DE is valid for BMSC and it can be adopted here to calculate the threshold SNR of a specific ensemble of LDPC codes. DE tracks the change of LLRs during the Sum-Product decoding process which has been described in Chapter 3. In this section, we will show how to use DE for uncorrelated generalized fading channels with SαS noise.

DE assumes that the channel output is symmetric and here we prove the symmetry property for fading channels with SαS noise as follows:

$$\begin{aligned} P(y|x=1,a) &= \frac{1}{2\pi}\int_{-\infty}^{\infty} \exp(-\gamma^{\alpha}|t|^{\alpha}) e^{-jt(y-a)} dt \\ &= \frac{1}{2\pi}\int_{-\infty}^{\infty} \exp(-\gamma^{\alpha}|t|^{\alpha}) e^{-jt[-(y-a)]} dt \\ &= P(-y|x=-1,a), \end{aligned} \tag{5.30}$$

hence $P(y|x=1) = P(-y|x=-1)$. If we know the side information (SI), the initial message $v^{(0)}$ is given as

$$v^{(0)} = \ln \frac{P(x=+1|y,a)}{P(x=-1|y,a)} = \ln \frac{f_{\alpha}(y-a;\gamma)}{f_{\alpha}(y+a;\gamma)}. \tag{5.31}$$

The pdf of (5.31) has no analytic expression except for $\alpha = 2$ which cannot be

calculated numerically, hence, a Monte-Carlo simulation with a histogram method is used to obtain the conditional density function $p(v^{(0)}|a)$ of $v^{(0)}$. Finally, to obtain the unconditional density function of $v^{(0)}$, we average $p(v^{(0)}|a)$ over the pdf of a as

$$p_v^{(0)} = \int_0^\infty p(v^{(0)}|a)p(a)da, \tag{5.32}$$

where $p(a)$ is the pdf of the fading amplitude a. After the calculation of the pdf of the initial LLR, the DE of the check node update and variable node update are the same as we previously introduced.

The optimal receiver in (5.31) requires the calculation of the pdf of SαS noise which has a high complexity and is not practical. Hence some sub-optimal receivers are required to reduce the computational cost but achieve good performance. In this chapter, two types of sub-optimal receivers are examined for generalized fading channels with SαS channels. The first type of sub-optimal receiver approximates the SαS pdf by a closed-form expression, such as the BCGM model [91] and the Cauchy distribution. The other type of sub-optimal receivers employs simple non-linear operations such as hole-punching or clipping on the received signal or the LLR to reduce the effect of the presence of impulses. In Chapter 4, our DE method has shown its effectiveness for these sub-optimal receivers. For fading channels, it is still applicable as a tool to analyze the asymptotic performance of LDPC codes. Similar to optimal receivers, the conditional pdf $p(v^{(0)}|a)$ of $v^{(0)}$ for sub-optimal receivers should be calculated by a simulation-based approach.

5.5.2 Waterfall Performance Analysis of LDPC codes

As in Chapter 4, we define the observed BER $P_{b,\text{obs}}^{\alpha}$ as the BER of any received codeword of length N, implying $P_{b,\text{obs}}^{\alpha}$ is a random variable. Each bit of the codeword has a probability $P_b^{\alpha,\text{F}}$ of being in error and the probability mass function (pmf) is obtained as

$$f_{P_{b,\text{obs}}^{\alpha}}(N, P_{b,\text{obs}}^{\alpha}) = \binom{N}{K}(P_b^{\alpha,\text{F}})^K(1-P_b^{\alpha,\text{F}})^{N-K}, \tag{5.33}$$

where $K = NP_{b,\text{obs}}^{\alpha}$ is the number of errors in a codeword of length N, which follows a binomial distribution $B(N, P_b^{\alpha,\text{F}})$. When $N \to \infty$, the pmf of K becomes a Gaussian distribution $\mathcal{N}(NP_b^{\alpha,\text{F}}, NP_b^{\alpha,\text{F}}(1-P_b^{\alpha,\text{F}}))$. Hence the pdf of $P_{b,\text{obs}}^{\alpha}$ can be

approximated by $\mathcal{N}(P_b^{\alpha,\mathrm{F}}, P_b^{\alpha,\mathrm{F}}(1-P_b^{\alpha,\mathrm{F}})/N)$.

To find P_B^α of a specific ensemble of LDPC codes, first the threshold γ_{th} for an ensemble of LDPC codes is obtained through DE. Then the obtained threshold dispersion is used to calculate the corresponding threshold BEP P_{th}. According to (5.5), we have

$$P_{\mathrm{th}} = \int_0^\infty Q_\alpha\left(\sqrt{4R_c C_g^{(\frac{2}{\alpha}-1)}\omega}\right) p\left(\omega; \left(\frac{E_b}{N_0}\right)_{\mathrm{th}}\right) d\omega, \tag{5.34}$$

where $\left(\frac{E_b}{N_0}\right)_{\mathrm{th}}$ is the corresponding threshold SNR defined by γ_{th}. Then the block-error probability is obtained by calculating the probability that $P_{b,\mathrm{obs}}^\alpha > P_{\mathrm{th}}$.

$$\begin{aligned} P_{\mathrm{B}}^\alpha(N,\lambda,\rho) &= \int_{P_{\mathrm{th}}}^1 f_{P_{b,\mathrm{obs}}^\alpha}(N,x)dx \\ &= Q\left(\frac{P_{\mathrm{th}} - \mu_{P_{b,\mathrm{obs}}^\alpha}}{\sigma_{P_{b,\mathrm{obs}}^\alpha}}\right), \end{aligned} \tag{5.35}$$

where $P_{\mathrm{B}}^\alpha(N,\lambda,\rho)$ is our estimated block error probability for an ensemble of LDPC codes with block length N and degree distributions $\lambda(x)$ and $\rho(x)$. Also, $\mu_{P_{b,\mathrm{obs}}^\alpha} = P_b^{\alpha,\mathrm{F}}$ and $\sigma_{P_{b,\mathrm{obs}}^\alpha} = P_b^{\alpha,\mathrm{F}}(1-P_b^{\alpha,\mathrm{F}})/N$.

The bit-error probability $P_{\mathrm{b}}^\alpha(N,\lambda,\rho)$ can be derived from $P_{\mathrm{B}}^\alpha(N,\lambda,\rho)$. Each block has probability $P_{\mathrm{B}}^\alpha(N,\lambda,\rho)$ of being in error, hence the coded BEP is given as

$$P_{\mathrm{b}}^\alpha(N,\lambda,\rho) = P_e^{(l_{\max})} P_{\mathrm{B}}^\alpha(N,\lambda,\rho). \tag{5.36}$$

5.6 Results and Discussion

5.6.1 Uncoded BER for fading channels with SαS noise

As shown in Fig. 5.5-5.7, the analytic BEP closely matches the simulated BER for Rician, Nakagami-m and Rayleigh fading channels with SαS noise for different levels of impulsiveness. Another observation is when the degradation caused by fading is not very strong, even very slightly impulsive noise will severely degrade the performance at low values of SNR. For example, even when $\alpha = 1.99$, there are very few impulses but it leads to a 6dB degradation at BER $= 10^{-5}$ compared with Gaussian noise ($\alpha = 2$) on Rician fading channels. When the fading effect becomes stronger, this performance loss due to impulsive noise becomes smaller. As shown

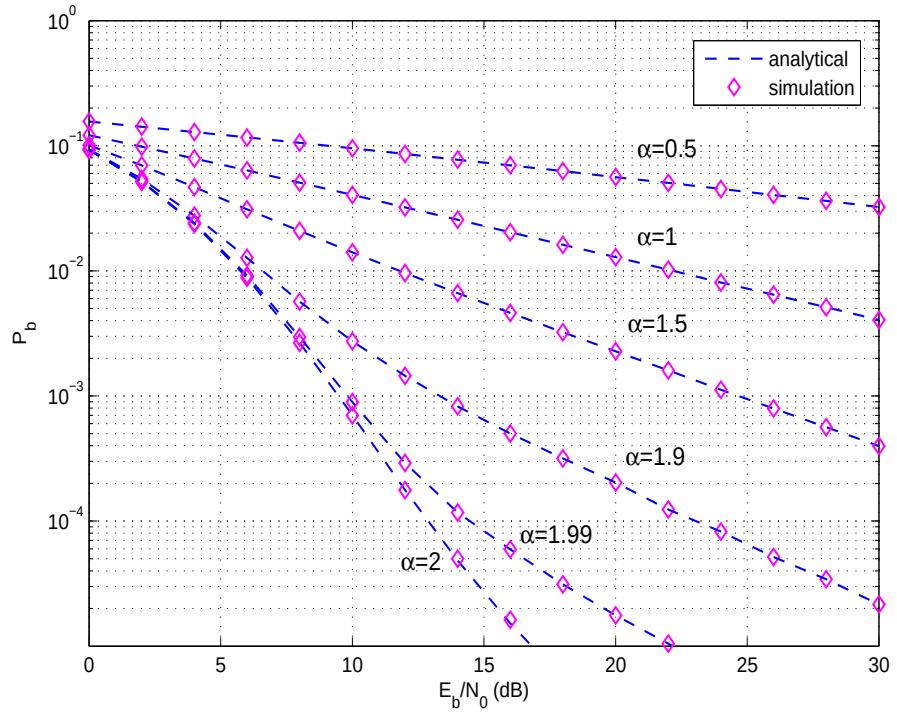

Figure 5.5: Uncoded performance of BPSK on the Rician fading channel ($K = 10$) with SαS noise at $\alpha = 2, 1.99, 1.9, 1.5, 1$ and 0.5 respectively.

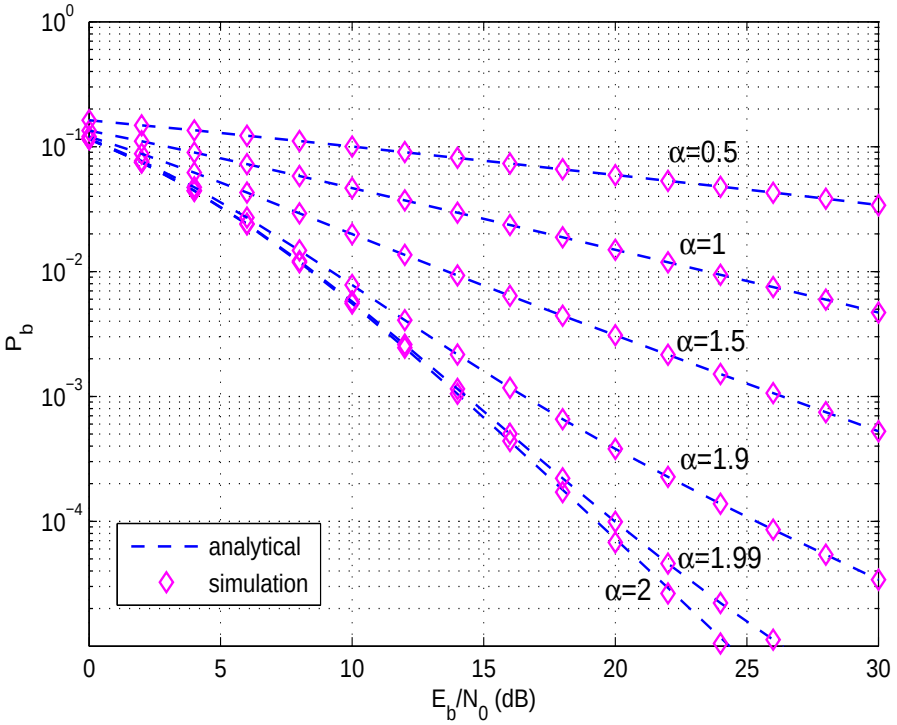

Figure 5.6: Uncoded performance of BPSK on the Nakagami-m fading channel ($m = 2$) with SαS noise at $\alpha = 2, 1.99, 1.9, 1.5, 1$ and 0.5 respectively.

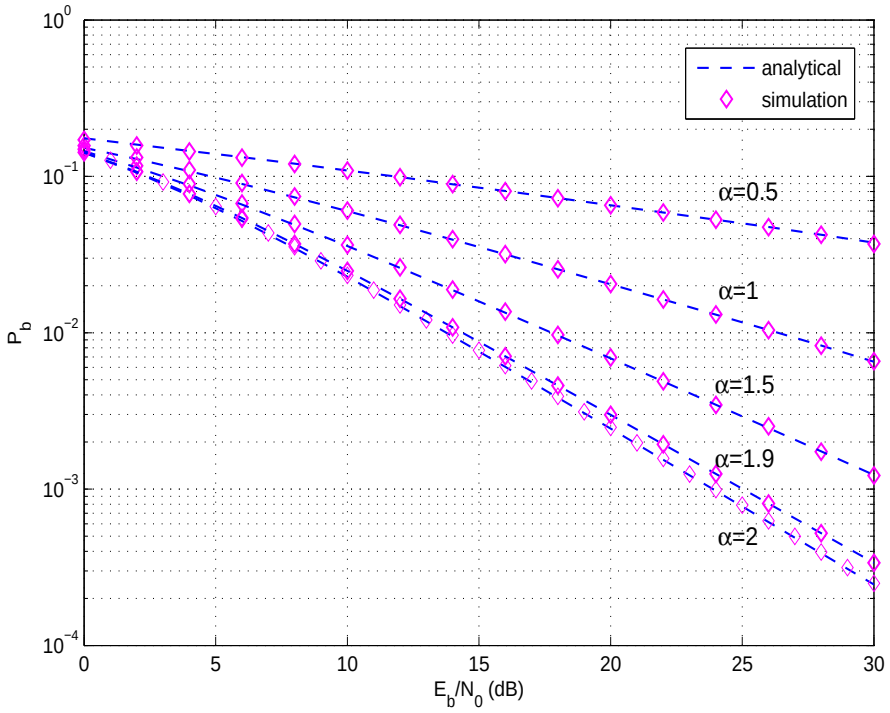

Figure 5.7: Uncoded performance of BPSK on the Rayleigh fading channel with SαS noise at $\alpha = 2, 1.9, 1.5, 1$ and 0.5 respectively.

in Fig. 5.6, the loss is about only 2 dB for Nakagami-m fading with $m = 2$. For the Rayleigh fading channel, which is a special case of Nakagami-m fading with $m = 1$, the influence of slightly impulsive noise is not obvious. As illustrated in 5.7, even when $\alpha = 1.9$, the performance loss due to impulses is small.

When the SαS channel is very impulsive ($\alpha = 1$), it always leads to a large performance degradation for different fading channels. For example, the gap at BER $= 10^{-2}$ between $\alpha = 1$ and $\alpha = 2$ for Rician, Nakagami-m and Rayleigh fading channels are 16, 15 and 12 dB, respectively.

5.6.2 Coded BER for fading channels with SαS noise

In this section, the asymptotic and waterfall performance of regular and irregular LDPC codes on fading channels with SαS noise will be investigated by numerical and simulated results. The rate 1/2 regular $(3, 6)$ LDPC codes and irregular LDPC codes with two pairs of degree distributions $\lambda(x) = 0.247x + 0.339x^2 + 0.414x^3$, $\rho(x) = 0.1x^4 + 0.9x^5$ and $\lambda(x) = 0.4x^2 + 0.4x^5 + 0.2x^8$, $\rho(x) = x^8$ are considered with the following block sizes: $N = 1000, 4000, 20000$. LDPC codes with short and medium code length ($N \leq 4000$ bits) are constructed using the PEG algorithm [1] to

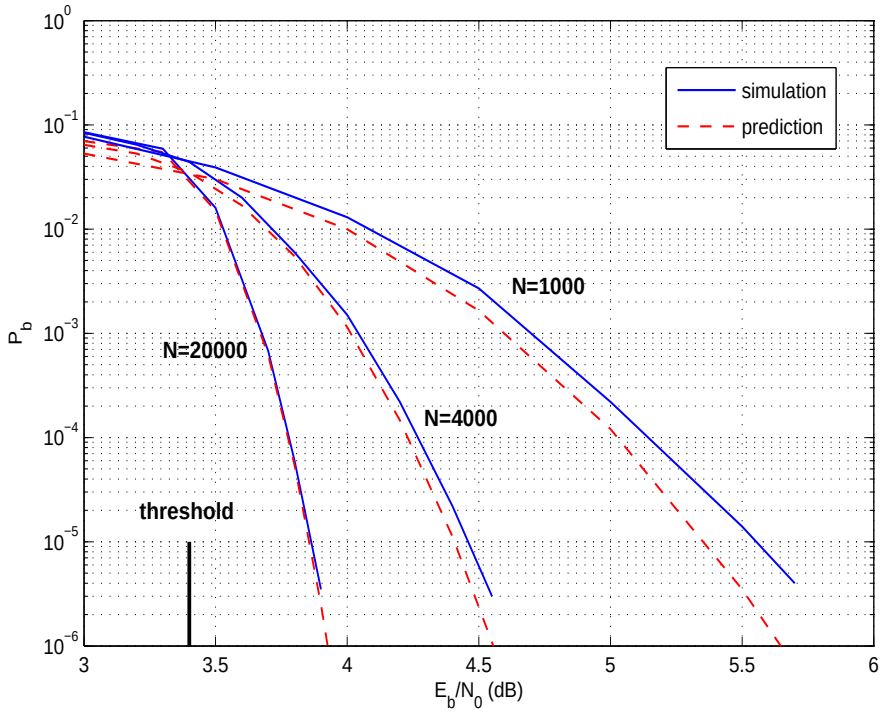

Figure 5.8: Performance of regular LDPC codes with different length on Rayleigh fading channels with SαS noise at $\alpha = 1.9$.

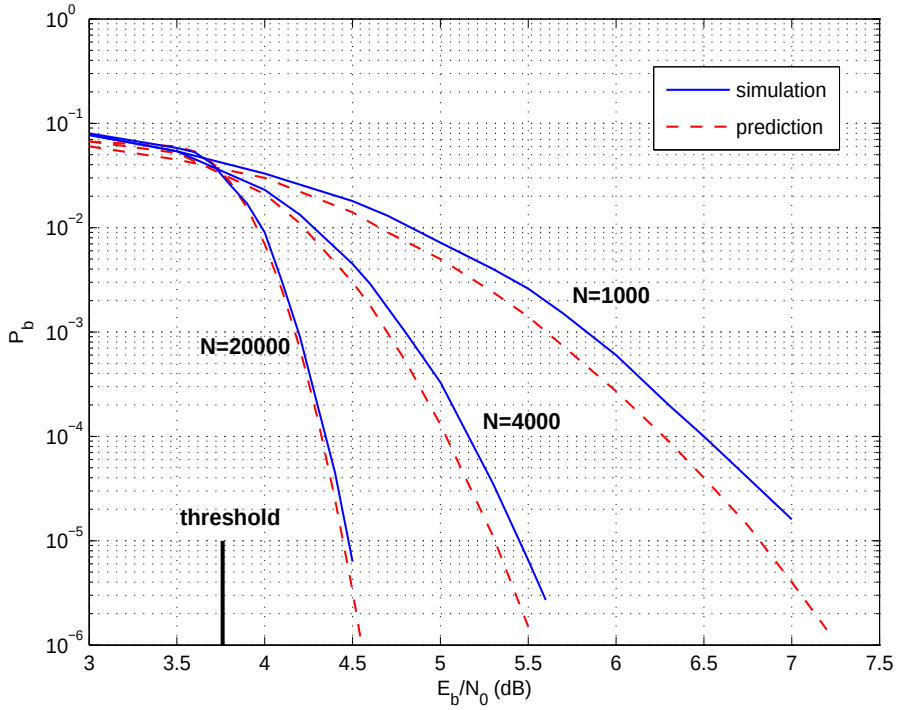

Figure 5.9: Performance of regular LDPC codes with different length on Rician fading channels ($K = 10$) with SαS noise at $\alpha = 1$.

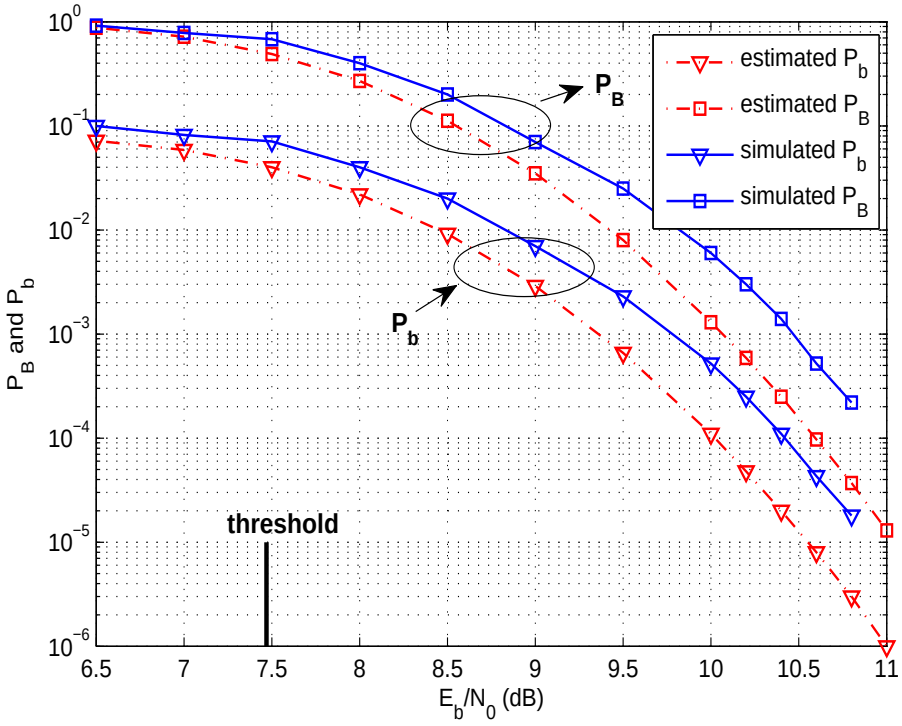

Figure 5.10: Block and bit error probability of irregular LDPC codes ($N = 4000$) with degree distributions $\lambda(x) = 0.4x^2+0.4x^5+0.2x^8$ and $\rho(x) = x^8$ on Nakagami-m fading channels ($m = 3$) with SαS noise at $\alpha = 0.5$.

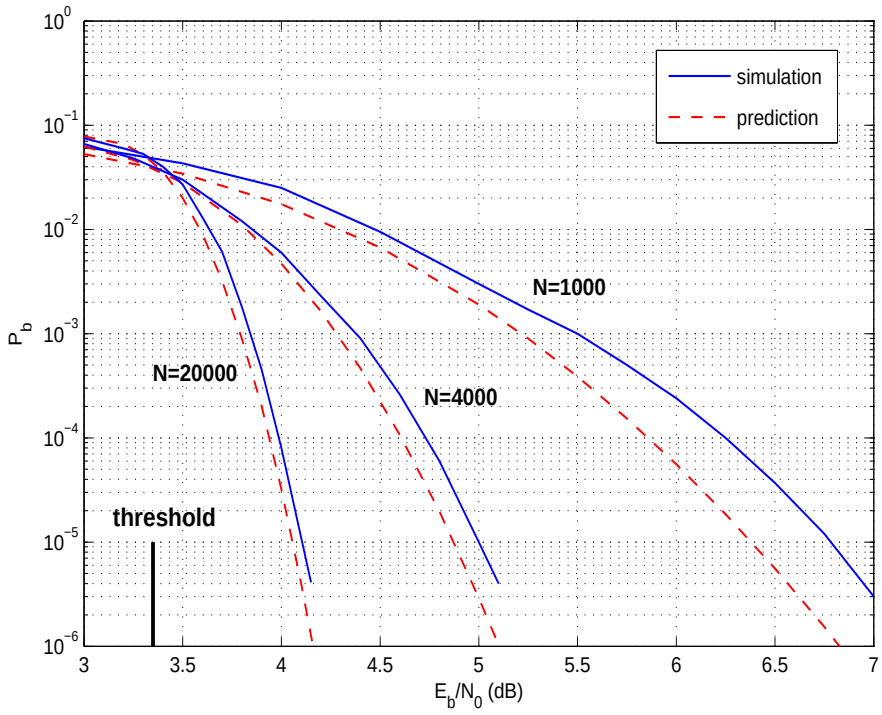

Figure 5.11: Performance of irregular LDPC codes with degree distributions $\lambda(x) = 0.247x + 0.339x^2 + 0.414x^3$ and $\rho(x) = 0.1x^4 + 0.9x^5$ on Rician fading channels ($K = 10$) with SαS noise at $\alpha = 1$.

maximizes the girth properties. For long LDPC codes ($N = 20000$), we use Mackay's construction method since the PEG's complexity is too high when constructing long codes. The maximum number of the decoding iterations is set to 100.

As shown in Fig. 5.8-5.9, the numerical results from our analytic expression accurately predict the performance of finite length regular $(3, 6)$ LDPC codes with different lengths on Rayleigh fading channels and Rician fading channels with SαS noise at different degrees of impulsiveness ($\alpha = 1.9$ and $\alpha = 1$, respectively). As the code length increases, the prediction becomes more and more accurate. When $N = 20000$, our prediction are almost identical to the simulation results. To adopt more generalizations, more case studies are presented to verify our analysis for irregular LDPC codes. As shown in Fig. 5.10, both our analytic block and bit error probability have closely predicted the simulated BER for $\alpha = 0.5$. The analytic P_b presents a 0.3 dB gap to the simulation result while the asymptotic performance is about 3.3 dB away from the practical performance at BER = 10^{-5}. As given in Fig. 5.11, our analysis is still effective for different lengths of LDPC codes and for a different irregular LDPC ensemble.

As we observed, the gap between the predicted and simulated results is larger for LDPC codes with shorter code length. The reason is that the pdf of $P^{\alpha}_{b,\text{obs}}$ is not well approximated by a Gaussian distribution when N is small. In addition, short cycles appear more frequently for short LDPC codes, which will degrade performance. As the concentration theorem states, the average behavior of LDPC codes concentrates around its expected behavior as the code length increases and this average behavior converges to cycle-free case [41].

In Fig. 5.12, we investigate the finite length performance of LDPC codes ($N = 20000$) with optimal and sub-optimal receivers (optimal, BCGM, Cauchy and clipper [71]) on Nakagami-m ($m = 2$) fading channels with moderate impulsive noise ($\alpha = 1.43$). The value of α is selected from [5] which is used to model the impulsiveness in wireless transceivers. Fig. 5.12 shows the thresholds of optimal sub-optimal receivers as well as the waterfall region estimation of each receiver, which is denoted by the dashed lines. The simulation results can verify the threshold obtained from DE and the waterfall performance estimation. One exception is the clipper, where the waterfall performance prediction is not as accurate as other receivers. The reason is due to the Gaussian assumption not holding in this situation when non-linear operations like clipping are performed on the LLRs. Nevertheless, even for

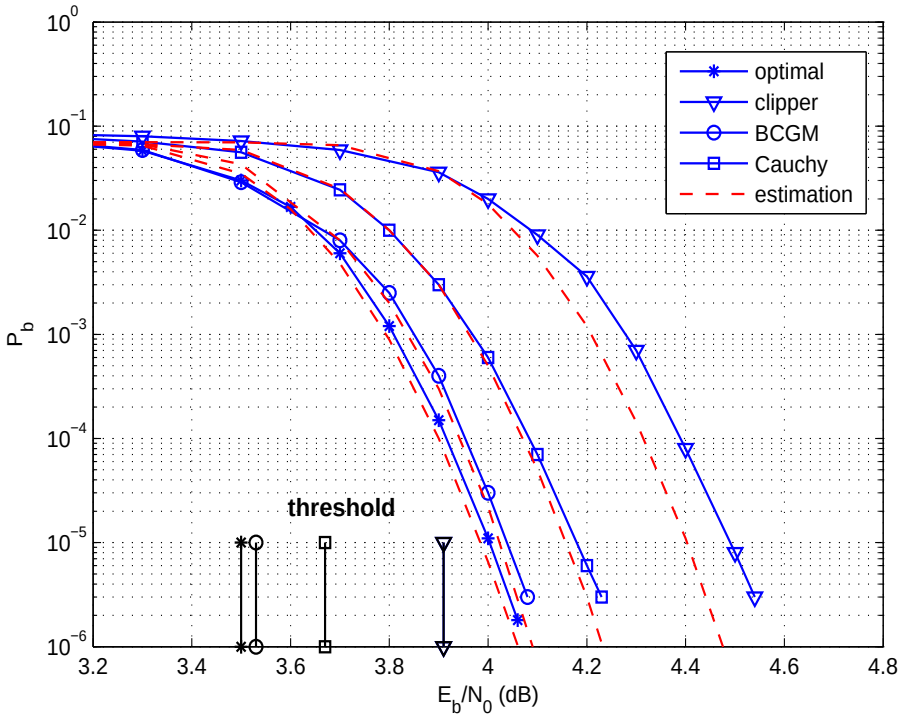

Figure 5.12: Performance of regular LDPC codes with different receivers on Nakagami-m ($m = 2$) fading channels with SαS noise at $\alpha = 1.43$.

the clipper, our estimation is still much closer to the simulated performance than the threshold.

5.7 Conclusion

In this chapter, we derive the theoretical BEP of the uncoded and coded BEP of generalized fading channels with SαS noise. Due to the high complexity in the calculation of the exact BEP, two closed-form approximations are proposed on Rayleigh fading channels with SαS noise, based on the BCGM model and an asymptotic approximation. The numerical and simulated results show that the BCGM model matches the high error-rate region of the exact BEP curve and becomes less accurate in the low error-rate region. In contrast, the asymptotic BEP can provide a good approximation for the exact BEP in the low error-rate region.

In terms of the LDPC coded performance, a DE analysis is performed to find the asymptotic performance of LDPC codes with optimal and sub-optimal receivers. Then, we accurately predict the waterfall performance of finite length LDPC codes on these channels by modeling the BER of each codeword as a random variable. As the code length increases, the accuracy of the predicted waterfall region compared

with the simulated BERs increases. At long block lengths ($N = 20000$ bits), the estimated bit error probabilities are almost identical to the simulated bit error rates, showing that our work is a useful tool to predict the actual performance of LDPC codes on fading channels with additive impulsive noise.

5.8 Appendix

5.8.1 Derivation of (5.12)

The standard BCGM distribution can be written by the sum of two SαS distributions:

$$\begin{aligned} f_{\mathrm{CG}}^{s} &= (1-\epsilon)\frac{1}{2\sqrt{\pi}}\exp\left(-\frac{x^2}{4}\right) + \epsilon\frac{1}{\pi(x^2+1)} \\ &= (1-\epsilon) f_{\alpha=2}(x;0,1) + \epsilon f_{\alpha=1}(x;0,1). \end{aligned} \tag{5.37}$$

Hence (5.12) can be simplified as

$$\begin{aligned} P_b^{\alpha,\mathrm{Ray}} &\approx \frac{1}{\Omega}\int_0^{\infty}\left(\int_{\sqrt{4C_1\omega}}^{\infty} f_{\mathrm{CG}}^{s}(t)dt\right)\exp\left(-\frac{\omega}{\Omega}\right)d\omega \\ &= \frac{1-\epsilon}{\Omega}\int_0^{\infty}\left(\int_{\sqrt{4C_1\omega}}^{\infty} f_{\alpha=2}(t;0,1)dt\right)\exp\left(-\frac{\omega}{\Omega}\right)d\omega \\ &+ \frac{\epsilon}{\pi\Omega}\int_0^{\infty}\left(\int_{\sqrt{4C_1\omega}}^{\infty} f_{\alpha=1}(t;0,1)dt\right)\exp\left(-\frac{\omega}{\Omega}\right)d\omega \\ &= P_b^{\mathrm{G}} + P_b^{\mathrm{C}}, \end{aligned} \tag{5.38}$$

where P_b^{G} is the component of BEP for Gaussian noise and P_b^{C} is the component of BEP for Cauchy noise on Rayleigh fading channels.

Since $0 < \omega < \infty$ and $\sqrt{4C_1\omega} \le t < \infty$, thus we have $0 < \omega \le t^2/4C_1$, where $C_1 = C_g^{(\frac{2}{\alpha}-1)}$. Then P_b^{G} is calculated as

$$\begin{aligned} P_b^{\mathrm{G}} &= \frac{1-\epsilon}{\Omega}\int_0^{\infty}\frac{1}{2\sqrt{\pi}}\exp\left(-\frac{t^2}{4}\right)\left(\int_0^{\frac{t^2}{4C_1}}\exp\left(-\frac{\omega}{\Omega}\right)d\omega\right)dt \\ &= \frac{1-\epsilon}{2\sqrt{\pi}}\int_0^{\infty}\exp\left(-\frac{t^2}{4}\right)\left(1-\exp\left(-\frac{t^2}{4C_1\Omega}\right)\right)dt \\ &= \frac{1-\epsilon}{2}\left(1-\sqrt{\frac{C_1\Omega}{1+C_1\Omega}}\right). \end{aligned}$$

Similar to P_b^{G}, P_b^{C} is calculated as

$$\begin{aligned} P_b^{\mathrm{C}} &= \frac{\epsilon}{\pi\Omega}\int_0^{\infty}\left(\int_{\sqrt{4C_1\omega}}^{\infty}\frac{1}{1+t^2}dt\right)\exp\left(-\frac{\omega}{\Omega}\right)d\omega \\ &= \frac{\epsilon}{\pi\Omega}\int_0^{\infty}\left(\int_0^{\frac{t^2}{4C_1}}\exp\left(-\frac{\omega}{\Omega}\right)d\omega\right)\frac{1}{1+t^2}dt \\ &= \frac{\epsilon}{2}\left(1-\exp\left(\frac{1}{4C_1\Omega}\right)\mathrm{erfc}\left(\sqrt{\frac{1}{4\mathrm{C}_1\Omega}}\right)\right) \end{aligned} \tag{5.39}$$

5.8.2 Derivation of (5.17)

In this Appendix, we simplify (5.17). The asymptotic BEP of uncoded BPSK on Rayleigh fading channels with SαS noise is given as

$$\begin{aligned} P_b^{\alpha,\mathrm{Ray}} &\to \int_0^{\infty} C_\alpha\left(\sqrt{4C_1\omega}\right)^{-\alpha}p(\omega)d\omega \\ &= \frac{C_\alpha}{(4C_1)^{\frac{\alpha}{2}}\,\Omega}\int_0^{\infty}\omega^{-\frac{\alpha}{2}}\exp(-\frac{\omega}{\Omega})d\omega \\ &= \frac{C_\alpha}{(4C_1\Omega)^{\frac{\alpha}{2}}}\int_0^{\infty}t^{-\frac{\alpha}{2}}\exp(-t)dt \\ &= \frac{C_\alpha}{(4C_1\Omega)^{\frac{\alpha}{2}}}\Gamma\left(1-\frac{\alpha}{2}\right) \end{aligned} \tag{5.40}$$

Chapter 6

Performance Analysis of LDPC-Coded Diversity Combining on Rayleigh Fading Channels with Impulsive Noise

6.1 Introduction

Diversity combining is an important technique that combats fading effects by exploiting spatial diversity. Conventional combining schemes such as MRC, EGC and SC are selected depending on the required trade-off between performance and complexity at the receiver. Conventionally, the noise added at each branch of the diversity combiner is assumed to be Gaussian. However, there are many applications where the interference can exhibit an impulsive behavior and it is important to take this impulsive nature into account when analyzing spatial diversity.

The contributions of this chapter are as follows: First, the analytic or semi-analytic BEPs of SC, EGC and MRC on Rayleigh fading channels with SαS noise with independent components are derived. In addition, the relationship of different combiners in terms of SNR is derived, regardless of fading types. Second, the asymptotic and waterfall performance of LDPC codes with different linear combiners on these channels is investigated in this chapter. Finally, a non-linear detector based on the bi-parameter Cauchy-Gaussian mixture (BCGM) model [91] is used to achieve near-optimal performance with a significantly reduced complexity than the

optimal detector.

6.2 System and Channel Models

6.2.1 Channel Model and SαS distributions

In this chapter, we consider a single-input-mutiple-output (SIMO) system where the transmitted signal is received over L_r independent flat Rayleigh fading channels. Assuming perfect phase and timing synchronization, the received signal of the l-th branch can be modeled as

$$r_l = h_l x + n_l, \quad 1 \leq l \leq L_r, \tag{6.1}$$

where r_l, h_l and n_l denote the received signal, channel gain and additive noise for the l-th branch, respectively. $h_l = a_l e^{j\phi_l}$ is the complex Gaussian channel gain, where a_l is Rayleigh distributed and ϕ_l is the phase of h_l. We also assume that $\{a_l\}_{l=1}^{L}$ are i.i.d. variables with $\mathbb{E}[a_l^2] = 1$. n_l is the SαS noise where the real and imaginary components are i.i.d. and follow the univariate SαS distribution. SαS distributed random variables share many interesting properties, which have been described in the Chapter 3. Here we recall three important properties that will be used in this chapter:

Property 1. If $v_i \sim S(\alpha, 0, 0, \gamma_i)$, $i = 1, 2, \cdots, N$, then $\sum_{i=1}^{N} v_i \sim S(\alpha, 0, 0, \gamma)$, where $\gamma = \left(\sum_{i=1}^{N} \gamma_i^{\alpha}\right)^{\frac{1}{\alpha}}$.

Property 2. Let $v \sim S(\alpha, 0, 0, \gamma)$ and c is an arbitrary constant. Then $cv \sim S(\alpha, 0, 0, |c|\gamma)$.

Property 3. Any real SαS random variable $v \sim S(\alpha, 0, 0, \gamma)$ can be written as $v = \sqrt{B}G$, where B and G are independent, with $B \sim S(\alpha/2, 1, 0, [\cos(\pi\alpha/4)]^{2/\alpha})$ and G is a Gaussian random variable with zero mean and variance σ^2.

According to Property 3, the complex SαS noise with i.i.d. components can be

described as

$$n_l = \sqrt{B_1}G_1 + j\sqrt{B_2}G_2, \tag{6.2}$$

where B_1 and B_2 are i.i.d. and have the same distribution as B. G_1 and G_2 are i.i.d. Gaussian random variables which follow $\mathcal{N}(0, \sigma^2)$. The SαS noise is assumed to be independent from channel to channel. The instantaneous SNR of the l-th branch is $\eta_l = (a_l^2 E_s)/N_l$, where E_s is the energy of the modulated symbol and N_l is the noise power for the l-th channel.

In the receiver, the noise parameters α and γ are usually not known. However, in the detection of SαS noise, the knowledge of parameters is very important since most soft detectors and decoders require knowledge of the noise statistics. Hence, parameter estimation methods are required. In Chapter 3, a fast estimation method [87] based on the extreme value theory was introduced. In this chapter, the LDPC-coded performance with exact and estimated parameters will be shown in the result section.

6.3 Uncoded BEP Analysis of Diversity Combining on Rayleigh fading channels with AWSαSN

In this section, the uncoded BEP of several linear diversity combining methods (SC, EGC and MRC) on Rayleigh fading channels with SαS noise will be derived analytically and semi-analytically. As discussed in previous chapters, the geometric SNR ($\mathrm{SNR_G}$) is used since the second order moment of SαS random variables does not exist. For a coded system, $\frac{E_b}{N_0}$ for BPSK modulation is defined as

$$\frac{E_b}{N_0} = \frac{1}{4R_c C_g^{(\frac{2}{\alpha}-1)}\gamma^2}, \tag{6.3}$$

where R_c is the code rate. The uncoded BEP of a point-to-point system on SαS channels has also been derived in Chapter 4 and is given as

$$P_{b,\alpha} = Q_\alpha\left(\frac{1}{\gamma}\right) = Q_\alpha\left(\sqrt{4R_c C_g^{(\frac{2}{\alpha}-1)}\frac{E_b}{N_0}}\right). \tag{6.4}$$

With the value of geometric SNR and derived $P_{b,\alpha}$, the uncoded BEP of conventional linear diversity combining schemes (SC, EGC and MRC) can be determined.

6.3.1 Uncoded BEP of Selection Combining

For SC, only the channel with the maximum output SNR is chosen and the combined signal y is given as

$$y = \sum_{l=1}^{L_r} w_l r_l = w_k r_k, \tag{6.5}$$

where

$$w_k = \begin{cases} 1, & \text{if } \eta_k = \max\limits_{l} \{\eta_l\} \\ 0, & \text{otherwise} \end{cases},$$

and $\eta_l = a_l^2 \frac{E_b}{N_0}$ is the output SNR of the l-th branch. Hence, the combined signal y can also be rewritten as

$$y = h_{\text{sc}} x + n_{\text{sc}}, \tag{6.6}$$

where $h_{\text{sc}} = a_{\text{sc}} e^{j\phi_{\text{sc}}}$ and n_{sc} are the channel gain and the noise of the branch with the largest output SNR, respectively. When we consider the fading effect, the uncoded BEP we obtained in (6.4) becomes a conditional BEP and it is denoted as

$$P_{b|a_{\text{sc}},\alpha}(\eta) = Q_\alpha \left(\sqrt{4R_c C_g^{(\frac{2}{\alpha}-1)} \eta} \right), \tag{6.7}$$

where $\eta = a_{\text{sc}}^2 \frac{E_b}{N_0}$. Since h_{sc} is random, (6.7) is then averaged over the pdf of η to obtain the unconditional BEP. The final expression of the uncoded BEP for SC on Rayleigh fading channels with AWSαSN is given as

$$\begin{aligned} P_{b,\alpha}^{\text{SC}} &= \int_0^\infty P_{b|a_{\text{sc}},\alpha}(\eta) p(\eta; \overline{\eta}) d\eta \\ &= \int_0^\infty Q_\alpha \left(\sqrt{4R_c C_g^{(\frac{2}{\alpha}-1)} \eta} \right) p(\eta; \overline{\eta}) d\eta, \end{aligned} \tag{6.8}$$

where $p(\eta; \overline{\eta})$ is the pdf of η for SC and $\overline{\eta} = \frac{E_b}{N_0}$. For SC, $p(\eta; \overline{\eta})$ can be obtained from the outage probability. The outage probability of SC on Rayleigh fading channels is given as

$$P_{\text{out}}(\eta_s) = P\left[\eta < \eta_s\right] = \prod_{l=1}^{L_r} P\left[\eta_l < \eta_s\right] = \left(1 - e^{-\eta_s/\overline{\eta}}\right)^{L_r}. \tag{6.9}$$

It is known that $P_{\text{out}}(\eta_s)$ also represents the cdf of the output SNR as a function of the threshold η_s. Hence, the pdf of the output SNR can be calculated by differenti-

ating (6.9). The resulting $p(\eta;\overline{\eta})$ is given as

$$p(\eta;\overline{\eta}) = \frac{dP_{\text{out}}(\eta)}{d\eta} = \frac{L_r}{\overline{\eta}} e^{-\eta/\overline{\eta}} \left(1 - e^{-\eta/\overline{\eta}}\right)^{L_r - 1}. \tag{6.10}$$

By substituting (6.10) to (6.8), the analytic BEP for SC can be obtained.

6.3.2 Uncoded BEP of Equal-Gain Combining

For EGC, all branches have the same unit gain and the combined signal y is obtained by dividing the received signal r_l by the phase of h_l:

$$y = \sum_{l=1}^{L_r} e^{-j\phi_l} r_l = x \sum_{l=1}^{L_r} a_l + \sum_{l=1}^{L_r} \tilde{n}_l, \tag{6.11}$$

where $\tilde{n}_l = n_l e^{-j\phi_l}$. If we represent the combined channel gain of EGC by a_{egc}, the combined signal y in (6.11) is rewritten as

$$y = a_{\text{egc}} x + n_{\text{egc}}, \tag{6.12}$$

where $a_{\text{egc}} = \sum_{l=1}^{L_r} a_l$ and $n_{\text{egc}} = \sum_{l=1}^{L_r} \tilde{n}_l$. In addition, $\tilde{n}_l = n_l e^{-j\phi_l}$ is also SαS distributed with the same α and γ as n_l. The proof is given in the Appendix. Hence, according to Property 1, $n_{\text{egc}} \sim S(\alpha, 0, \gamma_{\text{egc}}, 0)$, where the dispersion of n_{egc} is given as

$$\gamma_{\text{egc}} = L_r^{1/\alpha} \gamma. \tag{6.13}$$

Hence, the conditional BEP for EGC is given as

$$\begin{aligned} P_{b|a_{\text{egc}},\alpha} &= Q_\alpha \left(L_r^{-\frac{1}{\alpha}} \sqrt{4 R_c C_g^{(\frac{2}{\alpha}-1)} \frac{a_{\text{egc}}^2 E_b}{N_0}} \right) \\ &= Q_\alpha \left(a_{\text{egc}} L_r^{-\frac{1}{\alpha}} \sqrt{4 R_c C_g^{(\frac{2}{\alpha}-1)} \frac{E_b}{N_0}} \right). \end{aligned} \tag{6.14}$$

Finally, the uncoded BEP for EGC on Rayleigh fading channels with AWSαSN is calculated as

$$\begin{aligned} P_{b,\alpha}^{\text{EGC}} &= \int_0^\infty P_{b|a_{\text{egc}},\alpha} p(a_{\text{egc}}) da_{\text{egc}} \\ &= \int_0^\infty Q_\alpha \left(a_{\text{egc}} L_r^{-\frac{1}{\alpha}} \sqrt{4 R_c C_g^{(\frac{2}{\alpha}-1)} \frac{E_b}{N_0}} \right) p(a_{\text{egc}}) da_{\text{egc}}, \end{aligned} \tag{6.15}$$

$$p(a_{\text{egc}}) = \frac{a_{\text{egc}}^{(2L_r-1)} e^{-\frac{a_{\text{egc}}^2}{2b}}}{2^{L_r-1} b^{L_r} (L_r-1)!} - \frac{(a_{\text{egc}}-a_2)^{(2L_r-2)} e^{-\frac{a_1(a_{\text{egc}}-a_2)^2}{2b}}}{2^{(L_r-1)} b \left(\frac{b}{a_1}\right)^{L_r} (L_r-1)!} \times a_0 \left[b(2L_r a_{\text{egc}} - a_2) - a_1 a_{\text{egc}} (a_{\text{egc}}-a_2)^2\right] \tag{6.17}$$

where $p(a_{\text{egc}})$ is the pdf of the output channel gain a_{egc}. The exact pdf of a_{egc} cannot be evaluated in closed-form, but accurate closed-form approximations can be obtained. In [93,94], the pdf of Rayleigh sum distributions was proposed and here we use these models to find $p(a_{\text{egc}})$. When $L_r = 2$, a small argument approximation (SAA) proposed in [93] is used and the pdf of a_{egc} is given as

$$p(a_{\text{egc}}) = \frac{a_{\text{egc}}^{(2L_r-1)} e^{-\frac{a_{\text{egc}}^2}{2b}}}{2^{L_r-1} b^{L_r} (L_r-1)!}, \tag{6.16}$$

where

$$b = \frac{\sigma^2}{L_r} \left(\prod_{x=1}^{L_r} (2x-1) \right)^{1/L_r}.$$

When $L_r \geq 3$, a more accurate closed-form approximation of $p(a_{\text{egc}})$ is given in (6.17) and values of a_0, a_1 and a_2 for different L_r were given in [94]. In our case, we note that the standard deviation σ for Rayleigh distributions in the calculation of b in (6.17) should be normalized as $\sigma = \sqrt{\frac{L_r}{2}}$.

6.3.3 Uncoded BEP of Maximal-Ratio Combining

Compared with AWGN, the maximal-ratio combining does not exist for SαS noise when $\alpha \neq 2$ since the second order moment of SαS process is infinite [4]. Hence, the MRC here only refers to a particular choice of weights which is the same as AWGN.

In order to calculate the BEP of MRC, we must use a different approach that (6.11) is now divided by $\sum_{l=1}^{L_r} w_l a_l$. Since the weights are chosen as $w_l = h_l^* = a_l e^{-j\phi_l}$ for MRC, (6.11) becomes

$$\hat{y} = x + \hat{n}, \tag{6.18}$$

where

$$\hat{y} = \frac{y}{\sum_{l=1}^{L_r} a_l^2}, \tag{6.19}$$

and

$$\hat{n} = \frac{\sum_{l=1}^{L_r} a_l e^{-j\phi_l} n_l}{\sum_{l=1}^{L_r} a_l^2}. \tag{6.20}$$

It is known that the BEP will not change if y is divided by a positive constant. $\hat{n}$ is still an SαS random variable but with a different dispersion. According to Properties 1 and 2, the dispersion γ_{mrc} of $\hat{n}$ is calculated as

$$\gamma_{\text{mrc}} = \left(\sum_{l=1}^{L_r} \left| \frac{a_l e^{-j\phi_l}}{\sum_{l=1}^{L_r} a_l^2} \right|^{\alpha} \right)^{\frac{1}{\alpha}} \gamma = \frac{\left(\sum_{l=1}^{L_r} a_l^{\alpha} \right)^{\frac{1}{\alpha}}}{\sum_{l=1}^{L_r} a_l^2} \gamma. \tag{6.21}$$

Then the conditional BEP can be obtained by substituting (6.21) and (6.3) into (6.4). It is given as

$$P_{b|a_{\text{mrc}},\alpha} = Q_{\alpha} \left(\omega \sqrt{4 R_c C_g^{(\frac{2}{\alpha}-1)} \frac{E_b}{N_0}} \right), \tag{6.22}$$

where

$$\omega = \frac{\sum_{l=1}^{L_r} a_l^2}{\left(\sum_{l=1}^{L_r} a_l^{\alpha} \right)^{\frac{1}{\alpha}}}. \tag{6.23}$$

As shown in (6.23), $p(\omega)$ cannot be evaluated by an analytic expression, hence a Monte-Carlo simulation and histogram method is employed to find $p(\omega)$. Then a semi-analytic BEP on Rayleigh fading channels with AWSαSN is given as

$$P_{b,\alpha}^{\text{MRC}} = \int_0^{\infty} Q_{\alpha} \left(\omega \sqrt{4 R_c C_g^{(\frac{2}{\alpha}-1)} \frac{E_b}{N_0}} \right) p(\omega) d\omega. \tag{6.24}$$

6.3.4 SNR Comparison of linear Combiners

The SNR gain of optimal linear combiners over MRC and EGC was presented in [30,31]. In this subsection, the relationship of the dispersion of SC, EGC and MRC are derived to give an insight into the performance of different combiners. Similar to our BEP analysis for MRC, (6.6) and (6.12) are also rewritten as $\hat{y} = x + \hat{n}$. $\hat{n} = n_{\text{sc}}/h_{\text{sc}}$ for SC and $\hat{n} = n_{\text{egc}}/a_{\text{egc}}$ for EGC. Hence, the dispersions of the noise for SC and EGC are obtained as

$$\hat{\gamma}_{\text{sc}} = \frac{1}{a_m} \gamma \quad \text{and} \quad \hat{\gamma}_{\text{egc}} = \frac{L_r^{1/\alpha}}{\sum_{l=1}^{L_r} a_l} \gamma, \tag{6.25}$$

where $a_m = \max\{a_1, a_2, \cdots, a_{L_r}\}$. After some derivations, the relationship of the dispersions between these three combiners is given as

(a) When $0 < \alpha \leq 1$,

$$\hat{\gamma}_{\text{sc}} \leq \gamma_{\text{mrc}} \leq \hat{\gamma}_{\text{egc}} \leq L_r^{\frac{1}{\alpha}} \hat{\gamma}_{\text{sc}}, \tag{6.26}$$

(b) When $1 \leq \alpha < 2$,

$$L_r^{\frac{1}{\alpha}-1} \hat{\gamma}_{\text{sc}} \leq \gamma_{\text{mrc}} \leq \hat{\gamma}_{\text{egc}} \leq L_r^{\frac{1}{\alpha}} \hat{\gamma}_{\text{sc}}. \tag{6.27}$$

The relationships in (6.26) and (6.27) are independent of fading types since they are only related to the dispersion. The proof of (6.26) and (6.27) is given in the Appendix. According to the definition, the noise power is proportional to the dispersion of the noise. Hence,(6.26) and (6.27) imply that MRC should perform better than EGC in all cases. In particular, SC shows the best performance when the channel is very impulsive ($\alpha < 1$). In addition, the upper bound and lower bound of the performance for MRC and EGC can be determined by SC from (6.26) and (6.27). The numerical results of the SNR comparison of these combiners will be shown in the result section.

6.3.5 Optimal and Sub-optimal Detectors

The linear combiners just discussed are very simple to implement however, they do not take the impulsive nature of the interference into account. As presented in the literature, non-linear detectors usually achieve much better performance on impulsive noise channels [16, 31]. The decision metric of the optimal detector for fading channels with AWSαSN is denoted as

$$\lambda_{\text{op}} = \sum_{l=1}^{L_r} \ln \frac{P(x_l = +1 | r_l, a_l)}{P(x_l = -1 | r_l, a_l)} = \sum_{l=1}^{L_r} \ln \frac{f_\alpha(r_l - a_l; \gamma)}{f_\alpha(r_l + a_l; \gamma)}. \tag{6.28}$$

(6.28) also represents the initial log-likelihood ratios (LLRs) for soft-input-soft-output decoding.

The complexity in the calculation of (6.28) is high since the pdf of SαS distributions is not given in closed-form, thus reduced complexity sub-optimal detectors are required. In the literature, the Cauchy detector showed very good performance for a large range of α, especially when α is small and approaches one [95]. The Cauchy

detector is expressed as

$$\lambda_{\text{Cauchy}} = \sum_{l=1}^{L_r} \ln\left(\frac{\gamma^2 + (y_l + a_l)^2}{\gamma^2 + (r_l - a_l)^2}\right). \tag{6.29}$$

In contrast, the Cauchy detector will lead to a significant degradation when the channel is near Gaussian (α is close to two), since the Cauchy distribution is only a special case of SαS distributions at small α ($\alpha = 1$). In order to give a better approximation of SαS distributions as closed-form expressions, two classes of mixture models were proposed. One is called the Gaussian mixture model (GMM) which is the sum of scaled Gaussian pdfs. However, GMM cannot accurately estimate the tail behavior of SαS distributions. The other one is Cauchy-Gaussian mixture (CGM) model which is a mixture of Gaussian distribution and Cauchy distribution. The CGM model can better approximate the tail of SαS distributions since the Cauchy pdf is also heavy-tailed. The conventional CGM model requires three parameters: mixture ratio ϵ, the variance σ^2 of the Gaussian distribution and the dispersion γ of Cauchy distribution. The BCGM model is a new type of CGM model with only two parameters, a mixture ratio ϵ and γ, and it approximates SαS pdf well at $\alpha \in [1, 2]$ [91]. Hence the BCGM model can be used to achieve near-optimal performance. The BCGM pdf is given as

$$f_{\text{CG}}(x;\gamma) = (1-\epsilon)\frac{1}{2\sqrt{\pi}\gamma}\exp\left(-\frac{x^2}{4\gamma^2}\right) + \epsilon\frac{\gamma}{\pi(x^2+\gamma^2)}. \tag{6.30}$$

A near-optimal value of ϵ can be achieved when

$$\varepsilon = \frac{2\Gamma(-\omega/\alpha) - \alpha\Gamma(-\omega/2)}{2\alpha\Gamma(-\omega) - \alpha\Gamma(-\omega/2)}, \tag{6.31}$$

where the gamma function is defined as $\Gamma(x) = \int_0^\infty e^{-t}t^{x-1}dt$ and $\omega < \alpha$. By using this BCGM model, the decision metric of the detector is obtained by replacing the SαS pdf in (6.28) by (6.30). The BCGM model was only proposed for $\alpha \in [1, 2]$ and we note that when $\alpha < 1$, the BCGM detector reduces to a Cauchy detector. The complexity of this new detector is much lower than the optimal detector since its pdf is given in closed-form. The performance of optimal and sub-optimal detectors will also be presented in the result section.

6.4 Coded BEP analysis for linear diversity combining techniques

6.4.1 Asymptotic Performance of LDPC Codes

Similar to previous chapters, DE is used to calculate the threshold of a specific ensemble of LDPC codes. In this section, we will show how to apply DE to different linear combining techniques on Rayleigh fading channels with AWSαSN by deriving the initial pdf of the LLRs for these combiners.

Assuming the side information of the channel is known, the initial LLR of the decoder for SC or EGC is calculated as

$$v^{(0)} = \ln \frac{P(x=+1|y,a)}{P(x=-1|y,a)} = \ln \frac{f_\alpha(y-a;\gamma)}{f_\alpha(y+a;\gamma)}, \tag{6.32}$$

where a is the combining channel gain over i.i.d. Rayleigh fading channels, which is denoted as a_{sc} or a_{egc} for SC or EGC, respectively. Similarly, γ becomes γ_{egc} for EGC. The pdf of (6.32) has no analytic expression with the exception of $\alpha = 2$. Hence, Monte-Carlo simulations with a histogram method can be used to obtain the conditional pdf of $v^{(0)}$ as $p(v^{(0)}|a)$. The unconditional pdf of $v^{(0)}$ can be obtained by averaging $p(v^{(0)}|a)$ over the pdf of a as

$$p_v^{(0)} = \int_0^\infty p(v^{(0)}|a)p(a)da, \tag{6.33}$$

where $p(a)$ is the pdf of the combining channel gain a.

The pdf of a_{sc} for SC can be derived by changing the variable of (6.10), a_{sc}, using the relationship $p(\eta)d\eta = p(a_{\text{sc}})da_{\text{sc}}$ and $a_{\text{sc}}^2 = \eta/\overline{\eta}$. Hence, the pdf of a_{sc} is then given as

$$p(a_{\text{sc}}) = 2a_{\text{sc}}L_r e^{-a_{\text{sc}}^2}\left(1-e^{-a_{\text{sc}}^2}\right)^{L_r-1}. \tag{6.34}$$

For EGC, closed-form approximated pdfs of a_{egc} have already been given in (6.17). Alternatively, a simulation-based approach can also be employed to find the pdf of a_{egc} using a histogram method.

For MRC, we should use a different approach to calculate the pdf of the initial

LLRs. According to (6.18) and (6.21), the initial LLR can be written as

$$v^{(0)} = \ln \frac{f_\alpha(\hat{y}-1;\gamma_{\text{mrc}})}{f_\alpha(\hat{y}+1;\gamma_{\text{mrc}})}. \tag{6.35}$$

The relationship between γ_{mrc} and γ has been given in (6.21) as $\gamma_{\text{mrc}} = \xi\gamma$, where ξ is expressed as

$$\xi = \frac{\left(\sum_{l=1}^{L_r} a_l^\alpha\right)^{\frac{1}{\alpha}}}{\sum_{l=1}^{L_r} a_l^2}. \tag{6.36}$$

Hence the unconditional pdf of $v^{(0)}$ is obtained as

$$p_v^{(0)} = \int_0^\infty p(v^{(0)}|\xi)p(\xi)d\xi, \tag{6.37}$$

where $p(\xi)$ is the pdf of ξ. We note that $p(\xi)$ cannot be evaluated in closed-form and a similar simulation-based approach is used to find $p(\xi)$. After the initialization step, DE of the sum-product algorithm is then performed and it consists of DE for both the check node update and variable node update.

6.4.2 Waterfall Performance Estimation of LDPC Codes

In this section, we follow our analysis in previous chapters and an accurate estimation of block and bit-error probability of finite length LDPC codes on Rayleigh fading channels with AWSαSN for SC, EGC and MRC is given by observing the real-time channel quality.

$P_{b,\alpha}^c$ is the probability of a bit error and is denoted as either $P_{b,\alpha}^{\text{SC}}$, $P_{b,\alpha}^{\text{EGC}}$ or $P_{b,\alpha}^{\text{MRC}}$, depending on the type of linear combiner. When N is large, the pmf of $NP_{b,\alpha}^{\text{obs}}$ can be well approximated by a normal distribution $\mathcal{N}(NP_{b,\alpha}^c, NP_{b,\alpha}^c(1-P_{b,\alpha}^c))$. Hence, the pdf of $P_{b,\alpha}^{\text{obs}}$ is denoted as $\mathcal{N}(P_{b,\alpha}^c, P_{b,\alpha}^c(1-P_{b,\alpha}^c)/N)$. Finally, the block-error probability of LDPC codes with ensemble (λ,ρ) is given as

$$\begin{aligned} P_{\text{B}}^\alpha(N,\lambda,\rho) &= \int_{P_{\text{th}}}^1 f_{P_{b,\alpha}^{\text{obs}}}(N,x)dx \\ &= Q\left(\frac{P_{\text{th}} - \mu_{P_{b,\alpha}^{\text{obs}}}}{\sigma_{P_{b,\alpha}^{\text{obs}}}}\right), \end{aligned} \tag{6.38}$$

where $\mu_{P_{b,\alpha}^{\text{obs}}} = P_{b,\alpha}^c$ and $\sigma_{P_{b,\alpha}^{\text{obs}}} = P_{b,\alpha}^c(1-P_{b,\alpha}^c)/N$. P_{th} is the corresponding BEP of the threshold SNR $\left(\frac{E_b}{N_0}\right)_{\text{th}}$ and the block-error probability is $P_{b,\alpha}^{\text{obs}} > P_{\text{th}}$. We note

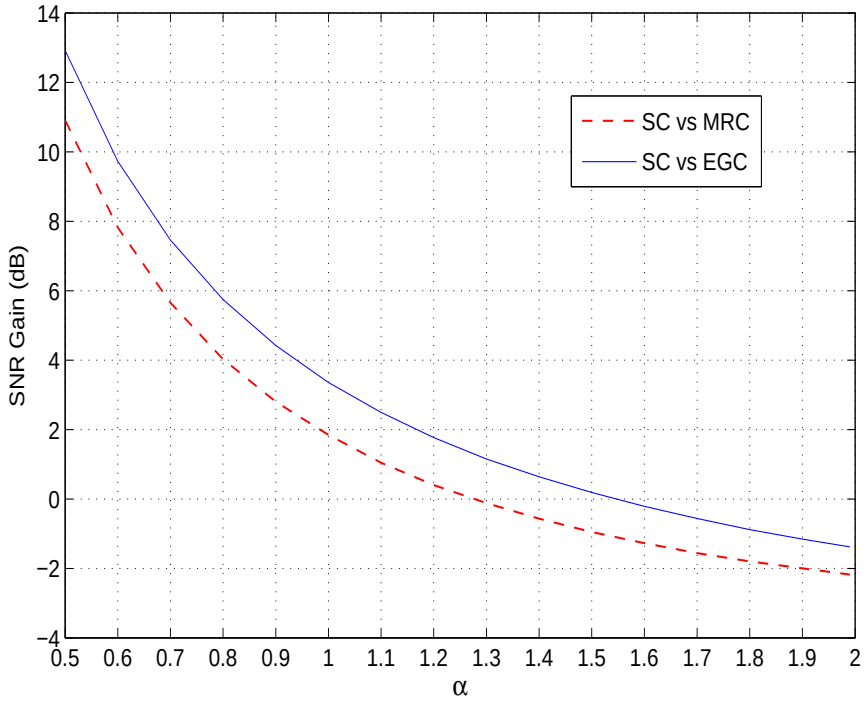

Figure 6.1: SNR gain of SC over EGC and MRC with different α for $L_r = 3$.

that the threshold SNR $\left(\frac{E_b}{N_0}\right)_{\text{th}}$ can be calculated from γ^* which has been found by DE in the previous section. Hence for SC, EGC and MRC, P_{th} is obtained by substituting $\left(\frac{E_b}{N_0}\right)_{\text{th}}$ into (6.8), (6.15) and (6.24), respectively.

The coded bit error probability $P_{\text{b}}^{\alpha}(N, \lambda, \rho)$ can be derived from $P_{\text{B}}^{\alpha}(N, \lambda, \rho)$. In the description of DE, we know that the decoder has a probability $P_e^{(l_{\max})}$ of failing, where $l_{\max}$ is the maximum number of iterations when DE is performed. The estimated coded BEP can be expressed as

$$P_{\text{b}}^{\alpha}(N, \lambda, \rho) = P_e^{(l_{\max})} P_{\text{B}}^{\alpha}(N, \lambda, \rho). \tag{6.39}$$

6.5 Results and Discussion

6.5.1 SNR Comparison

To verify the effectiveness of our SNR analysis for linear combiners (SC, EGC and MRC), the SNR gain of SC over EGC and MRC is shown in Fig. 6.1. The SNR gain in dB over EGC and MRC is defined as $20\log_{10}(\hat{\gamma}_{\text{egc}}/\hat{\gamma}_{\text{sc}})$ and $20\log_{10}(\gamma_{\text{mrc}}/\hat{\gamma}_{\text{sc}})$, respectively. As shown in Fig. 6.1, MRC always performs better than EGC for each α, which agrees with our theoretical results in (6.26) and (6.27). Moreover, we find

that SC achieve the best performance when α is small. However, it will degrade as α increases and starts to present no gain (SNR gain is 0 dB) over MRC and EGC from $\alpha = 1.3$ and $\alpha = 1.55$, respectively. The SNR comparison of different combiners provide us a very good insight into their performance, regardless of fading effects. In the following subsections, these observations from Fig. 6.1 will be verified by results of our uncoded and LDPC-coded BEP.

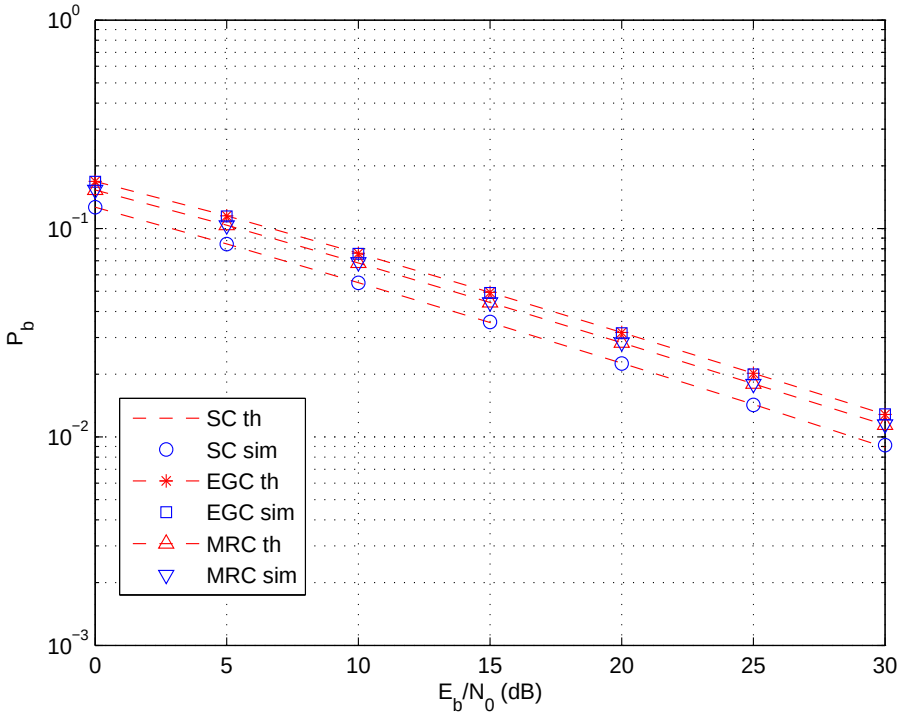

Figure 6.2: Uncoded BEP of SC, EGC and MRC with $L_r = 2$ on Rayleigh fading channels with SαS noise at $\alpha = 0.8$.

6.5.2 Uncoded BEP

In this subsection, both numerical results of analytic performance and simulated performance of different combiners on Rayleigh fading channels with AWSαSN are investigated. Moreover, the performance of non-linear detectors is also presented. As seen in Fig. 6.2 - 6.7, our derived analytic BEP matches with simulated BER for SC, EGC and MRC at different α ($\alpha = 0.8, 1.4, 1.9$) and different number of branches ($L_r = 2, 4$).

As seen in Fig. 6.2 and 6.3, compared with EGC and MRC, SC achieves the best performance at small values of α ($\alpha = 0.8$) and this result agrees with the observations in the literature [31]. The relationship of the uncoded BEP for SC,

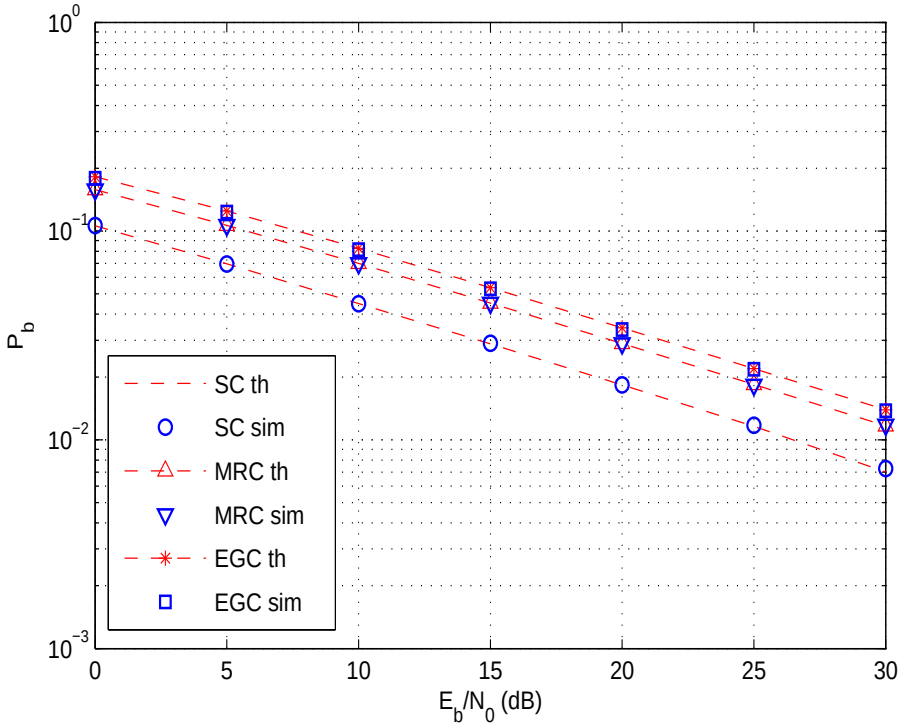

Figure 6.3: Uncoded BEP of SC, EGC and MRC with $L_r = 4$ on Rayleigh fading channels with SαS noise at $\alpha = 0.8$.

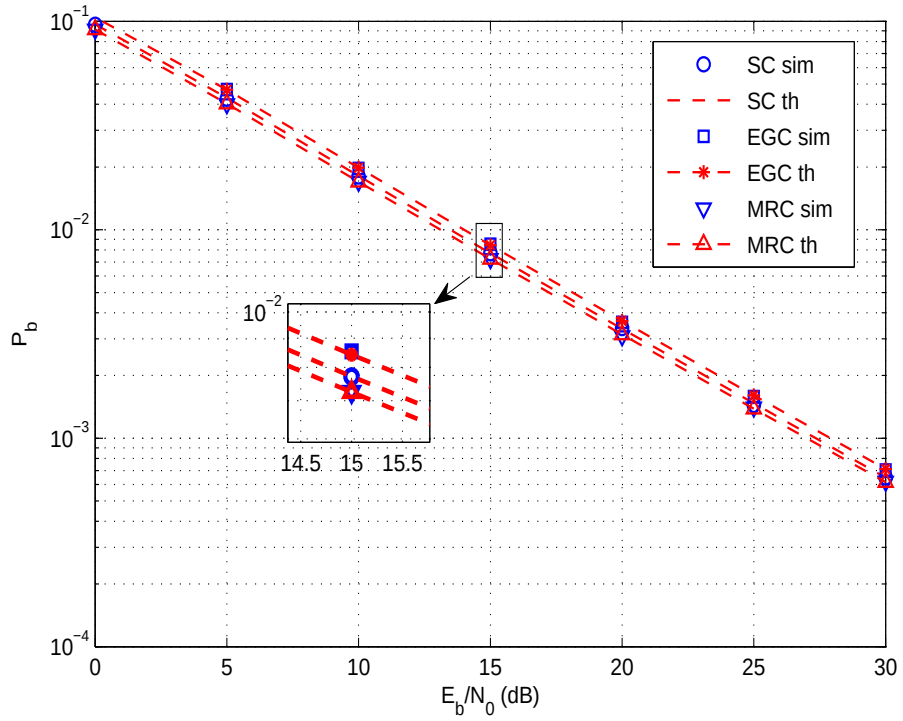

Figure 6.4: Uncoded BEP of SC, EGC and MRC with $L_r = 2$ on Rayleigh fading channels with SαS noise at $\alpha = 1.4$.

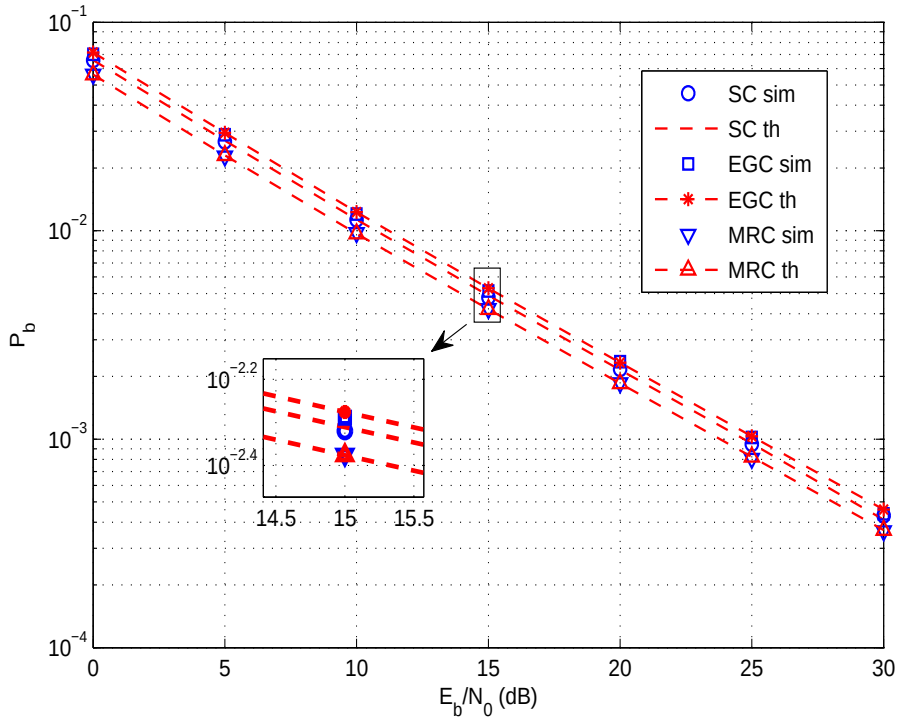

Figure 6.5: Uncoded BEP of SC, EGC and MRC with $L_r = 4$ on Rayleigh fading channels with SαS noise at $\alpha = 1.4$.

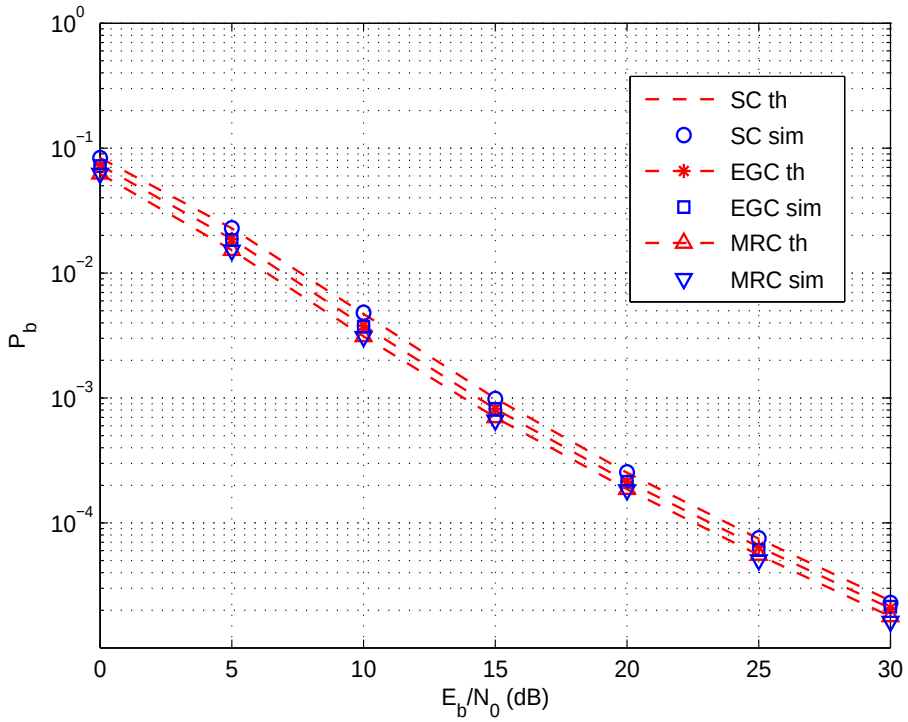

Figure 6.6: Uncoded BEP of SC, EGC and MRC with $L_r = 2$ on Rayleigh fading channels with SαS noise at $\alpha = 1.9$.

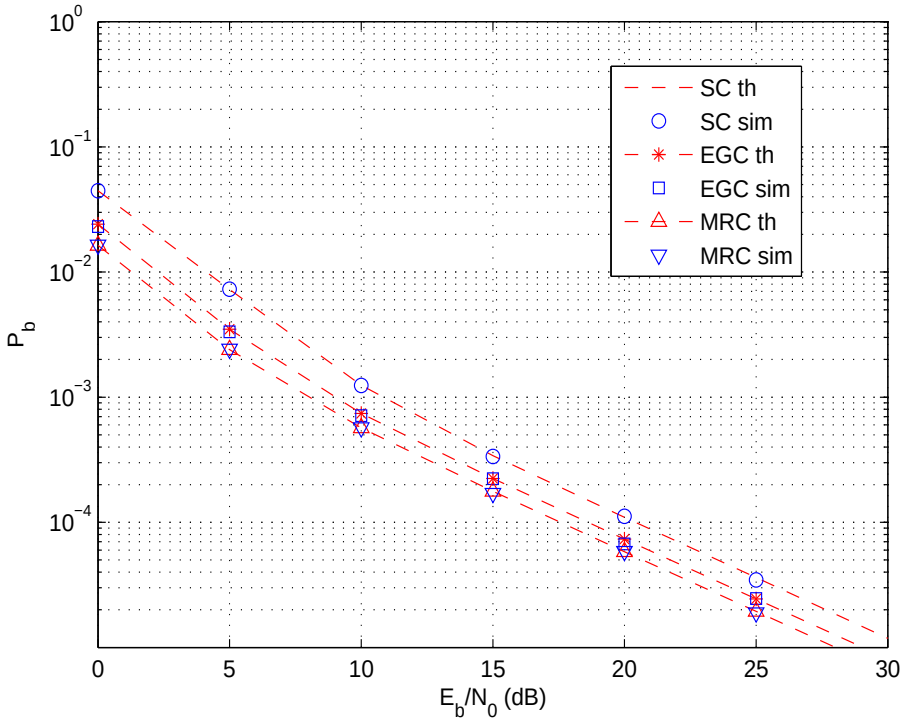

Figure 6.7: Uncoded BEP of SC, EGC and MRC with $L_r = 4$ on Rayleigh fading channels with SαS noise at $\alpha = 1.9$.

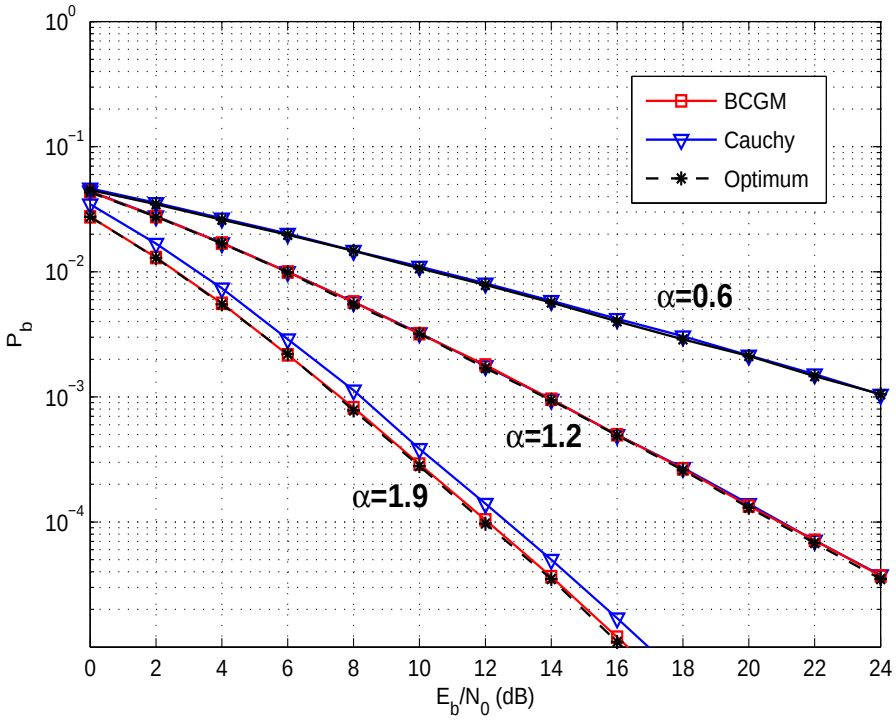

Figure 6.8: BER performance of different detectors with $L_r = 3$ on Rayleigh fading channels with SαS noise at $\alpha = 1.9, 1.2, 0.6$.

EGC and MRC is $P_{b,\alpha}^{\mathrm{SC}} < P_{b,\alpha}^{\mathrm{MRC}} < P_{b,\alpha}^{\mathrm{EGC}}$. Moreover, it is observed that SC achieves more gain for additional number of branches in this extremely impulsive noise, while the performance of EGC and MRC is even worse for $L_r = 4$. When the channel is less impulsive ($\alpha = 1.4$), compared with EGC and MRC, the performance of SC degrades and we have $P_{b,\alpha}^{\mathrm{MRC}} < P_{b,\alpha}^{\mathrm{SC}} < P_{b,\alpha}^{\mathrm{EGC}}$, which agrees with the result in Fig. 6.1 that SC becomes worse than MRC and EGC at $\alpha = 1.3$ and $\alpha = 1.55$ since $1.3 < 1.4 < 1.55$. When the channel exhibits very few impulses ($\alpha = 1.9$), as shown in Fig. 6.6 and 6.7, SC gives the worst performance among these three linear combiners and we have $P_{b,\alpha}^{\mathrm{MRC}} < P_{b,\alpha}^{\mathrm{EGC}} < P_{b,\alpha}^{\mathrm{SC}}$. In addition, when the number of branches increases, MRC can achieve a larger gain over SC and MRC.

We observe that SC can achieve superior performance when the channel is more impulsive and the performance starts to degrade as α increases. Although MRC only refers to a particular set of weights, it can still achieve a very good performance when compared with SC and EGC, especially when the noise is near Gaussian. To conclude, the uncoded BEP we obtained in Fig. 6.2 - 6.7 illustrates good agreement with our observations from the SNR gain in Fig. 6.1.

The simulated performance of optimal, Cauchy and BCGM detectors are shown in Fig. 6.8. When the channel is extremely impulsive ($\alpha = 0.6$), the BCGM detector reduces to the Cauchy detector and shows near-optimal performance. When α is close to one ($\alpha = 1.2$), both BCGM and Cauchy detectors achieve almost optimal performance. However, when α approaches two which means the channel is slightly impulsive, the Cauchy detector presents a significant degradation. As shown in Fig. 6.8, when $\alpha = 1.9$ and $L_r = 3$, the optimal detector shows about 0.8 dB gain over the Cauchy detector. In contrast, the BCGM detector shows superior performance for all α.

6.5.3 Coded BEP

In this subsection, the asymptotic and waterfall performance of regular and irregular LDPC codes are evaluated with both numerical and simulation results. The rate 1/2 regular (3,6) LDPC codes and for irregular LDPC codes, the degree distribution is $\lambda(x) = 0.4x^2 + 0.4x^5 + 0.2x^8$, $\rho(x) = x^8$. The codeword lengths are $N = 1000, 4000, 20000$ bits. For short and moderate length LDPC codes ($N \leq 4000$), PEG algorithm is employed and for very long LDPC codes ($N = 20000$), Mackay's

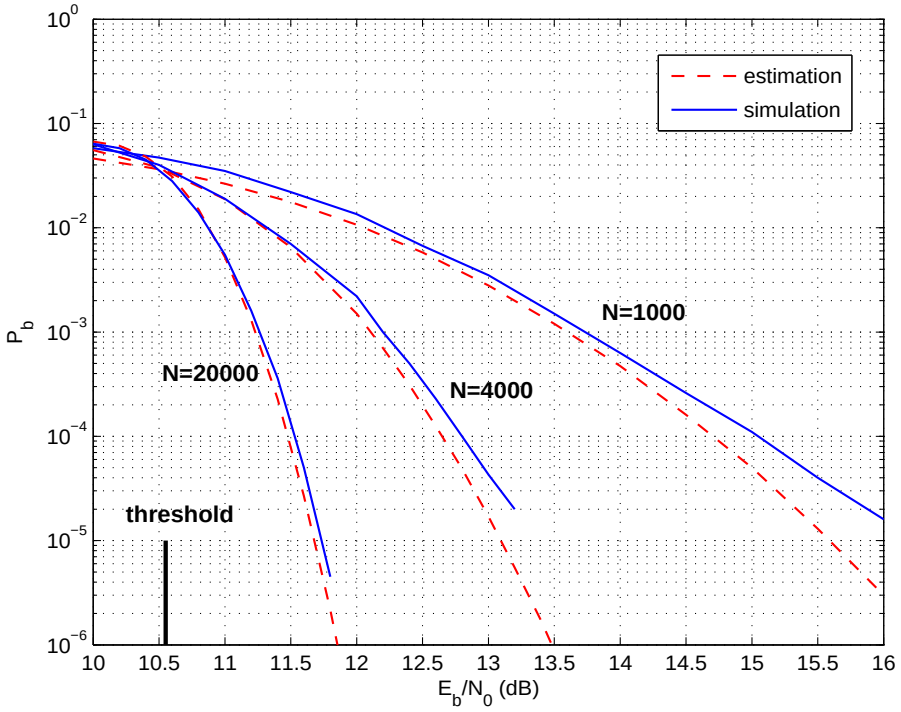

Figure 6.9: Performance of regular $(3, 6)$ LDPC codes with EGC for $N = 1000, 4000, 20000$ at $L_r = 2$ on Rayleigh fading channels with SαS noise at $\alpha = 0.6$.

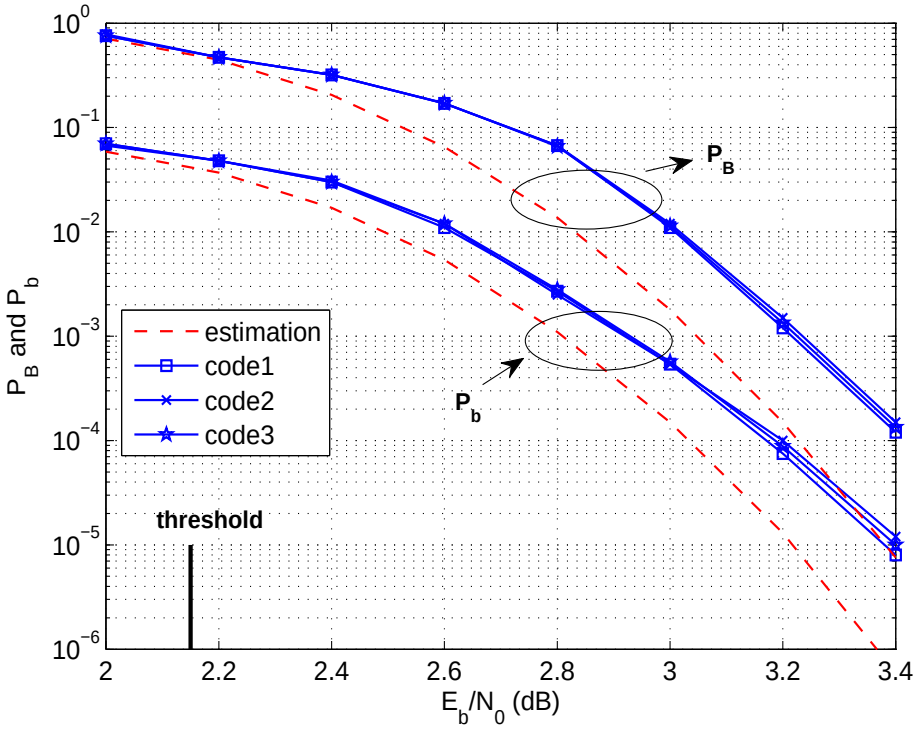

Figure 6.10: Performance of irregular LDPC codes with SC at $L_r = 2$ and $N = 4000$ on Rayleigh fading channels with SαS noise at $\alpha = 1.5$.

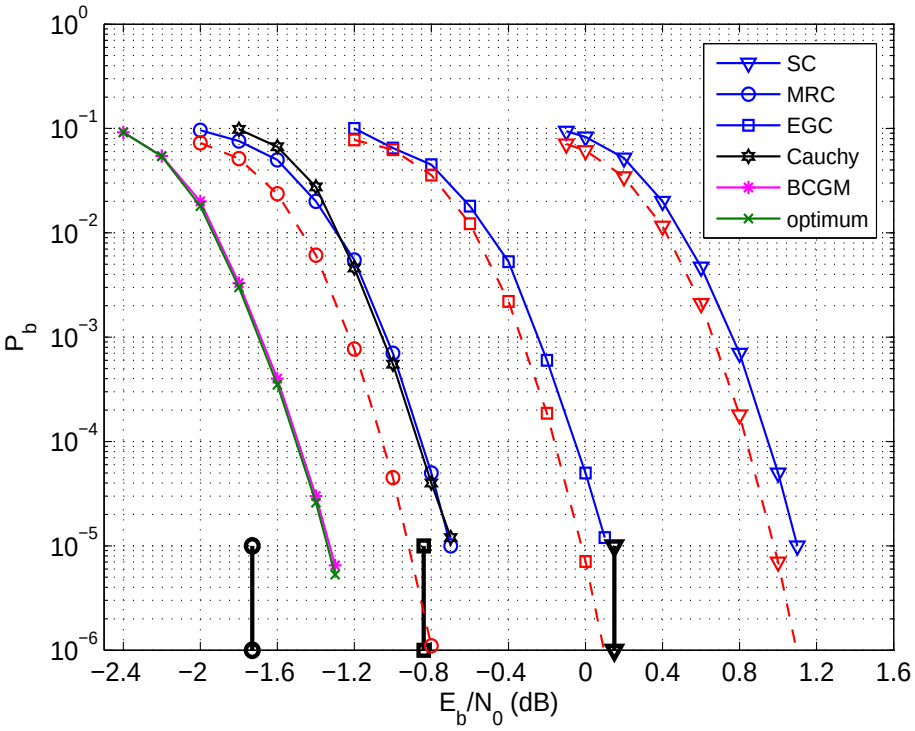

Figure 6.11: Performance of irregular LDPC codes with different combiners at $L_r = 3$ and $N = 4000$ on Rayleigh fading channels with SαS noise at $\alpha = 1.8$.

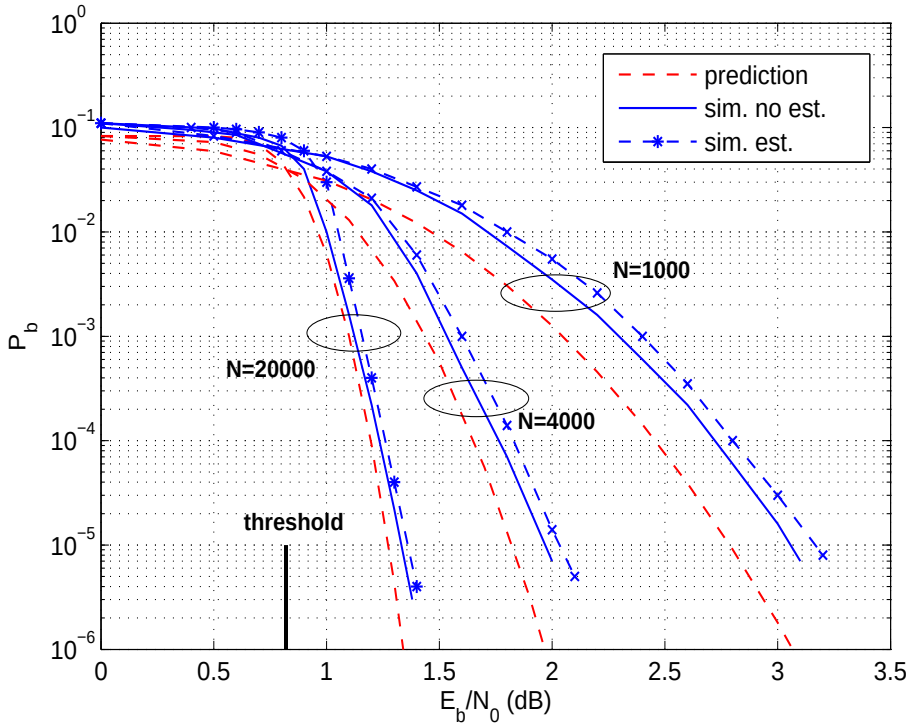

Figure 6.12: Performance of irregular LDPC-coded SC with exact and estimated parameters on Rayleigh fading channels with SαS noise at $\alpha = 1.5$ and $L_r = 3$.

Table 6.1: The threshold SNRs in dB of regular LDPC codes with SC, EGC and MRC for Rayleigh fading channels with SαS noise

	$L_r = 2$			$L_r = 4$		
	SC	EGC	MRC	SC	EGC	MRC
$\alpha = 1.8$	0.91	0.52	-0.18	-1.02	-2.31	-3.43
$\alpha = 1.4$	1.90	2.44	1.53	-0.19	0.37	-0.98
$\alpha = 1$	3.02	5.32	4.10	0.92	4.93	3.16
$\alpha = 0.6$	4.32	10.55	9.15	2.17	14.31	12.10

construction method is used since the complexity of PEG is very high in this case.

As shown in Table 6.1, the threshold SNRs of $(3, 6)$ regular LDPC codes for SC, EGC and MRC are given. The relationship of asymptotic performance of LDPC codes we obtained for these combiners show good agreement with the uncoded performance we analyzed for different linear combiners. As shown in Table 6.1, SC presents the best performance for strongly impulsive noise ($\alpha = 0.6$ and $\alpha = 1$) for $L_r = 2$ and $L_r = 4$. When the effect of impulses is moderate ($\alpha = 1.4$), MRC outperforms SC and when the channel is only slightly impulsive, the performance of MRC is better the gap between MRC and SC is larger. As an example, the threshold SNR of MRC is 1.53 dB at $\alpha = 1.4$ and $L_r = 2$, which is 0.37 dB smaller than SC. When $\alpha = 1.8$, the gap increases to 1.09 dB. For EGC, it only shows good performance for a slightly impulsive channel ($\alpha = 1.8$).

Furthermore, there is an interesting observation that more branches do not always give better performance for impulsive noise channels. As shown in Table 6.1, as α decreases, $L_r = 4$ has a smaller gain than $L_r = 2$ over EGC and MRC, respectively. When the channel is extremely impulsive ($\alpha = 0.6$), thresholds of EGC and MRC for $L_r = 4$ are even larger than for $L_r = 2$. It indicates that strong impulses will lead to a larger degradation with EGC and MRC when more branches are used, which implies that the received signals from other branches become a source of interference.

In addition to the asymptotic performance obtained in Table 6.1, the numerical results of predicted waterfall performance and simulation results for LDPC codes are presented in Figs. 6.9 - 6.12. As shown in Fig. 6.9, the estimated performance closely matches the simulation results very closely for EGC at $\alpha = 0.6$. Also, a reduction is found in the gap between the predicted and simulated results as the block length N increases. The estimation inaccuracy decreases from 0.3 dB to 0.15 dB as N increases from 1000 to 4000. When $N = 20000$, the estimated and

simulated performance are almost identical. On the other hand, when compared with the asymptotic performance, even for long LDPC codes ($N = 20000$), the gap between the threshold SNR and simulation results is 1.3 dB which is much larger than our predicted performance.

Fig. 6.10 shows both the estimated and simulated block and bit error rates for irregular LDPC codes with $N = 4000$ when $\alpha = 1.5$. To show the generalization of our method, three individual LDPC codes are constructed from the same degree distribution we have given and their performance is presented. As shown in Fig. 6.10, the performance is accurately predicted by our analytic P_B and P_b in (6.38) and (6.39) with a 0.2 dB gap at the error rate of 10^{-5}, while the gap between asymptotic and simulated performance is 1.25 dB.

Linear combiners and non-linear detectors in slightly impulsive noise are compared in Fig. 6.11. For linear combiners SC, EGC and MRC, the threshold SNR and numerical predictions are given. It is shown that the coded BEP of different combiners agrees with the uncoded BEP we obtained above, where MRC outperforms SC and EGC for slightly impulsive noise. Meanwhile, the non-linear detectors perform better than the linear combiners due to the utilization of the noise statistics. The performance of the optimal detector and our proposed detector are almost identical, which achieve 0.7 dB gain over the Cauchy detector and MRC.

To examine the accuracy of the parameter estimation algorithm and the robustness of the decoder. The performance with known and estimated α and γ is presented in Fig. 6.12. The curves named "sim. no est." and "sim. est." represent simulated performance with exact and estimated parameters, respectively. In our simulations, the average estimation errors of α are found to be $8\%, 6\%$ and 4% at $N = 1000, 4000$ and 20000, respectively. The corresponding estimation errors of γ are $16\%, 17\%$ and 18% at $E_b/N_0 = 0$ dB ($\gamma = 0.64$). As presented in Fig. 6.12, the difference between the performance with known and estimated parameters is small, which is less than 0.1 dB. It shows that the LDPC decoder is very robust against estimation errors.

It has been observed that the waterfall performance prediction of LDPC codes is more accurate when N is large. The reasons are as follows: first, the P_{th} is obtained from DE and DE assumes the LDPC codes are cycle-free and the codeword length is infinite. However, the effect of cycles cannot be avoided and ignored. It is more serious at short block length which will degrade the performance. For LDPC codes

with long block length, the concentration theorem states that the average behavior of individual codes will converge to the cycle-free case as the code length grows [41]. Hence the our estimation becomes more accurate in this case. Second, it worth examining the accuracy of Gaussian approximation since according to central limit theorem, the pdf of P_{obs}^{α} converges to Gaussian pdf when N is large.

To numerically evaluate the accuracy of the Gaussian approximation, the KL divergence is employed to calculate the difference between the two pdfs. In our case, the binomial pdf $B(N, P_{b,\alpha}^{c})$ is the true pdf and the normal distribution $\mathcal{N}(P_{b,\alpha}^{c}, P_{b,\alpha}^{c}(1-P_{b,\alpha}^{c})/N)$ is an approximation of $B(N, P_{b,\alpha}^{c})$. It is obvious that these two pdfs are both determined by N and $P_{b,\alpha}^{c}$ which is related to α. In order to examine the influence of N and α on the accuracy of the approximation, we take Fig. 6.9 and Fig. 6.12 as examples. As shown in Fig. 6.9, the channel is extremely impulsive with $\alpha = 0.6$. $N = 1000, 4000, 20000$ and $P_{b,\alpha}^{c}$ can be calculated by (6.15). The accuracy of the Gaussian approximation improves as N increases and $P_{b,\alpha}^{c}$ is not near to 0 or 1. Hence, in order to investigate the validity of our approximation, for the worst case, we choose the smallest $P_{b,\alpha}^{c} = 0.0948$ which can be calculated from (6.15) at $E_b/N_0 = 16$ dB in Fig. 6.9. Hence the KL divergence between the pdf of P_{obs}^{α} and Gaussian distribution is obtained as $6.4 \times 10^{-4}, 1.6 \times 10^{-4}, 3.2 \times 10^{-5}$ for $N = 1000, 4000, 20000$, respectively. Similarly, as shown in Fig. 6.12, when the channel is moderate impulsive ($\alpha = 1.5$), the KL divergence at $E_b/N_0 = 3$ dB is obtained as $9.2 \times 10^{-4}, 2.3 \times 10^{-4}, 4.6 \times 10^{-5}$ for $N = 1000, 4000, 20000$, respectively. Hence, the Gaussian approximation is very accurate even for short length LDPC codes ($N = 1000$), since the KL divergence is very small. In addition, we observe that the value of α has little impact on the accuracy of approximation.

6.6 Conclusion

In this chapter, we investigate the uncoded and coded performance of linear diversity combining schemes on Rayleigh fading channels with AWSαSN noise. The asymptotic performance of LDPC codes is also derived using DE to verify the effectiveness of our analysis. In addition, a closed-form expression of the waterfall performance is given that reduces the gap between the asymptotic and simulated performance of LDPC codes. As discussed in the result section, MRC is no longer the optimal linear combiner, especially when the channel becomes more impulsive,

and SC shows superior performance when the effect of impulses is very strong. An interesting result is found when the channel is very impulsive. In this case, more branches have no benefit and may even degrade the performance of EGC and MRC. Meanwhile, non-linear detectors present a better performance than linear combiners, but with higher complexity. We have proposed a reduced complexity detector by approximating the SαS pdf through a closed-form BCGM pdf which can achieve near optimal performance for all α.

6.7 Appendix

6.7.1 The noise distribution of EGC

The noise of the combined signal for EGC in (6.12) is given as

$$n_{\text{egc}} = \sum_{l=1}^{L_r} \tilde{n}_l, \tag{6.40}$$

where $\tilde{n}_l = n_l e^{-j\phi_l}$ and n_l is an complex SαS random variable with i.i.d. components. Hence, according to (6.2), $\tilde{n}_l$ is written as

$$\begin{aligned} \tilde{n}_l &= \sqrt{B_1} G_1 e^{-j\phi_l} + j\sqrt{B_2} G_2 e^{-j\phi_l} \\ &= \sqrt{B_1} G_1^{'} + j\sqrt{B_2} G_2^{'}, \end{aligned} \tag{6.41}$$

where $G_1^{'} = G_1 e^{-j\phi_l}$ and $G_2^{'} = G_2 e^{-j\phi_l}$. According to the isotropic property of Gaussian random variables, $G_1^{'}$ and $G_1^{'}$ are also Gaussian with the same mean and variance as G_1 and G_2. Hence $\tilde{n}_l$ also follows SαS distribution with the same α and γ as n_l.

6.7.2 The relationship of the dispersion between SC, MRC and EGC

First, we start from proving $\gamma_{\text{mrc}} \leq \hat{\gamma}_{\text{egc}}$ for $0 < \alpha < 2$. According to the power mean inequality, for real numbers k_1, k_2 and positive real numbers $a_1, a_2, \cdots, a_n$. If $k_1 \leq k_2$, we have

$$\left(\frac{\sum_{i=1}^{n} a_i^{k_1}}{n} \right)^{\frac{1}{k_1}} < \left(\frac{\sum_{i=1}^{n} a_i^{k_2}}{n} \right)^{\frac{1}{k_2}}. \tag{6.42}$$

Then by using this inequality we can obtain

$$\left(\sum_{l=1}^{L_r} a_l^{\alpha}\right)^{\frac{1}{\alpha}} \leq L_r^{\frac{1}{\alpha}-\frac{1}{2}} \left(\sum_{l=1}^{L_r} a_l^2\right)^{\frac{1}{2}}. \tag{6.43}$$

For MRC, by substituting (6.43) to (6.21), we have

$$\gamma_{\text{mrc}} \leq \frac{L_r^{\frac{1}{\alpha}-\frac{1}{2}}}{\left(\sum_{l=1}^{L_r} a_l^2\right)^{\frac{1}{2}}}\gamma \leq \frac{L_r^{\frac{1}{\alpha}}}{\left(\sum_{l=1}^{L_r} a_l\right)}\gamma = \hat{\gamma}_{\text{egc}}. \tag{6.44}$$

After the proof of $\gamma_{\text{mrc}} \leq \hat{\gamma}_{\text{egc}}$, for EGC, one obtains

$$\hat{\gamma}_{\text{egc}} = \frac{L_r^{1/\alpha}}{\sum_{l=1}^{L_r} a_l}\gamma \leq \frac{L_r^{1/\alpha}}{a_m}\gamma = L_r^{1/\alpha}\hat{\gamma}_{\text{sc}}. \tag{6.45}$$

When $0 < \alpha \leq 1$, it was proved that $\hat{\gamma}_{\text{sc}} \leq \gamma_{\text{mrc}}$ in [31]. Hence, the relationship of the dispersions of SC, MRC and EGC is given as

$$\hat{\gamma}_{\text{sc}} \leq \gamma_{\text{mrc}} \leq \hat{\gamma}_{\text{egc}} \leq L_r^{1/\alpha}\hat{\gamma}_{\text{sc}}. \tag{6.46}$$

When $1 \leq \alpha < 2$, $\hat{\gamma}_{\text{sc}}$ is not always less than γ_{mrc}. Again by using (6.42), the relationship is obtained as

$$\begin{aligned}
\gamma_{\text{mrc}} &\geq \frac{\sum_{l=1}^{L_r} a_l}{\sum_{l=1}^{L_r} a_l^2} L_r^{\frac{1}{\alpha}-1}\gamma \\
&\geq \frac{\sum_{l=1}^{L_r} a_l}{\sum_{l=1}^{L_r} a_l a_m} L_r^{\frac{1}{\alpha}-1}\gamma \\
&= \frac{1}{a_m} L_r^{\frac{1}{\alpha}-1}\gamma = L_r^{\frac{1}{\alpha}-1}\hat{\gamma}_{\text{sc}}.
\end{aligned} \tag{6.47}$$

Finally, the relationship of the dispersion for SC, MRC and EGC when $1 \leq \alpha < 2$ is given as

$$L_r^{\frac{1}{\alpha}-1}\hat{\gamma}_{\text{sc}} \leq \gamma_{\text{mrc}} \leq \hat{\gamma}_{\text{egc}} \leq L_r^{1/\alpha}\hat{\gamma}_{\text{sc}}. \tag{6.48}$$

Chapter 7

Conclusions and Future Research

7.1 Conclusion

When the noise or interference can be modeled as SαS distributions, this thesis addresses the signal detection in LDPC-coded system on such impulsive noise channels. The optimal LLR demapper in SαS noise is too complex since the pdf is not given in closed-form. Hence in this thesis, we compare different sub-optimal receivers and propose a new near-optimal receiver. In terms of the coded performance in additive impulsive noise, the asymptotic and finite length performance of LDPC codes are investigated. Furthermore, by considering the fading effect, the uncoded and coded performance are also analyzed. Finally, by exploiting the spatial diversity to combat the fading, the performance of diversity combining techniques are explored.

In Chapter 4, we have investigated the performance of LDPC codes on SαS noise channels with different receivers designed to mitigate the effect of impulses. We have proposed a low-complexity sub-optimal receiver that produces a very good approximation of the LLRs but does not require the knowledge of the dispersion. The asymptotic performance of LDPC codes was presented by a DE analysis of each receiver on impulsive noise channels with different levels of impulsiveness to derive the threshold SNR that indicates the beginning of the waterfall region. The numerical results from DE and the simulation results show that our receiver can achieve near-optimal performance. We have also observed that the clipper is suitable for slightly impulsive noise channels due to its simplicity and good performance, whereas the Cauchy receiver is suitable when the channel presents severe impulses.

Although the threshold of LDPC codes can be found by DE, there is still a large

gap between the threshold and the actual performance. Hence, we have performed a finite length analysis of regular and irregular LDPC codes to derive the block and bit error probabilities on additive impulsive noise channels with SαS pdfs. At long block lengths ($N = 20000$ bits), the estimated bit error probabilities are almost identical to the simulated bit error rates for different values of α, but it has been observed that the gap between theoretical and simulation results increases as the block length decreases. Furthermore, our analysis implies that for a given uncoded BEP and threshold, the prediction of the actual performance for short LDPC codes could be accomplished on more general memoryless channels.

In Chapter 5, we have first derived the exact uncoded BEP of BPSK on generalized fading channels with SαS noise. In addition, to reducing the computational cost, we have derived two approximations of the exact BEP on Rayleigh fading channels with SαS noise, which are based on the BCGM model and the asymptotic expansion of the SαS process. The BCGM model has been shown to match the high error-rate region of the exact BEP. The asymptotic BEP has consistently provided a good approximation for the BEP in the low error-rate region. Most importantly, these two approximations have closed-from expressions, which greatly reduces the computational complexity.

Then we investigated the LDPC-coded BEP of generalized fading channels with SαS noise. The DE analysis is performed to find the asymptotic performance of LDPC codes with optimal and sub-optimal receivers on these channels. Finally, we accurately predict the waterfall performance of finite length LDPC codes on these channels by modeling the BER of each codeword as a random variable. For large block sizes the estimated bit error probabilities are almost identical to the simulated bit error rates, showing that this work is a useful tool to predict the actual performance of LDPC codes on fading channels with additive impulsive noise.

In Chapter 6, we investigate the uncoded and coded performance of linear diversity combining schemes (SC, EGC and MRC) and non-linear detectors on Rayleigh fading channels with independent SαS noise. The asymptotic performance of LDPC codes is derived using DE to verify the effectiveness of our analysis. In addition, a closed-form expression of the waterfall performance is given that reduces the gap between the asymptotic and simulated performance of LDPC codes. As discussed in the results section, MRC is not the best linear combiner, especially when the channel becomes more impulsive, and SC shows superior performance when the effect of

impulses is very strong. An interesting result is when the channel is very impulsive, where more branches have no benefit and can even degrade the performance with EGC and MRC. Meanwhile, non-linear detectors show a better performance than linear combiners with higher complexity and we proposed a reduced complexity detector by approximating the SαS pdf through a closed-form BCGM pdf which can achieve near optimal performance for all α.

In conclusion, this thesis investigates the uncoded and coded performance of communication systems in the presence of impulsive noise. We derive the theoretical uncoded BEP for the SISO (single-input single-output) system with fading or without fading. To reduce the effect of fading, diversity combining methods are also examined for the SIMO (single-input multiple-output) system. For coded performance, LDPC codes with different receivers are examined. In addition, the asymptotic performance of LDPC codes on these channels are derived. Finally, to reduce the gap between the asymptotic and simulated performance, we propose a framework to derive the finite length performance of LDPC codes on impulsive noise channels.

7.2 Future Research

In this thesis, the performance of LDPC codes on impulsive noise channels is examined. However, the LDPC codes we employ are not optimized codes for these channels. In the literature, the optimized degree distributions were only presented for AWGN channels. Although the codes designed for AWGN channels should also be good choices for other channels, the codes optimized for the specific channel are expected to perform slightly better. Hence, it is still an open problem to design LDPC codes for non-Gaussian channels.

In more and more applications, MIMO (multiple-input multiple-output) is adopted to achieve diversity or multiplexing. For future work, an LDPC-coded analysis of MIMO system on impulsive noise can be carried out. Furthermore, the error correction codes we use are not only restricted to LDPC codes, but more advanced codes such as polar codes. As we know, power-line communications employ LDPC codes in the most recent standard. However, we might find other coding schemes which are more suitable on impulsive noise channels and thus further improve the performance.

Furthermore, the code design and performance analysis can also be performed on frequency selective channels with impulsive noise since they are more realistic models of applications like power-line channels. Finally, as we have modeled the noise as SαS distributions, the accurate estimation of the parameters is very important on the performance of a communication system since the detector requires the knowledge of the noise. Hence a real-time and simple estimation method is required. Naturally, we also need to design a robust detector or decoder that can reduce the degradation caused by inaccurate estimation of parameters.

References

[1] X.-Y. Hu, E. Eleftheriou, and D.-M. Arnold, "Regular and irregular progressive edge-growth tanner graphs," *IEEE Trans. Inf. Theory*, vol. 51, no. 1, pp. 386–398, 2005.

[2] D. Middleton, "Non-Gaussian noise models in signal processing for telecommunications: new methods an results for class a and class b noise models," *IEEE Trans. Inf. Theory*, vol. 45, no. 4, pp. 1129–1149, 1999.

[3] T. Shongwey, A. H. Vinck, and H. C. Ferreira, "On impulse noise and its models," in *2014 18th IEEE International Symposium on Power Line Communications and its Applications (ISPLC)*. IEEE, 2014, pp. 12–17.

[4] M. Shao and C. L. Nikias, "Signal processing with fractional lower order moments: stable processes and their applications," *Proc. IEEE*, vol. 81, no. 7, pp. 986–1010, 1993.

[5] M. Nassar, K. Gulati, M. R. DeYoung, B. L. Evans, and K. R. Tinsley, "Mitigating near-field interference in laptop embedded wireless transceivers," *Journal of Signal Processing Systems*, vol. 63, no. 1, pp. 1–12, 2011.

[6] G. Laguna-Sanchez and M. Lopez-Guerrero, "On the use of alpha-stable distributions in noise modeling for plc," *IEEE Trans. Power Del.*, vol. 30, no. 4, pp. 1863–1870, 2015.

[7] M. Zimmermann and K. Dostert, "Analysis and modeling of impulsive noise in broad-band powerline communications," *IEEE Trans. Electromagn. Compat.*, vol. 44, no. 1, pp. 249–258, 2002.

[8] B. Hu and N. C. Beaulieu, "On characterizing multiple access interference in TH-UWB systems with impulsive noise models," in *2008 IEEE Radio and Wireless Symposium*, 2008.

[9] M. Chitre, J. Potter, and O. S. Heng, "Underwater acoustic channel characterisation for medium-range shallow water communications," in *OCEANS'04. MTTS/IEEE TECHNO-OCEAN'04*, vol. 1. IEEE, 2004, pp. 40–45.

[10] A. Rajan and C. Tepedelenlioğlu, "Diversity combining over rayleigh fading channels with symmetric alpha-stable noise," *IEEE Trans. Wireless Commun.*, vol. 9, no. 9, pp. 2968–2976, 2010.

[11] J. Lee and C. Tepedelenlioğlu, "Space-time coding over fading channels with stable noise," *IEEE Trans. Veh. Technol.*, vol. 60, no. 7, pp. 3169–3177, 2011.

[12] V. A. Aalo, K. P. Peppas, G. P. Efthymoglou, M. M. Alwakeel, and S. S. Alwakeel, "Serial amplify-and-forward relay transmission systems in nakagami-fading channels with a poisson interference field," *IEEE Trans. Veh. Technol.*, vol. 63, no. 5, pp. 2183–2196, 2014.

[13] Y. Han and K. C. Teh, "Performance study of asynchronous FFH/MFSK communications using various diversity combining techniques with MAI modeled as alpha-stable process," *IEEE Trans. Wireless Commun.*, vol. 6, no. 5, pp. 1615–1618, 2007.

[14] S. Rappaport and L. Kurz, "An optimal nonlinear detector for digital data transmission through non-gaussian channels," *IEEE Trans. Commun. Technol.*, vol. 14, no. 3, pp. 266–274, 1966.

[15] D. H. Johnson, "Optimal linear detectors for additive noise channels," *IEEE Trans. Signal Process.*, vol. 44, no. 12, pp. 3079–3084, 1996.

[16] G. A. Tsihrintzis and C. L. Nikias, "Performance of optimum and suboptimum receivers in the presence of impulsive noise modeled as an alpha-stable process," *IEEE Trans. Commun.*, vol. 43, no. 234, pp. 904–914, 1995.

[17] S. Ambike, J. Ilow, and D. Hatzinakos, "Detection for binary transmission in a mixture of gaussian noise and impulsive noise modeled as an alpha-stable process," *IEEE Signal Process. Lett.*, vol. 1, no. 3, pp. 55–57, 1994.

[18] T. S. Saleh, I. Marsland, and M. El-Tanany, "Suboptimal detectors for alpha-stable noise: Simplifying design and improving performance," *IEEE Trans. Commun.*, vol. 60, no. 10, pp. 2982–2989, 2012.

[19] E. E. Kuruoglu, W. J. Fitzgerald, and P. J. Rayner, "Near optimal detection of signals in impulsive noise modeled with a symmetric/spl alpha/-stable distribution," *IEEE Commun. Lett.*, vol. 2, no. 10, pp. 282–284, 1998.

[20] K. Gulati, A. Chopra, R. W. Heath Jr, B. L. Evans, K. R. Tinsley, and X. E. Lin, "MIMO receiver design in the presence of radio frequency interference," in *Global Communications Conference, IEEE GLOBECOM*. IEEE, 2008, pp. 1–5.

[21] E. Conte, M. Di Bisceglie, and M. Lops, "Optimum detection of fading signals in impulsive noise," *IEEE Trans. Commun.*, vol. 43, no. 2/3/4, pp. 869–876, 1995.

[22] S. Buzzi, E. Conte, and M. Lops, "Optimum detection over rayleigh-fading, dispersive channels, with non-gaussian noise," *IEEE Trans. Commun.*, vol. 45, no. 9, pp. 1061–1069, 1997.

[23] R. S. Blum, R. J. Kozick, and B. M. Sadler, "An adaptive spatial diversity receiver for non-gaussian interference and noise," *IEEE Trans. Signal Process.*, vol. 47, no. 8, pp. 2100–2111, 1999.

[24] C. Tepedelenlioglu and P. Gao, "On diversity reception over fading channels with impulsive noise," *IEEE Trans. Veh. Technol.*, vol. 54, no. 6, pp. 2037–2047, 2005.

[25] A. Nasri, R. Schober, and Y. Ma, "Unified asymptotic analysis of linearly modulated signals in fading, non-gaussian noise, and interference," *IEEE Trans. Commun.*, vol. 56, no. 6, pp. 980–990, 2008.

[26] G. Samoradnitsky and M. S. Taqqu, *Stable non-Gaussian random processes: stochastic models with infinite variance*. Chapman and Hall/CRC, 1994.

[27] A. Mahmood, M. Chitre, and M. A. Armand, "PSK communication with passband additive symmetric α-stable noise," *IEEE Trans. Commun.*, vol. 60, no. 10, pp. 2990–3000, 2012.

[28] ——, "On single-carrier communication in additive white symmetric alpha-stable noise," *IEEE Transactions on Communications*, vol. 62, no. 10, pp. 3584–3599, 2014.

[29] Z. Mei, M. Johnston, S. Le Goff, and L. Chen, "Density evolution analysis of LDPC codes with different receivers on impulsive noise channels," in *2015 IEEE/CIC International Conference on Communications in China (ICCC)*. IEEE, 2015, pp. 1–6.

[30] S. Niranjayan and N. C. Beaulieu, "The BER optimal linear rake receiver for signal detection in symmetric alpha-stable noise," *IEEE Trans. Commun.*, vol. 57, no. 12, pp. 3585–3588, 2009.

[31] ——, "BER optimal linear combiner for signal detection in symmetric alpha-stable noise: small values of alpha," *IEEE Trans. Wireless Commun.*, vol. 9, no. 3, pp. 886–890, 2010.

[32] R. G. Gallager, "Low-density parity-check codes," *IRE Trans.Inf. Theory*, vol. 8, no. 1, pp. 21–28, 1962.

[33] R. M. Tanner, "A recursive approach to low complexity codes," *IEEE Trans. Inf. Theory*, vol. 27, no. 5, pp. 533–547, 1981.

[34] D. J. MacKay, "Good error-correcting codes based on very sparse matrices," *IEEE Trans. Inf. Theory*, vol. 45, no. 2, pp. 399–431, 1999.

[35] M. C. Davey and D. J. MacKay, "Low density parity check codes over GF(q)," in *Information Theory Workshop, 1998*. IEEE, 1998, pp. 70–71.

[36] L. Barnault and D. Declercq, "Fast decoding algorithm for ldpc over GF(2^q)," in *Information Theory Workshop, 2003. Proceedings. 2003 IEEE*. IEEE, 2003, pp. 70–73.

[37] H. Wymeersch, H. Steendam, and M. Moeneclaey, "Log-domain decoding of LDPC codes over GF(q)," in *2004 IEEE International Conference on Communications*, vol. 2. IEEE, 2004, pp. 772–776.

[38] D. Declercq and M. Fossorier, "Decoding algorithms for nonbinary LDPC codes over GF(q)," *IEEE Trans. Commun.*, vol. 55, no. 4, pp. 633–643, 2007.

[39] V. Savin, "Min-max decoding for non binary ldpc codes," in *2008 IEEE International Symposium on Information Theory*. IEEE, 2008, pp. 960–964.

[40] A. Voicila, D. Declercq, F. Verdier, M. Fossorier, and P. Urard, "Low-complexity decoding for non-binary ldpc codes in high order fields," *IEEE Trans. Commun.*, vol. 58, no. 5, pp. 1365–1375, 2010.

[41] T. Richardson and R. Urbanke, "The capacity of low-density parity-check codes under message-passing decoding," *IEEE Trans. Inf. Theory*, vol. 47, no. 2, pp. 599–618, 2001.

[42] T. Richardson, M. A. Shokrollahi, and R. Urbanke, "Design of capacity-approaching irregular low-density parity-check codes," *IEEE Trans. Inf. Theory*, vol. 47, no. 2, pp. 619–637, 2001.

[43] S.-Y. Chung, G. D. Forney, T. J. Richardson, and R. Urbanke, "On the design of low-density parity-check codes within 0.0045 db of the shannon limit," *IEEE Commun. lett.*, vol. 5, no. 2, pp. 58–60, 2001.

[44] S.-Y. Chung, T. J. Richardson, and R. L. Urbanke, "Analysis of sum-product decoding of low-density parity-check codes using a gaussian approximation," *IEEE Trans. Inf. Theory*, vol. 47, no. 2, pp. 657–670, 2001.

[45] S. Ten Brink, "Convergence behavior of iteratively decoded parallel concatenated codes," *IEEE trans. Commun.*, vol. 49, no. 10, pp. 1727–1737, 2001.

[46] J. Hagenauer, "The exit chart-introduction to extrinsic information transfer in iterative processing," in *Proc. 12th European Signal Processing Conference (EUSIPCO)*. Citeseer, 2004, pp. 1541–1548.

[47] S. ten Brink, G. Kramer, and A. Ashikhmin, "Design of low-density parity-check codes for modulation and detection," *IEEE Trans. Commun.*, vol. 52, no. 4, pp. 670–678, 2004.

[48] C. Di, D. Proietti, T. J. Richardson, R. L. Urbanke *et al.*, "Finite-length analysis of low-density parity-check codes on the binary erasure channel," *IEEE Trans. Inf. Theory*, vol. 48, no. 6, pp. 1570–1579, 2002.

[49] A. Amraoui, A. Montanari, T. Richardson, and R. Urbanke, "Finite-length scaling for iteratively decoded LDPC ensembles," *IEEE Trans. Inf. Theory*, vol. 55, no. 2, pp. 473–498, 2009.

[50] R. Yazdani and M. Ardakani, "An efficient analysis of finite-length ldpc codes," in *IEEE International Conference on Communications, ICC*. IEEE, 2007, pp. 677–682.

[51] ——, "Waterfall performance analysis of finite-length LDPC codes on symmetric channels," *IEEE Trans. Commun.*, vol. 57, no. 11, pp. 3183–3187, 2009.

[52] M. Noor-A-Rahim, K. D. Nguyen, and G. Lechner, "Finite length analysis of LDPC codes," in *presentation in IEEE Wireless Comm. and Networking Conference (WCNC)*, 2014.

[53] M. Noor-A-Rahim, N. Zhang, and S. Wang, "Performance estimation of finite-length repeat–accumulate codes," *IET Communications*, vol. 9, no. 15, pp. 1902–1905, 2015.

[54] V. Oksman and S. Galli, "G. hn: The new ITU-T home networking standard," *IEEE Commun. Mag.*, vol. 47, no. 10, pp. 138–145, 2009.

[55] R. Pighi, M. Franceschini, G. Ferrari, and R. Raheli, "Fundamental performance limits of communications systems impaired by impulse noise," *IEEE Trans. Commun.*, vol. 57, no. 1, pp. 171–182, 2009.

[56] J. Fahs and I. Abou-Faycal, "On the capacity of additive white alpha-stable noise channels," in *Information Theory Proceedings (ISIT), 2012 IEEE International Symposium on*. IEEE, 2012, pp. 294–298.

[57] J. Wang, E. E. Kuruoglu, and T. Zhou, "Alpha-stable channel capacity," *IEEE Communications Letters*, vol. 15, no. 10, pp. 1107–1109, 2011.

[58] T. S. Saleh, I. Marsland, and M. El-Tanany, "Simplified LLR-based viterbi decoder for convolutional codes in symmetric alpha-stable noise," in *25th IEEE Canadian Conference on Electrical and Computer Engineering (CCECE)*. IEEE, 2012, pp. 1–4.

[59] ——, "Low-complexity near-optimal map decoder for convolutional codes in symmetric alpha-stable noise," in *Electrical & Computer Engineering (CCECE), 2012 25th IEEE Canadian Conference on*. IEEE, 2012, pp. 1–4.

[60] T. Q. Bui and H. H. Nguyen, "Error performance of bicm-id in impulsive noise," in *2006 Canadian Conference on Electrical and Computer Engineering*. IEEE, 2006, pp. 259–262.

[61] M. Shafieipour, H.-S. Lim, and T.-C. Chuah, "Decoding of turbo codes in symmetric alpha-stable noise," *ISRN Signal Processing*, vol. 2011, 2011.

[62] D. Umehara, H. Yamaguchi, and Y. Morihiro, "Turbo decoding in impulsive noise environment," in *Global Telecommunications Conference, 2004. GLOBECOM'04.*, vol. 1. IEEE, 2004, pp. 194–198.

[63] T. Faber, T. Scholand, and P. Jung, "Turbo decoding in impulsive noise environments," *Electronics letters*, vol. 39, no. 14, p. 1, 2003.

[64] W. Gu and L. Clavier, "Decoding metric study for turbo codes in very impulsive environment," *IEEE Commun. Lett.*, vol. 16, no. 2, pp. 256–258, 2012.

[65] H. Nakagawa, D. Umehara, S. Denno, and Y. Morihiro, "A decoding for low density parity check codes over impulsive noise channels," in *International Symposium on Power Line Communications and Its Applications, 2005.* IEEE, 2005, pp. 85–89.

[66] M. Ardakani, F. R. Kschischang, and W. Yu, "Low-density parity-check coding for impulse noise correction on power-line channels," in *International Symposium on Power Line Communications and Its Applications, 2005.* IEEE, 2005, pp. 90–94.

[67] N. Andreadou and F.-N. Pavlidou, "Mitigation of impulsive noise effect on the plc channel with QC–LDPC codes as the outer coding scheme," *IEEE Trans. Power Del.*, vol. 25, no. 3, pp. 1440–1449, 2010.

[68] H.-M. Oh, Y.-J. Park, S. Choi, J.-J. Lee, and K.-C. Whang, "Mitigation of performance degradation by impulsive noise in LDPC coded OFDM system," in *2006 IEEE International Symposium on Power Line Communications and Its Applications.* IEEE, 2006, pp. 331–336.

[69] C. Hsu, N. Wang, W.-Y. Chan, and P. Jain, "Improving homeplug power line communications with ldpc coded ofdm," in *INTELEC 06-Twenty-Eighth International Telecommunications Energy Conference.* IEEE, 2006, pp. 1–7.

[70] A. Ayyar, M. Lentmaier, K. Giridhar, and G. Fettweis, "Robust initial llrs for iterative decoders in presence of non-gaussian noise," in *2009 IEEE International Symposium on Information Theory*. IEEE, 2009, pp. 904–908.

[71] H. B. Mâad, A. Goupil, L. Clavier, and G. Gellé, "Clipping demapper for LDPC decoding in impulsive channel," *IEEE Commun. Lett.*, vol. 17, no. 5, pp. 968–971, 2013.

[72] V. Dimanche, A. Goupil, L. Clavier, and G. Gelle, "On detection method for soft iterative decoding in the presence of impulsive interference," *IEEE Commun. Lett.*, vol. 18, no. 6, pp. 945–948, 2014.

[73] Y. Hou, R. Liu, and L. Zhao, "A non-linear LLR approximation for LDPC decoding over impulsive noise channels," in *2014 IEEE/CIC International Conference on Communications in China (ICCC)*. IEEE, 2014, pp. 86–90.

[74] S. W. Kim, S.-J. Park, and W. Chang, "Diversity selection combining to enhance the coding gain," in *Vehicular Technology Conference, 2004. VTC2004-Fall. 2004 IEEE 60th*, vol. 3. IEEE, 2004, pp. 1861–1864.

[75] S. Gounai and T. Ohtsuki, "Performance analysis of ldpc code with spatial diversity," in *IEEE Vehicular Technology Conference*. IEEE, 2006, pp. 1–5.

[76] B. S. Tan, K. H. Li, and K. C. Teh, "Performance analysis of ldpc codes with selection diversity combining over identical and non-identical rayleigh fading channels," *IEEE Communications Letters*, vol. 14, no. 4, pp. 333–335, 2010.

[77] ——, "Performance analysis of ldpc codes with maximum-ratio combining cascaded with selection combining over nakagami-m fading," *IEEE Trans. Wireless Commun.*, vol. 10, no. 6, pp. 1886–1894, 2011.

[78] ——, "Efficient ber computation of ldpc coded sc/mrc systems over rayleigh fading," in *Signal Processing and Communication Systems (ICSPCS), 2010 4th International Conference on*. IEEE, 2010, pp. 1–5.

[79] Y. Fang, P. Chen, L. Wang, F. C. Lau, and K.-K. Wong, "Performance analysis of protograph-based low-density parity-check codes with spatial diversity," *IET Commun.*, vol. 6, no. 17, pp. 2941–2948, 2012.

[80] E. E. Kuruoğlu, C. Molina, and W. J. Fitzgerald, "Approximation of α-stable probability densities using finite gaussian mixtures," in *The 9th European Signal Processing Conference (EUSIPCO)*. IEEE, 1998, pp. 1–4.

[81] X. Wang and H. V. Poor, "Robust multiuser detection in non-gaussian channels," *IEEE Trans. Signal Process.*, vol. 47, no. 2, pp. 289–305, 1999.

[82] M. Ghosh, "Analysis of the effect of impulse noise on multicarrier and single carrier qam systems," *IEEE Trans. Commun.*, vol. 44, no. 2, pp. 145–147, 1996.

[83] M. Nassar, K. Gulati, Y. Mortazavi, and B. L. Evans, "Statistical modeling of asynchronous impulsive noise in powerline communication networks," in *Global Telecommunications Conference (GLOBECOM 2011), 2011 IEEE*. IEEE, 2011, pp. 1–6.

[84] H. El Ghannudi, L. Clavier, N. Azzaoui, F. Septier, and P. A. Rolland, "α-stable interference modeling and cauchy receiver for an ir-uwb ad hoc network," *IEEE Trans. Commun.*, vol. 58, no. 6, pp. 1748–1757, 2010.

[85] J. G. Gonzalez, J. L. Paredes, and G. R. Arce, "Zero-order statistics: a mathematical framework for the processing and characterization of very impulsive signals," *IEEE Trans. Signal Process.*, vol. 54, no. 10, pp. 3839–3851, 2006.

[86] J. M. Chambers, C. L. Mallows, and B. Stuck, "A method for simulating stable random variables," *Journal of the american statistical association*, vol. 71, no. 354, pp. 340–344, 1976.

[87] G. Tsihrintzis, C. L. Nikias *et al.*, "Fast estimation of the parameters of alpha-stable impulsive interference," *IEEE Trans. Signal Process.*, vol. 44, no. 6, pp. 1492–1503, 1996.

[88] S. J. Johnson, *Iterative error correction: turbo, low-density parity-check and repeat-accumulate codes*. Cambridge University Press, 2009.

[89] T. Richardson and R. Urbanke, *Modern coding theory*. Cambridge University Press, 2008.

[90] J. P. Nolan, "Numerical calculation of stable densities and distribution functions," *Communications in statistics. Stochastic models*, vol. 13, no. 4, pp. 759–774, 1997.

[91] X. Li, J. Sun, L. Jin, and M. Liu, "Bi-parameter CGM model for approximation of a-stable PDF," *Electron. Lett.*, vol. 44, no. 18, pp. 1096–1097, 2008.

[92] K. Cho and D. Yoon, "On the general BER expression of one-and two-dimensional amplitude modulations," *IEEE Trans. Commun.*, vol. 50, no. 7, pp. 1074–1080, 2002.

[93] M. Schwartz, W. R. Bennett, and S. Stein, *Communication systems and techniques*. John Wiley & Sons, 1995.

[94] J. Hu and N. C. Beaulieu, "Accurate simple closed-form approximations to rayleigh sum distributions and densities," *IEEE Commun. Lett.*, vol. 9, no. 2, pp. 109–111, 2005.

[95] H. B. Mâad, A. Goupil, L. Clavier, and G. Gelle, "Asymptotic performance of LDPC codes in impulsive non-gaussian channel," in *Signal Processing Advances in Wireless Communications (SPAWC), 2010 IEEE Eleventh International Workshop on*. IEEE, 2010, pp. 1–5.